UNIVERSITY OF CALIFORNIA,
IRVINE

Laboratory Studies of New Particle Formation and Growth from Methanesulfonic Acid Amines and Water

DISSERTATION

submitted in partial satisfaction of the requirements
for the degree of

DOCTOR OF PHILOSOPHY

in Chemistry

by

Matthew L. Dawson

Dissertation Committee:
Professor Barbara J. Finlayson-Pitts, Chair
Professor Donald R. Blake
Professor Sergey A. Nizkorodov

2014

TABLE OF CONTENTS

LIST OF FIGURES

LIST OF TABLES

ACKNOWLEDGMENTS

I would first like to thank Fabian Batchkin, for his unwaivering belief that I would some day 'get it.'

My advisor, Prof. Finlayson-Pitts has been a tremendous source of encouragement and motivation throughout my time at UCI. I will always be grateful for the time and energy she has invested in me and I hope that my future work will be characterized by the scientific curiosity, strong work ethic, and attention to detail that she works to instill in all of her students.

I am also very grateful to the entire Finlayson-Pitts group (current, former and extended members) for creating and maintaining such a friendly, supportive and productive working environment. Dr. Veronique Perraud and Micheal Ezell have, in particular, endured many, many hours of working with me, and have each provided valuable scientific and technical training, support and encouragement.

This work is the result of several collaborations, from which I have benefited a great deal. Specifically, I would like to thank Prof. R. Benny Gerber and Dr. Mychel Varner who provided the theoretical calculations and insight into the mechanisms underlying all of our experimental observations. I am grateful to Prof. Donald Dabdub, Dr. Andrew Martinez and Jeff Ngarmboonta for their collaboration and advice related to the development of the flow reactor model. I would like to thank Dr. Alla Zelenyuk for the training and collaboration using SPLAT-II, the many informative discussions at PNNL and various conferences, and her support throughout my time in graduate school. I am also grateful to Greg DeMattia, Jim Soulek, Jeff Tompkins and Metrohm USA for the use of the ion chromatograph, and for their generous support in developing the amine sampling technique. I would also like to thank Profs. Sergey Nizkorodov and Donald Blake for their support and for serving on both my advancement and dissertation committees.

Funding for the work presented here was provided by the Department of Energy and the National Science Foundation through AirUCI. I am grateful to the ARCS Foundation for an ARCS Scholar award and to Metrohm USA for the 2012 Methrohm Young Chemist award. I would like to thank Jennifer Bentson-Gebel, the Gebel family and the UC Irvine Department of Chemistry for the Michael Gebel award. Finally, I would like to thank the Lee family and the UC Irvine Department of Chemistry for an Edward K.C. Lee award.

CURRICULUM VITAE

Matthew L. Dawson

EDUCATION

University of California, Irvine *Irvine, CA*
Ph.D. in Chemistry **2009–2014**
GPA: 3.997
Advisor: Prof. Barbara J. Finlayson-Pitts

University of Pittsburgh *Pittsburgh, PA*
B.S. in Chemistry, summa cum laude **2007–2009**
GPA: 3.976
Advisor: Prof. Sunil Saxena

Community College of Allegheny County *Pittsburgh, PA*
GPA: 4.000 **2005–2006**

RESEARCH EXPERIENCE

Graduate Research Assistant **2009–2014**
University of California, Irvine *Irvine, CA*

- Gas-phase Ammonia and Amine Measurement
  - Developed a method for measuring gas-phase ammonia and amines at the part-per-trillion level by collection onto a weak cation exchange resin followed by extraction and analysis by ion chromatography.
- New Particle Formation
  - Performed laboratory simulations of new particle formation in the atmosphere from methanesulfonic acid, amines and water. Quantified nucleation rates using a variety of precursor concentrations and developed a kinetics mechanism describing particle formation from this system. Tested this mechanism in a comprehensive aerosol chemistry and physics model.
- Formation of Aromatic Compounds from VOC oxidation
  - Laboratory measurement of p-cymene (an aromatic hydrocarbon) formation in the oxidation of -pinene by OH under atmospherically relevant conditions.

Undergraduate Research Assistant **2008–2009**
University of Pittsburgh *Pittsburgh, PA*

- Modeling Protein Dynamics
  - Modeled conformational isomers of the spin-labeled EcoRI protein by molecular dynamic simulations to aid in the interpretation of experimental electron spin resonance (ESR) data.

AWARDS AND HONORS

Edward K. C. Lee Award **May 2014**

Metrohm Young Chemist Award **October 2012**
An award for novel research or an innovative approach to the applications of titration, ion chromatography and/or electrochemistry

ARCS Scholar **September 2012**
ARCS Foundation advances science and technology in the United States by providing financial awards to academically outstanding U.S. citizens studying to complete degrees in science, engineering and medical research.

AAAR Particulars **Spring 2012**
Highlighted in the *Who are these aerosol scientists?* section of the American Association for Aerosol Research newsletter

Gebel Award, UC, Irvine **May 2011**
An award recognizing excellence in graduate environmental chemistry research and service to the community

Contributions to Education by a Chemistry Department TA **May 2011**

Phillips Medal, University of Pittsburgh **May 2009**
An award presented to the senior chemistry major with the most outstanding academic record

TEACHING EXPERIENCE

Teaching Assistant **Summer 2011, 2012, 2013**
AirUCI Summer Teacher Workshop *Irvine, CA*

Laboratory Assistant **Fall 2009, Winter–Spring, 2010, Winter 2011**
University of California, Irvine *Irvine, CA*
General, Advanced Analytical, and Quantitative Analytical Undergraduate Chemistry Labs

Tutor **Fall–Winter 2006**
Community College of Allengheny County *Pittsburgh, PA*
Introductory Computer Courses and Java Programming

ORGANIZATIONS

American Association for Aerosol Research **2011–Present**
American Geophysical Union **2013–Present**

REFEREED JOURNAL PUBLICATIONS

Dawson, M.L., Perraud, V., Gomez A., Arquero, K.D., Ezell, M.J., and Finlayson-Pitts, B.J. Measurement of Gas-Phase Ammonia and Amines in Air by Collection onto an Ion Exchange Resin and Analysis by Ion Chromatography, *Atmos. Meas. Technol. Discuss.* **7**, 1573-1602 (2014).

Nishino, N., Arquero, K.D., Dawson, M.L., Finlayson-Pitts, B.J. Infrared Studies of the Reaction of Methanesulfonic Acid with Trimethylamine on Surfaces, *Environ. Sci. Technol.* **48**, 323330 (2013).

Dawson, M.L., Varner, M.E., Perraud, V., Ezell, M.J., Gerber, R.B., Finlayson-Pitts, B.J. New Particle Formation from Methanesulfonic Acid, Amines and Water: Experiment, *ab initio* Calculations and a Simplified Mechanism. *PNAS* **109**, 18719-18724 (2012).

Doezema, L.A., Longin, T., Cody, W., Perraud, V., Dawson, M.L., Ezell, M.J., Greaves, J., Johnson, K.R., Finlayson-Pitts, B.J. Analysis of Secondary Organic Aerosols in Air using Extractive Electrospray Ionization Mass Spectrometry (EESI-MS). *RSC Advances* **2**, 2930-2938 (2012).

Gratien, A, Johnson, S.N., Ezell, M.E., Dawson, M.L., Bennett, R, Finlayson-Pitts, B.J. Surprising Formation of p-Cymene in the Oxidation of α-Pinene in Air by the Atmospheric Oxidants OH, O_3, and NO_3. *Environ. Sci. Technol.* **45**, 2755-2760 (2011).

CONFERENCE PRESENTATIONS

*Presenting author(s)
*Chen, H., *Varner, M.E., *Dawson, M.L., *Martinez, A.S., Perraud, V., Arquero, K. D., Gomez, A., Gerber, R.B., Dabdub, D., Finlayson-Pitts, B.J. Particles and Their Precursors: From the Angstrom to Regional Scales. *Collaborative Workshop in Chemistry at the Interfaces.* AirUCI. Surf and Sand Hotel, Laguna Beach, CA. Jan. 22-23, 2014. Conference Presentation.

*Dawson, M.L., Gomez, A.L., Arquero, K.D., Perraud, V., Finlayson-Pitts, B.J. A New Method for Measurement of Gas-Phase Ammonia and Amines in Air. *AGU Fall Meeting.* American Geophysical Union. Moscone Convention Center, San Francisco, CA. December 9-13, 2013. Poster Presentation.

*Dawson, M.L., Perraud, V., Ezell, M.J., Finlayson-Pitts, B.J. Accurately Predicting Particle Formation and Growth from Gas-Phase Precursors. *Pittcon 2013*. Pennsylvania Convention Center, Philadelphia, PA. March 19, 2013. Poster Presentation.

*Martinez, A.S., *Dawson, M.L., Varner, M.E., Perraud, V., Ezell, M.J., Gerber, R.B., Dabdub, D., Finlayson-Pitts, B.J. Utilizing a regional air quality model to estimate potential for particle formation from methanesulfonic acid and amines. *30th Informal Symposium on Kinetics and Photochemical Processes in the Atmosphere*. California Institute of Technology, Pasadena, CA. March 8, 2013. Poster Presentation.

*Dawson, M.L., *Varner, M.E., *Martinez, A.S., Perraud, V., Ezell, M.J., Gerber, R.B., Dabdub, D., Finlayson-Pitts, B.J. New Particle Formation from Methanesulfonic Acid and Amines in Air. *Collaborative Workshop in Chemistry at the Interfaces*. AirUCI. Surf and Sand Hotel, Laguna Beach, CA. Jan. 31-Feb. 1, 2013. Conference Presentation.

*Dawson, M.L., Varner, M.E., Perraud, V., Ezell, M.J., Gerber, R.B., Zelenyuk, A., Finlayson-Pitts, B.J. A Novel Kinetics Mechanism for Particle Formation from Methanesulfonic Acid, Amines, and Water. *AAAR 2012 Annual Conference*. American Association for Aerosol Research. Hyatt Regency, Minneapolis, MN. Oct. 8-12, 2012. Poster Presentation.

*Dawson, M.L., Varner, M.E., Perraud, V., Ezell, M.J., Wingen, L.M., Bruns, E.A., Kleinman, M.T., Gerber, R.B., Finlayson-Pitts, B.J. Atmospheric Particle Formation and Growth from Methanesulfonic Acid and Amines. *Spring 2012 National Meeting and Exhibition*. American Chemical Society. San Diego Convention Center, Sand Diego, CA. March 25-29, 2012. Poster Presentation.

*Dawson, M.L., Varner, M.E., Perraud, V., Ezell, M.J., Gerber, M.J., Zelenyuk, A., Finlayson-Pitts, B.J. Formation and Growth of Atmospheric Aerosol Particles from Methanesulfonic Acid, Amines and Water. *2012 Science Team Meeting*. Atmospheric System Research Department of Energy. Hyatt Regency Crystal City, Arlington, VA. March 12-16, 2012. Poster Presentation.

*Dawson, M.L., Varner, M.E., Perraud, V., Ezell, M.J., Wingen, L.M., Bruns, E.A., Kleinman, M.T., Gerber, R.B., Finlayson-Pitts, B.J. Particle Nucleation and Growth from Methanesulfonic Acid and Amines. *29th Informal Symposium on Kinetics and Photochemical Processes in the Atmosphere*. California State University, Fullerton, CA. February 24, 2012. Poster Presentation.

*Dawson, M.L., *Varner, M.E., Perraud, V., Ezell, M.J., Gerber, R.B., Zelenyuk, A., Finlayson-Pitts, B.J. Formation and Properties of MSA-Amine Particles. *Collaborative Workshop in Chemistry at the Interfaces*. AirUCI. Surf and Sand Hotel, Laguna Beach, CA. Jan. 26-27, 2012. Conference Presentation.

*Dawson, M.L., Varner, M.E., Perraud, V., Ezell, M.J., Wingen, L.M., Bruns, E.A., Kleinman, M.T., Gerber, R.B., Finlayson-Pitts, B.J. Particle Nucleation and Growth from Methanesulfonic Acid and Amines. *AAAR 2011 Annual Conference*. American Association for Aerosol Research. Rosen Shingle Creek Resort, Orlando, FL. October 3-7, 2011. Poster Presentation.

*Dawson, M.L., Perraud, V., Ezell, M.J., Wingen, L.M., Bruns, E.A., Kleinman, M.T., Varner, M.E., Gerber, R.B., Finlayson-Pitts, B.J. Methanesulfonic Acid as a Source of New Particles in the Atmosphere. *241st ACS National Meeting and Exposition*. American Chemical Society. Anaheim Convention Center, Anaheim, CA. March 27-31, 2011. Poster Presentation.

*Dawson, M.L., Perraud, V., Ezell, M.J., Wingen, L.M., Kleinman, M.T., Finlayson-Pitts, B.J. New Particle Formation from Methanesulfonic Acid in Air. *28th Informal Symposium on Kinetics and Photochemical Processes in the Atmosphere*. University of California, Irvine, CA. Mar. 3, 2011. Poster Presentation.

*Dawson, M.L., *Varner, M.E., Perraud, V., Ezell, M.J., Gerber, R.B., Kleinman, M.T., Finlayson-Pitts, B.J. Effects of Water on Nanoparticle Formation from Methanesulfonic Acid: Approaching the Limit of Interfaces in Complex Systems. *Collaborative Workshop in Chemistry at the Interfaces*. AirUCI. Surf and Sand Hotel, Laguna Beach, CA. Jan. 19-20, 2011. Conference Presentation.

*Dawson, M.L., Perraud, V., Ezell, M.J., Wingen, L.M., Bruns, E.A., Kleinman, M.T., Finlayson-Pitts, B.J. New Particle Formation from Methanesulfonic Acid in Air. *AGU Fall Meeting*. American Geophysical Union. Moscone Convention Center, San Francisco, CA. Dec. 13-17, 2010. Poster Presentation.

*Dawson, M.L., Perraud, V., Ezell, M.J., Wingen, L.M., Bruns, E.A., Kleinman, M.T., Finlayson-Pitts, B.J. New Particle Formation from Methanesulfonic Acid in Air. *Chemical Sciences Roundtable: Challenges in Characterizing Small Particles: Exploring Particles from the Nano- to Microscales*. National Academy of Sciences. The Washington Plaza Hotel, Washington, D.C. Oct. 25-26, 2010. Poster Presentation.

OTHER PRESENTATIONS

*Dawson, M.L. A Random Walk to Graduate School. *ACS High School Awards Dinner*. American Chemical Society. UCI Student Center, Irvine, CA. May 3, 2013. Invited Speaker.

ABSTRACT OF THE DISSERTATION

Laboratory Studies of New Particle Formation and Growth from Methanesulfonic Acid Amines and Water

By

Matthew L. Dawson

Doctor of Philosophy in Chemistry

University of California, Irvine, 2014

Professor Barbara J. Finlayson-Pitts, Chair

Atmospheric aerosols reduce visibility, adversely affect human health, and influence the climate. However, modeling the evolution of these systems is complicated by the large number of species involved and their complex interactions in both the gas and particle phase. To reduce this complexity, key species and generalized mechanisms of particle formation, growth and evolution are sought to aid development of computationally-feasible regional and global atmospheric models. These models, alongside simple, accurate measurement techniques for particles and key gas-phase precursors, will improve predictions of the effects of changing emissions on visibility, climate and human health.

This dissertation reports work identifying a new source of particles in the atmosphere, those formed from methanesulfonic acid (MSA), amines and water. Experiments performed in an aerosol flow reactor with MSA, water vapor, and dimethylamine or trimethylamine demonstrate that this system rapidly forms particles, and that all three species (MSA, water and amine) are required for significant particle formation. A simplified kinetics mechanism for particle formation from this system was developed based on these experiments and theoretical calculations of small clusters of these species, performed by the Gerber group. Predictions of particle formation from this mechanism agree well with our measurements, making

this computationally inexpensive calculation useful for large-scale atmospheric models. A more comprehensive aerosol model is under development to test this mechanism while incorporating the effects of wall losses, coagulation between particles, and growth based on particle-phase activity.

Predicting particle formation in the laboratory and the real atmosphere requires accurate measurement techniques for the gas-phase precursors. A major limitation to many existing techniques for measuring gas-phase amines is rapid loss of the analyte to instrument surfaces, such as inlet tubing. A new technique for measuring gas-phase ammonia and amines was developed that involves collection of the sample on weak ion-exchange resin in a cartridge designed to minimize the exposure of the incoming sample to surfaces prior to uptake on the resin. These cartridges are simultaneously extracted and analyzed by ion chromatography, using a novel instrument configuration designed to lower the detection limit of this method to the parts-per-trillion level in air for a 60 min sample. This technique using inexpensive, reusable cartridges is shown to efficiently measure ammonia and three aliphatic amines.

Unlike MSA, ammonia and amines have high vapor pressures and must be neutralized to remain in the particle phase. This opens the possibility of complex displacement reactions between gas- and particle-phase ammonia and amine species. Experiments were performed in collaboration with scientists at PNNL's EMSL User Facility using the SPLAT-II single-particle mass spectrometer to investigate the displacement of ammonia and amines in ammonium- and aminium-methanesulfonate particles on addition of a different gas-phase amine. The results suggest a complex system where the effects of particle-phase ammonium or aminium on hygroscopicity and particle phase result in different degrees of displacement by gas-phase amines.

The work presented here will aid in the development and evaluation of regional and global atmospheric models, by identifying and quantifying new sources of particles, understanding

complex reactions affecting particle growth, and facilitating simple, accurate measurements of gas-phase particle precursors in the field.

Chapter 1

Introduction

Particulate matter is ubiquitous in the atmosphere and has a variety of natural and anthropogenic sources. These particles reduce visibility[1], have be shown to adversely affect human health,[2–6] and influence the climate through their ability to scatter and absorb radiation and act as cloud condensation nucleii (CCN).[7–9]

In regard to human health effects, ambient particulate matter has been linked to increased mortality rates,[10] cardiovascular disease,[4] pulmonary function problems (especially among asthmatics),[2] and increases the risk of lung cancer.[3] There is evidence that even short term exposure to elevated levels of particulate matter carries significant health risks.[2] Quantifying the impact of particulate matter on human health is an open area of research as adverse health effects have been shown to depend not just on particle size, but also on particle composition.[11,12]

The effects of aerosol particles on climate are equally complex. The extent to which particles scatter and absorb radiation and their ability to act as CCN are dependent on their number, size and composition,[7,9,13] making this a difficult system to model.[14] Indeed, the effect

of aerosol particles on radiative forcing remains the largest uncertainty in global climate models.[8]

Detailed understanding of the formation, growth, composition and physical properties of particulate matter is therefore essential to determining their effects on human health and understanding the trajectory of climate change. However, modeling the evolution of atmospheric aerosol systems is complicated by the large number of species involved and their complex interactions in both the gas and particle phase. To reduce this complexity, key species and generalized mechanisms of particle formation and growth are sought to aid in the development of computationally-feasible regional and global atmospheric models. The goal of this work is to characterize an as-yet unexplored source of atmospheric aerosol particles, those formed from the gas-phase reaction of methanesulfonic acid (MSA, CH_3SO_3H), amines and water, to develop a simple model for particle formation from this system, and to determine the effects of these species on further particle growth.

1.1 New Particle Formation

Aerosol particles are emitted directly (primary sources) and are formed in the atmosphere by condensation of gas-phase species (secondary sources). In fact, 30-50% of particles that act as CCN are thought to form from these secondary sources.[15,16] However, few gas-phase species have sufficiently low vapor pressure to react to form a stable cluster.[15,17,18] Sulfuric acid has long been recognized as a key species in the initial formation of particles in the atmosphere, and gas-phase sulfuric acid concentrations are generally well-correlated with new particle formation events[19–31], with temperature and relative humidity (RH) having important affects on particle formation.[30,32] Despite its key role, models of new particle formation based solely on binary nucleation of sulfuric acid and water often under-predict the

number of particles formed in the atmosphere.[30,33,34] This suggests a role for co-condensing species and/or alternate sources of new particles.

Ammonia and more recently amines have been identified as potentially important co-condensing species with sulfuric acid. Ammonia, with concentrations that can reach the ppm level in the atmosphere,[35] has been shown to enhance particle formation from sulfuric acid.[36–39] Amines, despite much lower atmospheric concentrations than ammonia, have a greater enhancing effect on sulfuric acid nucleation,[34,37,40–42] and are present along with sulfate in ambient particles during nucleation events.[43] Amines have been shown to contribute to particle formation and growth through both acid-base reaction as well as by forming low-volatility oxidation products when reacted with atmospheric oxidants.[44,45] As such, they are increasingly being seen as important contributors to new particle formation, and inclusion of amines in models of new particle formation brings results closer in line with atmospheric observations.[40] Other co-condensing species, such as several atmospherically relevant organic compounds, have been investigated and shown to enhance particle formation from sulfuric acid,[46] while others have been shown to not lead to such an enhancement.[47]

MSA is routinely detected in the particle phase,[48–57] and has been identified as an important species in particle growth.[58] There are indications that the role of MSA in particle growth is particularly important for small newly-formed particles, as particle-phase MSA has been observed to be enhanced relative to sulfate in particles < 100 nm in diameter in field measurements.[48,55,56] While uptake of MSA onto particles is rapid,[59] its contribution to further growth may involve complicated interfacial reactions.[58]

In contrast to sulfuric acid, much less is known about the contribution of MSA to new particle formation, despite its role in particle growth and the fact that it has similar sources and ambient concentrations as sulfuric acid,[51,60] as will be discussed in more detail below. While particle nucleation from MSA and water vapor has been previously studied and shown to not be significant compared to the sulfuric acid/water system,[29,61] an investigation of nucleation

rates for MSA with ammonia and amines had not previously been carried out. Field studies have shown, however, a moderate correlation between methanesulfonate and diethylamine in the particle phase over the ocean[53] and amines are known to react with other gas-phase acids, such as nitric and sulfuric acids, to form particles.[34,37,40,44]

1.1.1 Gas-Phase Precursor Sources

1.1.1.1 MSA

MSA is formed alongside sulfuric acid in the oxidation of organosulfur compounds such as dimethyl sulfide (DMS) and methyl mercaptan and is widespread in the atmosphere.[7,59,62–68] These reduced-sulfur species are emitted primarily from biological activity in the oceans in large quantities,[69–74] with DMS alone accounting for about half of the natural sulfur emissions globally.[73,74] There are also inland sources of these reduced sulfur species,[75–80] and indications of unidentified MSA sources, possibly including animal sources.[52]

Organosulfur compounds such as DMS are oxidized in the atmosphere by a variety of atmopsheric oxidants including OH and NO_3, among others in both the gas and particle phase.[59,62–68,81–84] The competition between OH oxidation during the day and NO_3 oxidation at night affects both average DMS concentrations and the time of day when peak daily DMS concentrations are observed in going from clean to more polluted environments.[50,73,74] In clean environments, the oxidation by OH during the day is rapid enough to lead to large diurnal variations in DMS concentrations which peak in the early morning and reach a minimum by mid-afternoon.[73,74] However in more polluted areas, NO_3 night-time oxidation shifts these diurnal variations such that DMS concentrations peak at noon and reach a minimum at night.[50]

Gas-phase concentrations of MSA in the atmosphere have been measured from $< 10^4$ up to 10^7 molecules cm^{-3}.[50,51,60,85,86] The yield of MSA from organosulfur oxidation varies with a variety of factors including oxidizing species and the presence of organics,[59,62,68,82,87] and has been reported to be many times that of sulfuric acid under certain conditions.[82] MSA concentrations have been observed to range from 6-100% relative to sulfuric acid in the marine coastal environment.[51] The MSA/sulfate ratio in particles has been measured to be between 0.02 and 0.93, with the lowest ratios near the equator and the highest off the coast of Antarctica.[52] In polluted areas, oxidation of DMS by NO_3 at night becomes more important, for which MSA/sufuric acid yields have been measured at 1.2 – 3.0.[59]

1.1.1.2 Ammonia and Amines

Ammonia and amines are ubiquitous in the atmosphere and have a wide variety of both biogenic and anthropogenic sources.[35,77,88–99] Relative concentrations of gas- and particle-phase ammonia and amines vary with season,[89,100] temperature,[89,100] and molecular mass of the amine species.[100] The largest source of atmospheric ammonia in the U.S. is livestock emissions, but industrial sources, fertilizers, soil and vehicle emissions also contribute.[89] For amines, important sources include agricultural operations,[101–105] coal combustion,[100] ocean biota,[88,90] biomass burning,[88,106] and release from carbon capture and storage devices that use amines to trap CO_2, which could become a more important source of atmospheric amines and ammonia as the technology becomes more widely adopted.[88,107–111] Methylamine (MA; CH_3NH_2), dimethylamine (DMA; $(CH_3)_2NH$) and trimethylamine (TMA; $(CH_3)_3N$) are among the most prevalent amines in the atmosphere, with estimated global emission rates of 285 ± 78 Gg N a^{-1} for the three amines combined, while annual emissions of NH_3 are $(5\pm3)\times10^4$ Gg N a^{-1}.[88,105] However amine concentrations vary widely in the atmosphere, with background concentrations of several ppt or lower, but reaching > 100 ppb near sources.[88]

In addition to their ability to contribute to new particle formation through acid-base reactions, amines react rapidly with atmospheric oxidants such as OH, NO_3 and O_3.[44,88,107,111–114] These oxidation reactions along with gas-to-particle conversion result in short atmospheric lifetimes for gas-phase amines,[88] which when coupled with variations in source strength, windspeed and direction leads to widely variable atmospheric amine concentrations.[88,115]

1.1.2 Experimental Techniques

Potential sources of new particles have been investigated by field measurement and laboratory experiments. In both cases, measurement of gas-phase precursor concentrations as well as particle number, size and composition are often required and a variety of techniques are employed to accomplish this challenging set of measurements.

Particle concentrations are measured by scanning mobility particle sizers (SMPS) and/or condensation particle counters (CPC) and used to determine particle formation rates for a certain set of experimental or ambient conditions.[20,32,116–119] Detection limits of CPC systems can be lowered by optimizing conditions and choosing an approriate working fluid.[120–122] And, some commericially available 'booster' CPCs have recently become available, including a particle size magnifier (PSM) which is used to lower the detection limit of the CPC to ∼1.5 nm and has been used in several nucleation studies.[32,41] Particle composition measurements have been made using particle-into-liquid samplers (PILS) coupled with ion chromatography (IC),[68], ambient-ion-monitor ion chromatography (AIM-IC)[123], aerosol time-of-flight mass spectrometry (ATOFMS),[43,57] and single particle laser ablation time-of-flight mass spectrometry (SPLAT-II).[124,125] However, composition measurements of ambient particles are not well suited for investigating particle formation as they typically measure particles >50-100 nm in diameter,[43] where the contribution to particle mass by species involved in forming the initial cluster are dwarfed by the subsequently condensing species. Recently, techniques have

been developed that are capable of sampling small clusters containing only a few molecules and measuring their composition by mass spectrometry in an effort to learn more about the earliest steps in particle formation. These include the cluster chemical ionization mass spectrometer (cluster CIMS),[122,126,127] and fourier transform ion cyclotron resonance mass spectrometry (FTICR-MS) with surface-induced dissociation.[128]

In the atmosphere, particle formation from gas-phase precursors usually occurs in bursts, often associated with low temperature, high RH and low background aerosol concentration.[30] In field measurements, new particle formation events are identified based on particle number concentration measurements. Correlations between gas-phase species concentrations and these events are used to identify important precursor species and quantify particle formation from these sources.[43,31] Composition measurements of small ($<$ 10 nm) ambient particles have also been successfully used to identify key precursor species.[42] This approach has led to the development of several parameterizations of particle formation in the atmosphere, based on, *e.g.*, nucleation theory or the kinetics of cluster formation.[20,126,129]

In the laboratory, many studies of particle formation and growth involve either static chamber[39,40,44,68,118,130–132] or flow-reactor[26,29,32,37,61,117,119,133–135] experiments. In static chamber experiments, gas-phase species are introduced into a large Teflon[68] or stainless steel[118] chamber and allowed to react to form particles. These experiments require measurement techniques with fast time resolution as the system evolves quickly once the gas-phase species are introduced. Flow reactors are less demanding with respect to fast time resolution. In these systems, measurements made at a fixed distance from where the gas-phase species are introduced correspond to a specific reaction time after the system reaches a steady state.[134] While wall-losses are a concern in both chamber and flow reactor experiments,[136,137] decreasing the surface-to-volume ratio has been used to reduce the effects of wall loss in both systems.[118,134]

Theoretical calculations of the energetics and dynamics of formation of small clusters as well as their structures have proven indispensable in understanding the formation of small

clusters in the atmosphere.[40,128,138–148] These calculations have been performed for a variety of charged and neutral clusters of sufuric acid or MSA with ammonia, amines and water, and have provided insight into both cluster formation processes and ammonium-aminium exchange in small clusters.[128,138,149] These techniques are capable of exploring important processes that are beyond the scope of measurement techniques, such as identifying when proton transfer occurs, and how structure, especially near the interface, may affect further cluster growth.[138,149] Their results are integral to several models of particle formation, including the one presented in this work.[149]

1.2 Ammonia and Amine Measurement Techniques

The relatively recent identification of amines as important species in new particle formation has highlighted the need for quantitative data on amine sources and ambient concentrations. Even ammonia concentrations, for which more data are available, are difficult to accurately predict due to the multiple factors influencing emissions from any particular source.[89] A variety of techniques for measuring atmospheric ammonia and amines have been described in the literature. These include both on-line mass spectrometric techniques for gas- or particle-phase samples as well as off-line techniques. Off-line measurement typically involves: (1) collection of the gas- and/or particle-phase ammonia and amines, (2) extraction, sometimes followed by derivatization, (3) separation by chromatography and (4) detection. In some cases, these steps are automated (*e.g.*, in the PILS technique[150–152] and in the AIM-IC[123]).

Several on-line particle mass spectrometers have been developed capable of measuring particle composition (including ammonium and aminium species) along with physical particle properties (*e.g.* size, morphology, density).[44,153–155] These include ATOFMS,[44,153,154] SPLAT-II-MS,[125,156–158] cluster CIMS,[126,127] and FTICR-MS with surface-induced dissociation,[128] as mentioned previously. On-line gas-phase ammonia and amine measurements

have been performed by chemical ionization mass spectrometry,[159,160] ambient pressure proton transfer MS,[161] and proton-transfer-reaction mass spectrometry (PTR-MS)[75,107,162–164] among others.[115,165]

In off-line techniques, particle-phase ammonium and aminium can be collected on a Teflon filter[100] or by condensational growth in a chamber supersaturated with water followed by impaction.[150–152] Filter samples are typically extracted with an acidic solution.[100] An important limitation to the filter technique for separating gas- and particle-phase amines involves the equilibrium often established between gas- and particle-phase ammonia and amines (*e.g.*, in NH_4NO_3 particles([7] which may act to alter the composition of particles collected on the filter as the samples are collected.[166]

Off-line gas-phase measurements of ammonia and amines typically involve collection onto a substrate (*e.g.*, activated charcoal[167] or an acid-impregnated glass fiber filter[168]). Alternately, pure gas-phase samples or those that have been filtered to remove particulates can be bubbled through an acidic solution,[100,101,105,169] or a whetted glass frit[170] to collect the remaining gas-phase ammonia and amines. Diffusion based techniques for sampling gas-phase ammonia have also been developed.[171]

Samples in solution are often derivatized to aid detection.[100,101,170,172,173] For example, samples in aqueous solution can be extracted with chloroform and bis-2-ethylhexylphosphate followed by reaction with isobutylchloroformate to form the isobutyloxycarbonyl amine derivatives[100]. Formation of an indophenol complex which is measured spectrometrically has been developed for NH_3,[174,175] as have various techniques involving the formation of 1-sulfonatoisoindole followed by fluorescence measurement.[176,177]

Separation and detection of ammonia and amine samples or their derivatives are performed by gas chromatography (GC)[100,101,105,169,178,179] coupled with mass spectrometry,[100] flame ionization,[167,178] high-pressure liquid chromatography (HPLC) with fluorescence[170,172] or

electrochemical detection[173] or IC with conductivity detection.[35,90,150–152,171,180,181] Derivatized amines have also be detected using UV-VIS spectrometry.[101] At higher concentrations (>ppm), gas-phase amines have been detected using metalloporphyrin foils and UV-VIS spectroscopy.[182] Other techniques exist for more exotic environments.[183] For atmospheric ammonia measurement techniques, several inter-comparison studies, in both field and laboratory settings, have been reported in the literature.[92,184–189]

An important limitation to many existing techniques for measuring ammonia and amines is deposition of the gas-phase analyte onto instrument surfaces prior to measurement, which varies with the compound.[190] Also, it has recently been shown that amines are irreversibly taken up onto surfaces that have been exposed to a gas-phase acid, forming a non-volatile salt.[191] As a variety of acids and acid precursors are present in the atmosphere, this loss may have a significant effect on measurement efficiency for instrumentation where the gas-phase sample is in contact with surfaces such as tubing prior to measurement, even when these surfaces are heated.

1.3 Amine Displacement and Particle Growth

Relative to most atmospheric species, sulfuric acid and MSA have low vapor pressures and have both been predicted to displace other acids, such as HCl, in aerosol particles.[192,193] In contrast, ammonia and amines have relatively high vapor pressures and need to be neutralized by acids to remain in the particle phase.[34] It has been shown that this neutralization of acidic particles, especially at small sizes, has large effects on further particle growth.[194] The requirement that ammonia and amines must be neutraliezd by acid to remain condensed opens the possibility for competition between ammonia and amine species for limited 'space' in the particle phase. Thus, MA, DMA and TMA have been shown to displace NH_3 in small (1-2 nm) charged clusters of ammonium sulfate and ammonium nitrate at near the

kinetic limit, however the reverse reaction (NH_3 displacement of amines) does not occur.[195] Similarly, DMA displaces ammonia in small ammonium methanesulfonate clusters.[196]

Interestingly, even in small (several molecules) clusters, displacement of ammonia by DMA is size dependent, indicating that the salt core is more difficult for incoming DMA to penetrate.[196,197] These experiments were carried out for dry, charged salt clusters. However, in the atmosphere, water vapor is always present and is likely incorporated into small acid-amine clusters. Chan and Chan[198] examined displacement of NH_3 by triethylamine (TEA) in larger (15-35 μm) particles of a variety of ammonium salts including the sulfate and bisulfate salts under different RH conditions. They found that particle phase had a dramatic effect on the extent of displacement. Dry solid salt particles allowed minimal displacement while the same salt under higher RH conditions underwent complete displacement. A similar dependence on particle phase was found for displacement of NH_3 in ammonium sulfate particles by a variety of alkyl amines as well as the complementary reaction (amine displacement by NH_3).[199] Their experiments indicate that properties of the bulk salt such as phase (amorphous *vs.* crystalline solid), deliquescence and efflorescence points are key determinants of expected displacement by gas-phase amines.

1.4 Modeling Aerosol Systems

Due to the complexity of aerosol systems, a variety of modeling approaches have been applied depending on the nature of the desired predictions and the complexity of the system under investigation.[27,30,129,200–202,202–210] To model the time evolution of aerosol systems, the general dynamic equation (GDE, eq. 1.1) is typically used, where $p(r,t)$ is the particle size distribution.[200,201]

$$\frac{d}{dt}p(r,t) = \left(\frac{\partial p(r,t)}{\partial t}\right)_{\text{nucleation}} + \left(\frac{\partial p(r,t)}{\partial t}\right)_{\text{growth}} + \left(\frac{\partial p(r,t)}{\partial t}\right)_{\text{coagulation}} + \left(\frac{\partial p(r,t)}{\partial t}\right)_{\text{wall loss}} \tag{1.1}$$

Solving the four components of the GDE and integrating over the desired reaction time yields the time-resolved aerosol size distribution, that can include particle composition. Each of the four components of the GDE are discussed below in the context of modeling particle formation from MSA, amines and water in the flow reactor experiments presented here.

1.4.1 Nucleation Schemes

Several mechanisms for particle formation have been proposed such as ion-induced nucleation,[211,212] binary and ternary homogeneous nucleation,[23,29,36,61] and activated complex theory.[15,17,18,213] In laboratory and field studies of particle formation, variations of the nucleation theorem originally proposed by Kaschiev[214] have been used to relate the observed rate of particle formation and gas-phase precursor concentration to the number of molecules in the "critical cluster," *i.e.* the cluster corresponding to a maximum on a plot of free energy *vs.* cluster size (curve 'a' in Fig. 1.1).[215–217] The typical formulation[216] of the nucleation theorem is,

$$\left[\frac{\partial W(n^*)}{\partial \mu}\right]_{V,T} = -(n^* - \bar{n}) \tag{1.2}$$

Here, $W(n^*)$ is the work in forming the critical cluster of size n^* at constant volume, V and temperature, T, which can be related to the particle formation rate J, such that $J = Ae^{\frac{-W(n^*)}{kT}}$, where k is the Boltzmann constant. The gas-phase precursor concentration can be

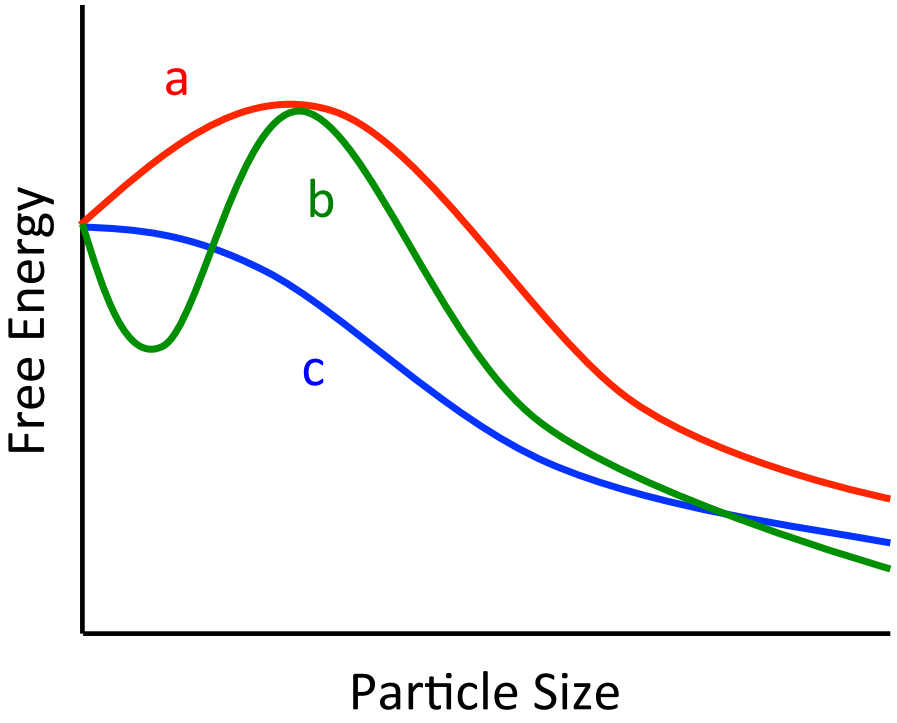

Figure 1.1: Free energy profiles for systems (a) described by the nucleation theorem, (b) with stable, pre-nucleation clusters, and (c) with barrierless nucleation

related to the chemical potential μ, and $\bar{n}$ is the number of gas-phase molecules that would occupy the same volume as the cluster, and is typically small (1–2).[218] For a single component system, a log-log plot of observed particle formation rate *vs.* precursor concentration is then able to give an indication of n^*.

The nucleation theorem has been derived using both thermodynamic[214,218] and kinetic[216] approaches, and has proven useful in interpreting laboratory and field data. However, several assumptions made in its derivation begin to lose validity for certain cases, such as non-ideal systems or those that have minima in their free energy profile prior to the critical cluster maximum,[216,219] and in multicomponent systems its application is limited to examining systems where all but one gas-phase precursor are held constant.[218,219] This makes formula-

tions of the particle formation rate J based on precursor concentrations in multicomponent systems complicated or unworkable using only the nucleation theorem.

More importantly, some atmospherically relevant systems have free energy profiles that are thought to deviate from those shown in Fig. 1.1a, for which nucleation theorem is derived. These include, for example, systems where no free energy barrier exists (Fig. 1.1c) and systems with stable, pre-nucleation clusters (Fig. 1.1b) which significantly change predictions based on the nucleation theorem.[33,219] In the latter case, cluster-cluster reactions, which are not addressed in the nucleation theorem become non-negligible and must be included.[219]

For these reasons, and to reduce computational burden, semi-empirical kinetics models for nucleation in acid-base systems have been proposed, including the one developed as part of this work.[126,149,220] These simple, semi-empirical models are based on parameterizations of the kinetics equations involved in forming key intermediate clusters and are designed to be easily implemented in regional and global models due to their minimal computational cost.

1.4.2 Particle Growth

Particle growth is the most complicated component of the GDE. In the simplest approximations, a rate of growth (*e.g.*, in nm/hr) is determined by gas-phase concentrations of condensing species. However, many factors are thought to affect growth of aerosol particles. These include: enhanced evaporation as a function of particle size due to the Kelvin effect,[7] evaporation of particle-phase species based on their activity in liquid particles,[194,221–223] particle phase effects[224] including multi-phase internally or externally mixed particles, and surface-specific effects on growth,[58] among others.

Several thermodynamic models have been developed to predict growth-related properties such as deliquescence RH and surface tension for both purely inorganic[221,225,226] or inor-

ganic/organic aerosols. Uptake of gas-phase species onto particles is often calculated at the kinetic limit, sometimes modulated by an species-specific uptake coefficient. Evaporation from particles typically requires knowledge of the activity of the particle-phase species, for which several models have been developed.[222,223,227–232] Dutcher et al.[231,232] described an activity model with an adjustable number of parameters based on variable layers of ion solvation in electrolytic solutions, which is used in this work to calculate water activity in MSA-amine-water particles. Typically, the parameters of these activity models are set by comparison with experimentally determined water activity. While the activities of water in several atmospherically relevant salt solutions have been reported over a range of concentrations and temperatures, those for MSA-amine and MSA-ammonia solutions have not. Highly accurate techniques for measurement of water activity have been developed,[233] and an experimental study of the MSA-amine and MSA-ammonia salt solutions would prove valuable for modeling aerosol systems that include these species.

1.4.3 Coagulation and Wall Losses

Long-range forces lead to an enhancement in coagulation (the collision of two particles resulting in the formation of one larger particle) over what would be expected from hard-sphere collision theory.[234,235] Thus, coagulation has been explored theoretically[236] and experimentally.[234] The enhancement due to these long range forces has been reported between 1 and 3 for sulfuric acid aerosol, but can reach higher values in other systems.[234]

Several analytical expressions have been derived to calculate particle wall losses in a variety of situations[237–239] including laminar flows in a cylinder, such as in the flow reactor used in this study.[240–243] These sometimes include the combined effects of diffusion and sedimentation,[241] although sedimentation losses are thought to be negligible over the timescales used here for the small particles observed ($<<$ 1 μm in diameter).

Chapter 2

Flow Reactor Studies

2.1 Research Goals

The goal of this study is to characterize new particle formation from MSA, amines and water. Specifically, DMA and TMA, two of the most prevalent amines in the atmosphere, are investigated to determine what, if any, enhancement to particle formation they induce over the MSA and water system. This is accomplished through laboratory experiments using a unique large-volume slow-flow aerosol flow tube reactor. The results of this study and a discussion of their importance in the atmosphere are presented in this chapter.

2.2 Experimental

2.2.1 Flow Reactor System

Laboratory studies of new particle formation from MSA, amines and water were carried out using a unique large-volume, slow-flow aerosol flow reactor (Figs. 2.1, 2.2) described in

Table 2.1: Reaction times and distances at each sampling and inlet port in the flow tube reactor for 40 L min^{-1} total flow. Inlet labels in parentheses refer to those shown in Figure 2.1a. Reaction times and distances are measured relative to addition of MSA in the downstream inlet as shown in Figure 2.1a.

Port	Distance (m)	Reaction Time (min)
peripheral inlet (RH)	-1.12	-4.5
1st spoked inlet (amine)	-1.05	-4.3
2nd spoked inlet (MSA)	0.0	0.0
sample port P0	0.02	0.07
sample port P1	1.04	4.2
sample port P2	2.26	9.2
sample port P3	3.48	14
sample port P4	4.70	19
sample port P5	5.92	24

detail elsewhere.[134] The flow reactor is designed for laminar flow and to have a low (10 m^{-1}) surface-to-volume ratio to minimize the effects of wall losses. A constant flow of clean, dry air from a purge gas generator (Parker Balston; model 75-62) was introduced along with gas-phase precursors into the initial 'mixing' section through several inlets (Fig. 2.1a). Two 'showerhead' discs[134] were used to provide additional mixing and ensure laminar flow, and are indicated by dashed lines in Figure 2.1. The total flow through the reactor was 40 L min^{-1}. Individual flows of air and precursor gases were maintained using five mass flow controllers (Alicat) labeled 'FC A'–'FC E' in Figure 2.1. Five sampling ports for particle measurements equally spaced down the length of the reactor correspond to between 4 and 24 min reaction time at 40 L min^{-1}, from the point of addition of MSA at the downstream inlet (Fig. 2.1a) and are labeled P1–P5. The distances and reaction times between inlets and sampling ports are given in Table 2.1. An additional sampling port (P0) corresponding to ∼4 s reaction time was used for gas-phase MSA sampling. Port P0 had been modified by fitting a length of 1/4" stainless steel tubing to the inside of the port, and positioning the tubing (blue line in Figure 2.1a) such that the effective reaction time from the MSA spoked-hub inlet was ∼4 s.

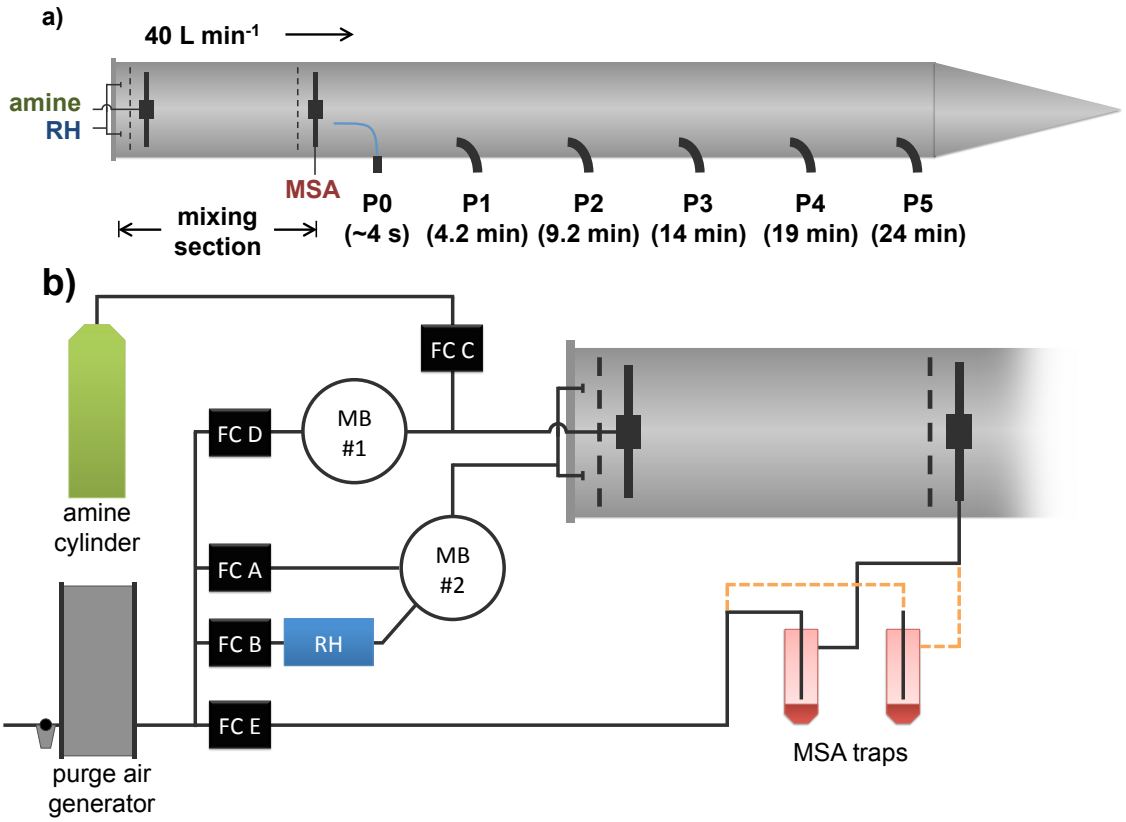

Figure 2.1: a) Schematic of the flow reactor system and b) detailed diagram of the gas-phase precursor introduction system. Black dashed lines indicate 'showerhead' discs, inlets labeled amine and MSA are spoked-hub inlets, and that labeled RH is the peripheral inlet as described in Ezell et al. 2010.[134] Sampling ports are labeled P0–P5, with their corresponding reaction times in parentheses. The blue line in (a) indicates the position of the 1/4" stainless steel tubing fitted to the inside of port P0. Circles labeled MB are 5 L glass mixing bulbs. Black boxes labeled FC are flow controllers whose letter corresponds to the flows listed in Table 2.3. Blue box marked RH is either a bubbler filled with nanopure water or a humidifer. Dashed orange lines indicate connection for two MSA traps in parallel.

2.2.2 Gas-Phase Precursor Generation

Water vapor was generated as shown in Figure 2.1b, where 3.0 – 18.5 L min^{-1} of clean dry from the purge gas generator was introduced into a mixing bulb ('MB #2' in Fig. 2.1b) along with 2.0 – 6.0 L min^{-1} of air from the purge gas generator that had been diverted through either a water bubbler filled with nanopure water or a humidifier (Perma Pure, LLC; model FC125-240-5MP). Flows of dry and humid air flowing into the mixing bulb were maintained

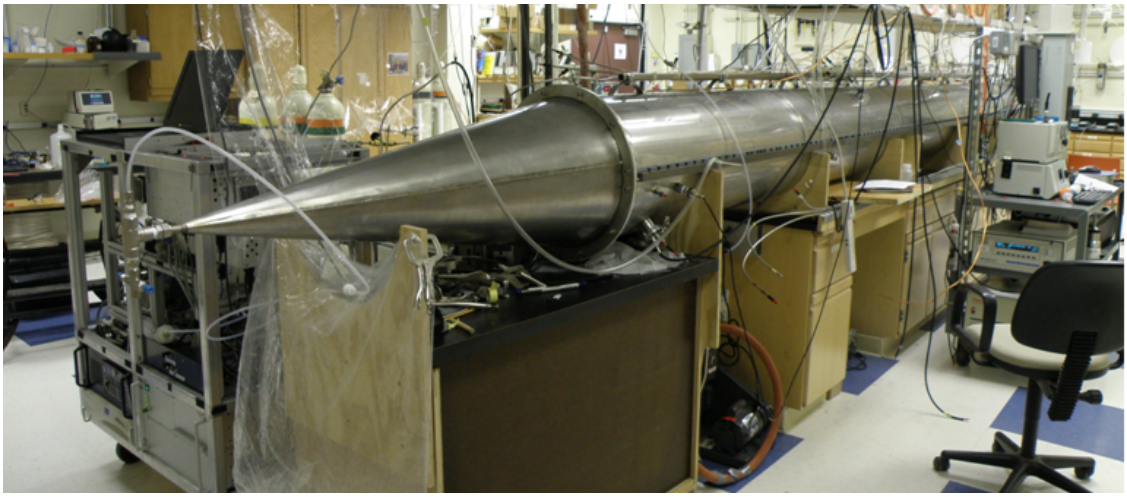

Figure 2.2: Photo of the flow reactor system.[134]

by flow controllers 'A' and 'B' (Fig. 2.1b). Water vapor concentrations were varied between 0.5 and 38.3 % RH by adjusting the fraction of air flowing through the bubbler or humidifier. In experiments performed under 'dry' conditions, no humidifer or bubbler was present, and clean dry air from the purge gas generator flowed into mixing bulb 2 from both inlets.

Clean dry air (18.0 – 20.5 L min^{-1}) from the purge gas generator was flowed through the mixing bulb labeled 'MB #1' in Figure 2.1a before being introduced into the first spoked hub inlet and was maintained using flow controller 'FC D' (Fig. 2.1b). To this flow of air, gas-phase DMA (1.0 ppm in N_2; Airgas) or TMA (13.4 ppm in N_2; Matheson) was added at 7.5 – 800 cm^3 min^{-1}. Amine concentrations in the flow tube were varied by adjusting the flow controller labeled 'FC C' in Figure 2.1b. It should be noted that these amine concentrations are based on the manufacturer stated concentrations, which may not be entirely accurate as discussed in section 3.3.1.

Gas-phase MSA was generated by passing 1.5 – 3.0 L min^{-1} of air from the purge gas generator through a glass trap containing ~10 mL liquid MSA (99%, Aldrich) before introduction into the flow reactor through the most downstream inlet, the second spoked-hub inlet, as indicated in Fig. 2.1a. MSA concentrations in the flow reactor were varied by adjusting

the flow through the glass trap using flow controller 'FC E' (Fig. 2.1b). When higher MSA concentrations were required, a second trap containing liquid MSA was connected in parallel to the first trap, as shown by the orange dashed lines in Figure 2.1b.

2.2.3 Gas-Phase Precursor and Particle Measurement

MSA concentrations in the flow tube were measured prior to introduction of amines by pumping a gas-phase sample from the flow reactor through a Durapore filter (25 mm x 0.45 μm; Millex HV) for 30 min at 1 L min^{-1}. Samples were taken from sampling ports P0 and P1. Samples were also taken directly from the outlet of the trap(s) containing MSA. Filters were then extracted in Nanopure water (Thermo Scientific; model 7146) and analyzed by UPLC-ESI-MS. Water vapor concentrations in the flow tube were measured using a RH probe (Vaisala; model HMP238) positioned in the flow reactor at a distance corresponding to a reaction time of 4.3 min after the introduction of MSA.

As discussed in the introduction, methods for measuring gas-phase amines are complicated by the rapid uptake of the analyte onto instrument surfaces, such as inlet tubing. A method for measuring gas-phase amines that minimizes wall loss effects was developed and is discussed below. However, for the results from the flow reactor experiments presented here, the amine concentrations were calculated based on the manufacturer labeled concentrations in the gas-cylinders and the known dilution in air from the purge gas generator. A summary of the experimental conditions explored are presented in Table 2.2.

Particle measurements were made using a SMPS, composed of a classifier (TSI; model 3080), a differential mobility analyzer (TSI; model 3081), and an ultra-fine CPC (TSI; model 3776). For all sets of experimental conditions, particle measurements were performed at sampling port P1 (Fig. 2.1a). For some sets of conditions, particle measurements were also taken at sampling ports P2–P5.

Table 2.2: Experimental conditions for flow tube experiments exploring particle formation from MSA, amines and water.

[MSA] (ppb)	Amine	[Amine] (ppb)	RH (%)
10	TMA	2.5	0.5
34	TMA	2.5	3.2, 8.4, 19.1, 29.3
5.3	TMA	7.3	0.5, 3.5, 8.7, 19.5
2.7	TMA	7.3	0.5, 3.7, 8.9, 20
6.2	TMA	2.5	0.5, 3.6, 8.8, 20
3.4	DMA	2.5	0.5
1.7	DMA	7.5	0.4, 3.0, 8.1, 18.4, 28.4
8.8	DMA	2.5	8.4, 19.3, 28.6
6.5	DMA	2.5	2.9, 7.8, 18.2, 27.9
2.1	DMA	2.5	3.0, 7.8, 12.8, 18.1, 27.7, 34.9
8.5	DMA	2.5	7.8, 11.6, 21.4
8.5	DMA	2.5, 5.0, 7.5, 10	7.5
8.5	DMA	20	7.8

2.3 Results and Discussion

Experimental conditions including calculated amine concentrations and measured MSA and water vapor concentrations are given in Table 2.2. These are included in Table 2.3 along with the flow rates, measured total particle concentrations and geometric mean diameters (GMD) at 4.2 min reaction time for each set of experimental conditions. The measured RH in experiments performed without a water bubbler or humidifier (*i.e.* under 'dry' conditions) was consistently 0.5% (Table 2.3). The RH probes used have a manufacturer stated accuracy of ±1% at 0–90% RH, which means 0% RH is within the uncertainty for experiments performed without added water vapor, however some water vapor likely makes it through the driers on the purge gas generator and is present in the flow tube under 'dry' conditions. The presence of water in 'dry' experiments will be discussed in more detail in section 2.3.4.

Size distributions at 4.2, 9.2, 14, 19 and 24 min reaction time were measured for each set of conditions for TMA experiments and for many of the DMA experiments. The total particle concentrations and GMD at each reaction time for these experiments are given in Table 2.4.

Table 2.3: Experimental conditions and measured particle concentrations at 4.2 min reaction time for flow tube experiments exploring particle formation from MSA, amines and water.

Flow Rates					Pre-cursor Concentrations				Measured	Measured
FC A (L min^{-1})	FC B (L min^{-1})	FC C (L min^{-1})	FC D (L min^{-1})	FC E (L min^{-1})	Amine	[Amine] (ppb)	[MSA] (ppb)	RH (%)	Particle Conc. (# cm^{-3})	GMD (nm)
5.00	14.00[a]	0.00	18.00	3.00[b]	none	0.0	8.5	0.5	23.8	69.5
15.00	4.00[c]	0.00	18.00	3.00[b]	none	0.0	8.5	8.5	681	14.2
11.00	8.00[c]	0.00	18.00	3.00[b]	none	0.0	8.5	15.6	1.98e3	18.0
7.00	12.00[c]	0.00	18.00	3.00[b]	none	0.0	8.5	23.3	7.14e3	23.0
17.00	2.00[c]	0.00	18.00	3.00[b]	none	0.0	8.5	3.4	1.11	135.8
16.90	2.00[c]	0.10	18.00	3.00[b]	DMA	2.5	8.5	3.5	1.40	57.3
14.90	4.00[c]	0.10	18.00	3.00[b]	DMA	2.5	8.5	7.8	4.85e3	19.2
12.90	6.00[c]	0.10	18.00	3.00[b]	DMA	2.5	8.5	11.6	1.05e5	19.8
6.90	12.00[c]	0.10	18.00	3.00[b]	DMA	2.5	8.5	21.4	1.90e5	20.2
14.80	4.00[c]	0.20	18.00	3.00[b]	DMA	5.0	8.5	7.5	4.48e5	20.4
14.70	4.00[c]	0.30	18.00	3.00[b]	DMA	7.5	8.5	7.5	4.46e5	23.5
14.60	4.00[c]	0.40	18.00	3.00[b]	DMA	10.0	8.5	7.5	7.06e5	26.1

[a]No bubbler or humidifier present.

[b]Two MSA traps in parallel.

[c]Water bubbler.

[d]Humidifier.

[e]One MSA trap.

[f]Particle measurements taken at multiple reaction times. See Table 2.4

Table 2.3: (continued)

Flow Rates					Pre-cursor Concentrations				Measured	Measured
FC A (L min^{-1})	FC B (L min^{-1})	FC C (L min^{-1})	FC D (L min^{-1})	FC E (L min^{-1})	Amine	[Amine] (ppb)	[MSA] (ppb)	RH (%)	Particle Conc. (# cm^{-3})	GMD (nm)
14.20	4.00[c]	0.80	18.00	3.00[b]	DMA	20.0	8.5	7.5	8.10e5	33.1
15.00	4.00[a]	0.00	18.00	3.00[b]	none	0.0	8.1	0.5	0.0	–
17.00	2.00[c]	0.00	18.00	3.00[b]	none	0.0	8.1	3.3	0.0	–
15.00	4.00[c]	0.00	18.00	3.00[b]	none	0.0	8.1	7.7	20.5	19.2
13.00	6.00[c]	0.00	18.00	3.00[b]	none	0.0	8.1	11.5	460	17.6
11.00	8.00[c]	0.00	18.00	3.00[b]	none	0.0	8.1	14.9	5.66e3	20.7
9.00	10.00[c]	0.00	18.00	3.00[b]	none	0.0	8.1	17.4	1.34e4	28.0
9.00	10.00[d]	0.00	18.00	3.00[b]	none	0.0	8.1	23.5	7.06e4	22.8
7.00	12.00[d]	0.00	18.00	3.00[b]	none	0.0	8.1	29.0	1.73e5	24.7
3.00	16.00[d]	0.00	18.00	3.00[b]	none	0.0	8.1	38.3	3.43e5	30.8
16.00	4.50[a]	0.00	18.00	1.50[e]	none	0.0	1.8	0.5	5.3	224.7
18.50	2.00[d]	0.00	18.00	1.50[e]	none	0.0	1.8	3.1	2.4	209.7
16.50	4.00[d]	0.00	18.00	1.50[e]	none	0.0	1.8	8.1	1.2	224.2

[a]No bubbler or humidifier present.

[b]Two MSA traps in parallel.

[c]Water bubbler.

[d]Humidifier.

[e]One MSA trap.

[f]Particle measurements taken at multiple reaction times. See Table 2.4

Table 2.3: (continued)

Flow Rates					Pre-cursor Concentrations				Measured	Measured
FC A (L min^{-1})	FC B (L min^{-1})	FC C (L min^{-1})	FC D (L min^{-1})	FC E (L min^{-1})	Amine	[Amine] (ppb)	[MSA] (ppb)	RH (%)	Particle Conc. (# cm^{-3})	GMD (nm)
14.50	6.00[d]	0.00	18.00	1.50[e]	none	0.0	1.8	13.6	686	17.9
12.50	8.00[d]	0.00	18.00	1.50[e]	none	0.0	1.8	19.0	5.85e3	23.5
10.50	10.00[d]	0.00	18.00	1.50[e]	none	0.0	1.8	23.8	1.55e4	29.9
8.50	12.00[d]	0.00	18.00	1.50[e]	none	0.0	1.8	28.3	2.06e4	31.6
4.50	16.00[d]	0.00	18.00	1.50[e]	none	0.0	1.8	36.2	4.03e4	31.6
18.50	2.00[d]	0.046	18.00	1.50[e]	DMA	1.2	2.1	2.8	13.9	40.6
16.50	4.00[d]	0.046	18.00	1.50[e]	DMA	1.2	2.1	7.8	30.3	114.0
14.50	6.00[d]	0.046	18.00	1.50[e]	DMA	1.2	2.1	12.8	355	19.2
14.50	6.00[d]	0.10	18.00	1.50[e]	DMA	2.5	2.1	12.8	1.29e5	18.7
16.50	4.00[d]	0.10	18.00	1.50[e]	DMA	2.5	2.1	7.8	8.69e4	19.2
18.50	2.00[d]	0.10	18.00	1.50[e]	DMA	2.5	2.1	3.0	7.57e3	21.5
12.50	8.00[d]	0.10	18.00	1.50[e]	DMA	2.5	2.1	18.1	2.71e5	19.9
8.50	12.00[d]	0.10	18.00	1.50[e]	DMA	2.5	2.1	27.7	5.07e5	20.9

[a]No bubbler or humidifier present.

[b]Two MSA traps in parallel.

[c]Water bubbler.

[d]Humidifier.

[e]One MSA trap.

[f]Particle measurements taken at multiple reaction times. See Table 2.4

Table 2.3: (continued)

Flow Rates					Pre-cursor Concentrations				Measured	Measured
FC A (L min^{-1})	FC B (L min^{-1})	FC C (L min^{-1})	FC D (L min^{-1})	FC E (L min^{-1})	Amine	[Amine] (ppb)	[MSA] (ppb)	RH (%)	Particle Conc. (# cm^{-3})	GMD (nm)
4.50	16.00[d]	0.10	18.00	1.50[e]	DMA	2.5	2.1	34.9	5.58e5[f]	21.6[f]
18.50	2.00[d]	0.10	18.00	1.50[e]	DMA	2.5	6.5	2.9	6.73e3[f]	25.1[f]
16.50	4.00[d]	0.10	18.00	1.50[e]	DMA	2.5	6.5	7.8	1.51e5[f]	21.5[f]
16.50	4.00[d]	0.10	18.00	1.50[e]	DMA	2.5	6.5	7.8	2.12e5[f]	23.7[f]
12.50	8.00[d]	0.10	18.00	1.50[e]	DMA	2.5	6.5	18.2	4.12e5[f]	21.7[f]
8.50	12.00[d]	0.10	18.00	1.50[e]	DMA	2.5	6.5	27.8	7.13e5[f]	20.6[f]
15.00	4.00[d]	0.10	18.00	3.00[b]	DMA	2.5	8.8	8.4	1.36e6[f]	17.1[f]
11.00	8.00[d]	0.10	18.00	3.00[b]	DMA	2.5	8.8	19.3	6.32e5[f]	20.5[f]
7.00	12.00[d]	0.10	18.00	3.00[b]	DMA	2.5	8.8	28.6	9.18e5[f]	21.9[f]
17.50	2.00[d]	0.30	18.00	1.50[e]	DMA	7.5	1.7	3.1	4.91e5[f]	43.0[f]
15.50	4.00[d]	0.30	18.00	1.50[e]	DMA	7.5	1.7	8.1	2.75e5[f]	27.7[f]
11.50	8.00[d]	0.30	18.00	1.50[e]	DMA	7.5	1.7	18.4	5.93e5[f]	19.6[f]
7.50	12.00[d]	0.30	18.00	1.50[e]	DMA	7.5	1.7	28.4	5.40e5[f]	17.5[f]

[a]No bubbler or humidifier present.

[b]Two MSA traps in parallel.

[c]Water bubbler.

[d]Humidifier.

[e]One MSA trap.

[f]Particle measurements taken at multiple reaction times. See Table 2.4

Table 2.3: (continued)

Flow Rates					Pre-cursor Concentrations				Measured	Measured
FC A (L min^{-1})	FC B (L min^{-1})	FC C (L min^{-1})	FC D (L min^{-1})	FC E (L min^{-1})	Amine	[Amine] (ppb)	[MSA] (ppb)	RH (%)	Particle Conc. (# cm^{-3})	GMD (nm)
12.00	6.00[a]	0.0075	19.00	3.00[b]	TMA	2.5	33.5	0.5	1.84e3[f]	61.5[f]
16.00	2.00[d]	0.0075	19.00	3.00[b]	TMA	2.5	33.5	3.2	5.10e5[f]	31.2[f]
14.00	4.00[d]	0.0075	19.00	3.00[b]	TMA	2.5	33.5	8.1	9.84e5[f]	25.2[f]
10.00	8.00[d]	0.0075	19.00	3.00[b]	TMA	2.5	33.5	19.2	1.69e6[f]	22.7[f]
6.00	12.00[d]	0.0075	19.00	3.00[b]	TMA	2.5	33.5	29.8	1.60e6[f]	22.3[f]
12.00	6.00[a]	0.0218	19.00	3.00[b]	TMA	7.3	5.3	0.5	6.65e5[f]	31.5[f]
16.00	2.00[d]	0.0218	19.00	3.00[b]	TMA	7.3	5.3	3.4	1.19e6[f]	25.6[f]
14.00	4.00[d]	0.0218	19.00	3.00[b]	TMA	7.3	5.3	8.6	1.25e6[f]	24.6[f]
10.00	8.00[d]	0.0218	19.00	3.00[b]	TMA	7.3	5.3	19.6	1.27e6[f]	23.7[f]
10.00	8.00[a]	0.0218	20.50	1.50[b]	TMA	7.3	2.7	0.5	2.70e5[f]	37.2[f]
16.00	2.00[d]	0.0218	20.50	1.50[b]	TMA	7.3	2.7	3.7	5.34e5[f]	24.3[f]
14.00	4.00[d]	0.0218	20.50	1.50[b]	TMA	7.3	2.7	8.9	4.79e5[f]	22.9[f]
10.00	8.00[d]	0.0218	20.50	1.50[b]	TMA	7.3	2.7	20.1	4.42e5[f]	21.5[f]

[a]No bubbler or humidifier present.

[b]Two MSA traps in parallel.

[c]Water bubbler.

[d]Humidifier.

[e]One MSA trap.

[f]Particle measurements taken at multiple reaction times. See Table 2.4

Table 2.3: (continued)

Flow Rates					Pre-cursor Concentrations				Measured	Measured
FC A (L min^{-1})	FC B (L min^{-1})	FC C (L min^{-1})	FC D (L min^{-1})	FC E (L min^{-1})	Amine	[Amine] (ppb)	[MSA] (ppb)	RH (%)	Particle Conc. (# cm^{-3})	GMD (nm)
10.00	8.00[d]	0.0075	20.50	1.50[b]	TMA	2.5	6.2	0.5	2.35e3[f]	59.7[f]
16.00	2.00[d]	0.0075	20.50	1.50[b]	TMA	2.5	6.2	3.6	1.31e5[f]	37.9[f]
14.00	4.00[d]	0.0075	20.50	1.50[b]	TMA	2.5	6.2	8.8	2.56e5[f]	30.6[f]
10.00	8.00[d]	0.0075	20.50	1.50[b]	TMA	2.5	6.2	20.1	4.73e5[f]	22.6[f]
10.00	8.00[a]	0.0075	19.00	3.00[b]	TMA	2.5	4.1	0.5	1.00e4[f]	56.1[f]

[a]No bubbler or humidifier present.

[b]Two MSA traps in parallel.

[c]Water bubbler.

[d]Humidifier.

[e]One MSA trap.

[f]Particle measurements taken at multiple reaction times. See Table 2.4

Table 2.4: Gas-phase precursor concentrations and measured particle concentrations at 4.2, 9.2, 14, 19 and 24 min reaction time for flow tube experiments exploring particle formation from MSA, amines and water.

Pre-cursor Concentrations				Measured Particle Concentration (# cm^{-3})					Geometric Mean Diameter (nm)				
Amine	[Amine] (ppb)	[MSA] (ppb)	RH (%)	Port 1	Port 2	Port 3	Port 4	Port 5	Port 1	Port 2	Port 3	Port 4	Port 5
DMA	2.5	2.1	34.9	5.58e5	2.52e5	2.55e5	2.00e5	1.80e5	21.6	27.5	27.8	29.8	30.6
DMA	2.5	6.5	2.9	6.73e3	2.07e4	n/a	n/a	n/a	25.1	32.3	n/a	n/a	n/a
DMA	2.5	6.5	7.8	1.51e5	8.21e4	8.76e4	8.29e4	8.04e4	21.5	28.1	28.3	28.8	28.8
DMA	2.5	6.5	7.8	2.12e5	1.01e5	9.55e4	1.06e5	1.04e5	23.7	28.0	28.2	28.3	28.6
DMA	2.5	6.5	18.2	4.12e5	2.06e5	2.30e5	1.93e5	1.70e5	21.7	26.7	25.7	27.1	27.6
DMA	2.5	6.5	27.8	7.13e5	2.89e5	3.35e5	2.54e5	2.24e5	20.6	27.8	26.8	29.5	30.2
DMA	2.5	8.8	8.4	1.36e6	3.32e5	3.94e5	2.76e5	2.57e5	17.1	23.0	22.3	24.7	25.3
DMA	2.5	8.8	19.3	6.32e5	3.80e5	4.70e5	3.73e5	2.98e5	20.5	24.9	23.6	25.5	27.6
DMA	2.5	8.8	28.6	9.18e5	4.27e5	4.93e5	4.04e5	3.30e5	21.9	27.6	26.0	28.1	30.5
DMA	7.5	1.7	3.1	4.91e4	5.84e4	8.50e4	5.77e4	n/a	43.0	56.9	58.3	57.2	n/a
DMA	7.5	1.7	8.1	2.75e5	2.23e5	2.48e5	n/a	n/a	27.7	39.3	39.7	n/a	n/a
DMA	7.5	1.7	18.4	5.93e5	3.40e5	4.09e5	n/a	n/a	19.6	33.0	31.8	n/a	n/a
DMA	7.5	1.7	28.4	5.40e5	3.60e5	4.16e5	n/a	n/a	17.5	29.8	28.9	n/a	n/a
TMA	2.5	33.5	0.5	1.84e3	2.17e3	2.22e3	2.28e3	2.32e3	61.5	66.0	73.5	71.3	70.1
TMA	2.5	33.5	3.2	5.10e5	2.80e5	3.14e5	2.52e5	2.47e5	31.2	33.4	33.5	35.9	36.1
TMA	2.5	33.5	8.1	9.84e5	4.16e5	4.71e5	3.84e5	3.76e5	25.2	33.5	32.5	35.2	35.4
TMA	2.5	33.5	24.6	1.69e6	5.19e5	5.65e5	4.53e5	4.38e5	22.7	35.5	34.5	37.0	37.3
TMA	2.5	33.5	29.8	1.60e6	5.40e5	6.56e5	4.27e5	4.14e5	22.3	38.2	35.9	41.9	42.0
TMA	7.3	5.3	0.5	6.65e5	5.71e5	4.53e5	3.63e5	3.46e5	31.5	34.6	38.8	40.5	41.3

Table 2.4: (continued)

Pre-cursor Concentrations				Measured Particle Concentration (# cm^{-3})					Geometric Mean Diameter (nm)				
Amine	[Amine] (ppb)	[MSA] (ppb)	RH (%)	Port 1	Port 2	Port 3	Port 4	Port 5	Port 1	Port 2	Port 3	Port 4	Port 5
TMA	7.3	5.3	3.4	1.19e6	5.24e5	6.03e5	4.72e5	4.58e5	25.6	38.9	37.3	40.0	40.3
TMA	7.3	5.3	8.6	1.25e6	5.52e5	6.33e5	4.87e5	4.84e5	24.6	39.2	37.9	41.3	41.4
TMA	7.3	5.3	19.6	1.27e6	5.59e5	6.28e5	4.80e5	4.64e5	23.7	41.6	39.9	43.7	44.0
TMA	7.3	2.7	0.5	2.70e5	2.56e5	2.79e5	2.44e5	2.44e5	37.2	43.4	43.5	44.7	44.7
TMA	7.3	2.7	3.7	5.34e5	3.59e5	3.99e5	3.17e5	3.04e5	24.3	37.2	36.4	38.4	38.8
TMA	7.3	2.7	8.9	4.79e5	3.67e5	3.96e5	3.00e5	2.85e5	22.9	35.1	34.6	38.0	38.5
TMA	7.3	2.7	20.1	4.42e5	3.68e5	3.94e5	3.08e5	2.92e5	21.5	34.1	33.9	37.3	37.3
TMA	2.5	6.2	0.5	2.35e3	2.72e3	2.66e3	2.23e3	1.96e3	59.7	59.8	60.9	58.1	57.2
TMA	2.5	6.2	3.6	1.31e5	1.20e5	1.19e5	1.04e5	9.93e4	37.9	43.0	43.1	42.7	42.3
TMA	2.5	6.2	8.8	2.56e5	2.20e5	2.35e5	1.89e5	1.83e5	30.6	38.1	37.3	39.2	39.0
TMA	2.5	6.2	20.1	4.73e5	2.87e5	3.13e5	2.42e5	2.34e5	22.6	34.6	33.1	36.0	36.2
TMA	2.5	4.1	0.5	1.00e4	6.97e3	6.49e3	5.96e3	5.64e3	56.1	67.7	66.8	60.7	60.2

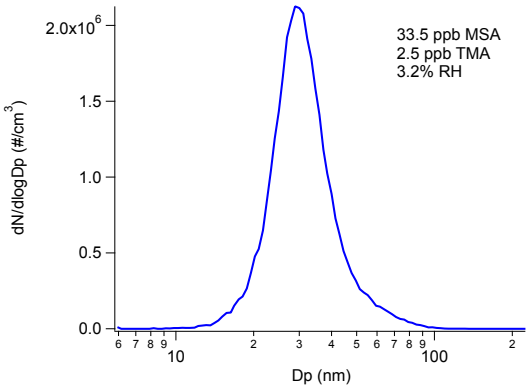

Figure 2.3: A typical particle size distribution measured at 4.2 min reaction time.

A typical particle size distribution measured at 4.2 min reaction time is shown in Figure 2.3. The CPC used in these experiments has a manufacturer stated cutoff at 2.5 nm but, the DMA and sheath and sample flows used result in a minimum detectable particle diameter of 5.8 nm. As can be seen in Figure 2.3, the size distributions measured are well above this lower limit, indicating that the majority of particles were being measured. It should be noted however that a bimodal distribution with a large number of small particles below the detection limit would not be measured under these conditions.

The majority of particle formation occurred prior to the first measured reaction time under all sets of experimental conditions. Some general observations about particle formation from this system can be made by comparison of the particle number concentrations measured at 4.2 min under different sets of experimental conditions. However, this requires that loss of gas- and particle-phase species to the walls and the decrease in particle number concentration due to coagulation between particles have negligible effects on the particle size distributions measured at 4.2 min compared to the effects of particle formation. This is found to be the case, as described in section 2.3.4. A rough approximation of particle formation rates can then be made based on measured particle concentrations at 4.2 min. These can be compared to previous work and used to make some general observations about this system, as described

in sections 2.3.1 and 2.3.2. A more rigorous approach to describing particle formation in this system is described in section 2.3.4.

2.3.1 MSA and Water

Seinfeld, Kreidenweis, Wyslouzil and coworkers studied particle formation from MSA and water, and found it to be considerably lower than that from sulfuric acid and water.[21,61,135] Their experiments were performed with higher initial gas-phase acid concentrations, but a comparison can be made to the results presented here. Figure 2.4a presents the particle size distribution reported by Wyslouzil et al. for [MSA] = 224 ppb and RH = 46 % at 18 s reaction time (blue trace) compared to that reported here for [MSA] = 8.5 and RH = 15.6 % at 4.2 min reaction time (red trace). Interestingly, the peak at lower particle diameter in the bimodal distribution from Wyslouzil et al. lines up with the trailing edge of the distribution reported here. In the time since their work, CPC detection limits have been lowered from tens of nm (for the TSI model 3760 CPC)[244] to only several nm (for the TSI model 3776 CPC used in this work)[245] and lower.[121,245] If a large number of small particles were present, it is likely that they would not be detected using the older CPC technology.

Figure 2.4b presents the calculated particle formation rates from Wyslouzil et al.[29] for sulfuric acid (blue triangles) and MSA (blue squares). Their results indicate that several orders of magnitude higher MSA concentrations are required to form particles at the same rate as an equivalent concentration of sulfuric acid. However, if small MSA+water particles were present but unaccounted for, these particle formation rates for MSA and water may be an underestimate. Taking results from this work for MSA under similar RH conditions (15%), a rough estimate of particle formation rates can be made by dividing the measured particle concentration at 4.2 min (252 s) reaction time by 252 s (red diamonds). This gives a particle formation rate in # cm^{-3} s^{-1}, which can be compared to the values obtained by Wyslouzil et

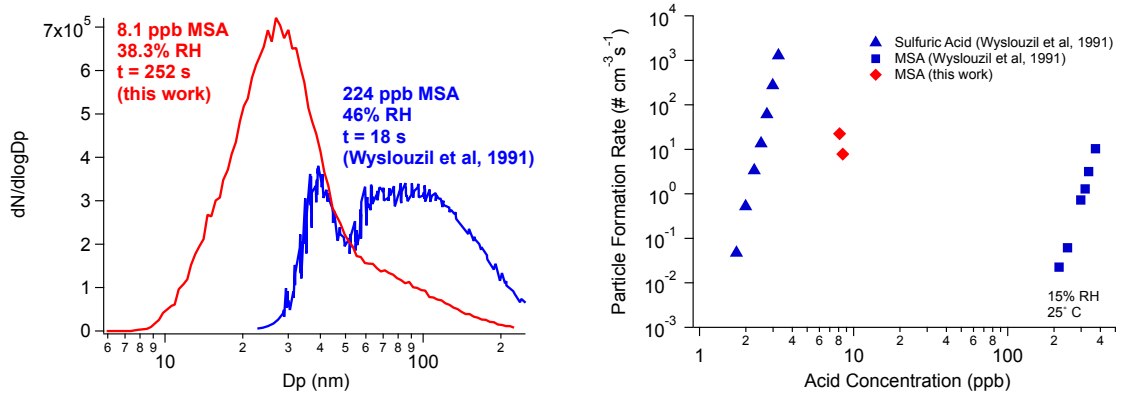

Figure 2.4: A comparison of a) typical size distributions and b) particle formation rates from MSA or sulfuric acid at 15% RH from this work (red) and Kreidenweis et al.[135] and Wyslouzil et al.[29,61] (blue). Data points in b) were calculated from particle formation rates and relative acidities reported by Wyslouzil et al.[29,61] along with vapor pressures (VP): $VP_{SA} = 1.3 \times 10^{-8}$ atm[246] and $VP_{MSA} = 7.4 \times 10^{-7}$ atm.[247]

al.[29]. These estimates suggest that the rate of particle formation from MSA and water may be more comparable to that of sulfuric acid and water than previously thought (Fig. 2.4b).

According to nucleation theory, the slope of a log-log plot of particle formation rate vs. precursor concentration is approximately equal to the number of precursor molecules in the 'critical cluster.' As discussed in section 1.4.1, many systems, such as those of more than two components or no free energy barrier to particle formation, are difficult to interpret in this manner. But, the simple two component MSA-water system may lend itself to this type of analysis. Figure 2.5 shows such a plot for experiments involving only MSA and water. Interpretation of the slope of the least-squares fit line using nucleation theory suggests that there are about 5 molecules of water in the critical cluster under these conditions ([MSA] = 1.8, 8.1 or 8.5 ppb). As this was not the primary system of interest of this work, insufficient data at constant RH conditions and varying [MSA] exist for a similar evaluation of the number of MSA molecules in the 'critical cluster.' A further exploration of the MSA-water system may be warranted given these results.

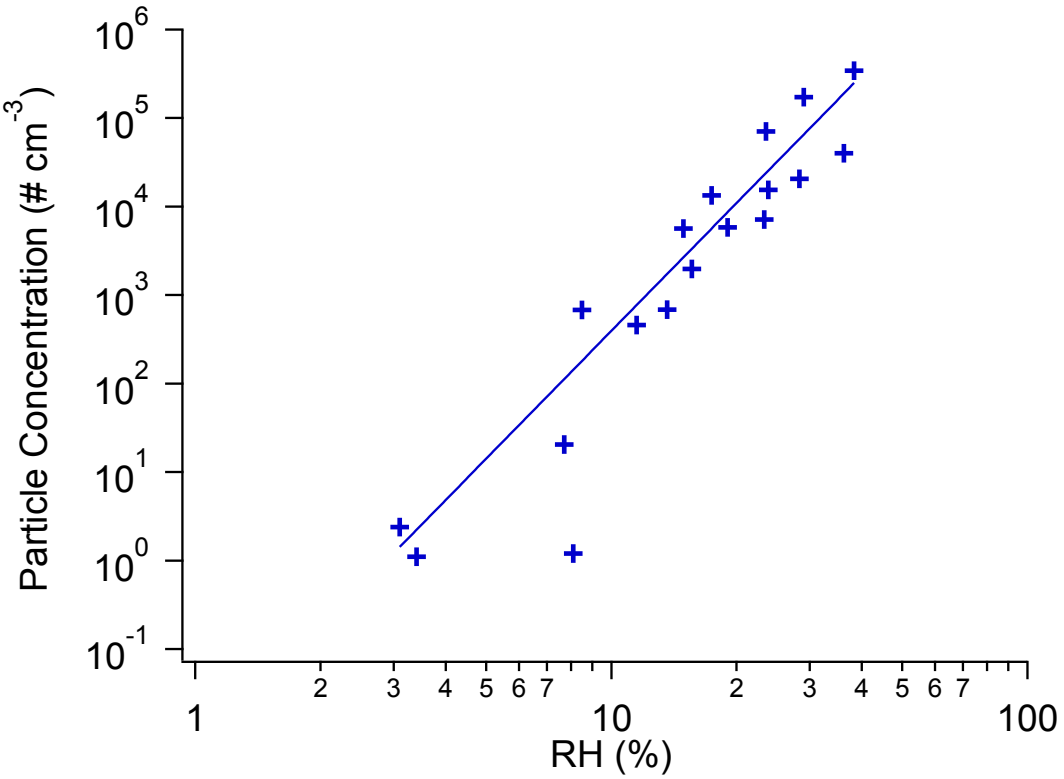

Figure 2.5: Log-log plot of particle concentration at 4.2 min reaction time for experiments involving only MSA and water. Included are data from experiments where the initial [MSA] = 1.8, 8.1 or 8.5 ppb. Points with zero measured particles and those performed without added water vapor have been excluded. A least squares fit (blue line) to the data has a slope $= 4.8 \pm 1.7(1s)$ and intercept $= -2.2 \pm 2.7(1s)$.

2.3.2 Enhancement of Particle Formation from Amines

Particle concentrations measured at 4.2 min reaction time are presented in Figure 2.6 as a function of precursor concentrations. Several general observations may be made about these results. First, a significant enhancement (several orders of magnitude) in particle concentration is observed upon addition of amine to the MSA/water system. These results are similar to those reported for amine enhancement in the sulfuric acid/water system.[41] Second, water is observed to be necessary for significant particle formation. Under dry conditions, particle concentrations for the MSA/amine system are comparable to those of MSA and water alone, and several orders of magnitude lower than when all three species are

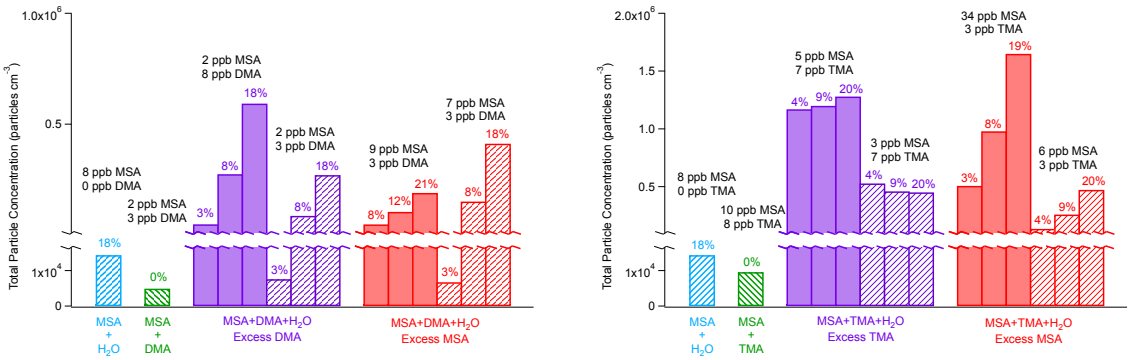

Figure 2.6: Total particle concentrations measured at 4.2 min reaction time for a variety of initial gas-phase concentrations and experiments with MSA, water and a) DMA or b) TMA. Numbers shown above histogram bars are percent RH.

present. Finally, in the TMA system, when excess amine is present, little if any dependence of measured particle concentration on initial water concentration is observed, although water is necessary. In contrast, the DMA system shows a strong water dependence in both the excess amine and excess MSA cases.

2.3.3 Computational Results

To aid in identification of the underlying physical processes involved in forming particles in the MSA/amine/water system, theoretical calculations were made on the structure and energies of formation of several small clusters of these species. This work was performed by Dr. Mychel Varner of the Gerber group at UCI and is presented in Figures 2.7, 2.8 and 2.9. In contrast to MSA-water complexes, which are predicted to require three[148] or four[248] water molecules for proton transfer, or MSA-NH_3-water which requires two water molecules,[249] the most energetically favorable structures of MSA-DMA and MSA-TMA clusters (Fig. 2.7) are those which have undergone proton transfer, even in the absence of water. The experimental observation of the necessity of water vapor for significant particle formation cannot then be explained simply by the need for water in order to form a stable, ionic cluster.

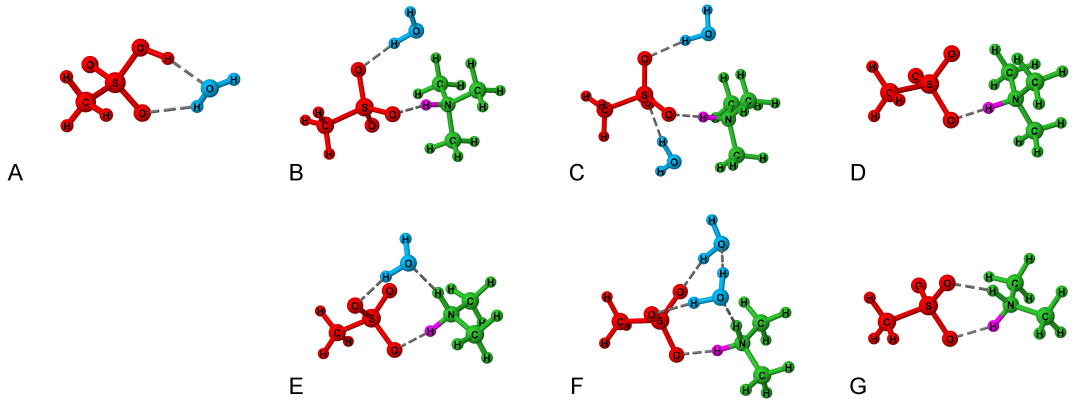

Figure 2.7: Calculated structures for A) MSA-H_2O, B) MSA-TMA-H_2O, C) MSA-TMA-$2H_2O$, D) MSA-TMA, E) MSA-DMA-H_2O, E) MSA-DMA-$2H_2O$ and F) MSA-DMA. MSA is shown in red, amines in green and transferred protons in pink. (Calculated by Dr. Mychel Varner of the Gerber Group, UCI)[149]

Based on the experimental observations and theoretical calculations, an attempt was made to identify clusters that act as key intermediates in the formation of particles. Clusters were evaluated based on energetic stability and structural elements. These include whether a cluster has accessible hydrogen-bond acceptor or donor sites available that could provide a site for the addition of incoming gas-phase species. For example, two MSA and two amine molecules form a very stable tetramer ($(MSA)_2-(DMA)_2$ ΔG=-64 kcal mol^{-1}; $(MSA)_2-(TMA)_2$ ΔG=-50 kcal mol^{-1}, relative to the gas-phase species). However, the closed ring structure (Fig. 2.8) does not present accessible donor or acceptor sites to which incoming gas-phase species could hydrogen bond, and would not then be expected to play a key role in particle formation, but may result in a pool of unreactive clusters.

Using the theoretical calculations and experimental data, the following pathway to particle formation is proposed. Particle formation begins with the formation of the MSA-water complex. Both MSA and methylamines are present as hydrates in the atmosphere,[29,61,135,147,250] but MSA-water complexes are more energetically favorable than are those of MSA-amines (Fig. 2.9)[144,148,251] and so were chosen as the starting complex in this scheme. From there, addition of an amime yields a stable trimer for both the DMA and TMA systems (Fig. 2.9).

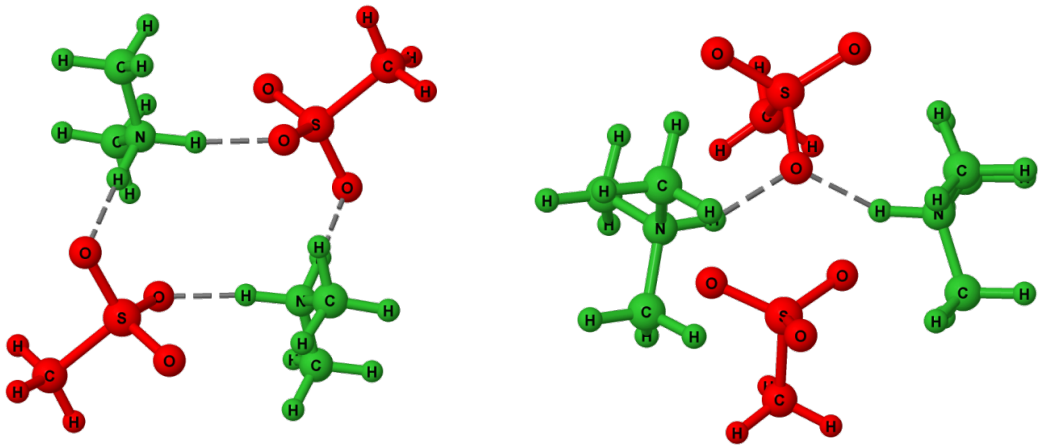

Figure 2.8: Calculated structures of a) $(MSA)_2-(DMA)_2$ and b) $(MSA)_2-(TMA)_2$ showing the closed ring formation. (Calculated by Dr. Mychel Varner of the Gerber Group, UCI)

Further addition of MSA, amine or water to the trimer results in a still-more stable tetramer. Besides the addition reactions, loss of water from the MSA-amine-water trimer is accessible, though not favorable. From the dry MSA-amine cluster, addition of MSA or amine forms a lower energy trimer, while addition of water reforms the MSA-amine-water trimer.

2.3.4 Kinetics Mechanism

A simplified, semi-empirical mechanism for particle formation from this system was developed based on the pathway described above and is shown in Figure 2.10. Reaction to form the MSA hydrate and MSA-amine-H_2O trimer from either the MSA hydrate or MSA-amine dimer are assumed to be collision limited. The second-order rate constants for these reactions are calculated according to equation 2.1,[7]

$$k_f = \pi \left(r_i + r_j\right)^2 \sqrt{\frac{8k_B T}{\pi \mu}} \tag{2.1}$$

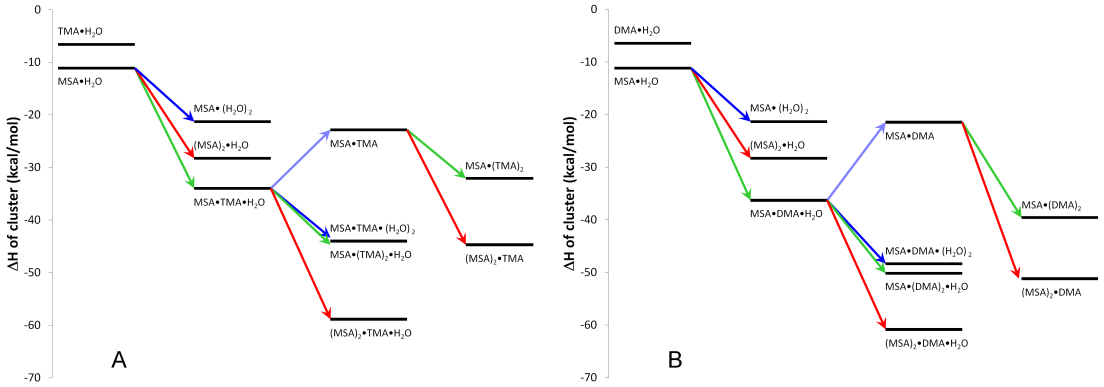

Figure 2.9: Enthalpies of formation for clusters of A) MSA, TMA and H_2O and B) MSA, DMA and H_2O. Arrows indicate addition of MSA (red), amine (green) and water (blue). (Calculated by Dr. Mychel Varner of the Gerber Group, UCI) [149]

where μ is the reduced mass of these species, k_B is the Boltzmann constant and T is temperature. The hard sphere collision radii of the reacting species, r_i and r_j, are estimated as the largest interatomic distance in gas-phase molecules and clusters shown in Figure 2.7. While these are only approximations, results from kinetics based particle formation mechanisms have been shown to not depend significantly on hard sphere collision radii approximations. [143] The forward and reverse rate constants based on unitless partial pressures ($k_f^{'}$ and $k_r^{'}$, respectively) are related by the theoretical energies of formation, ΔE, and are calculated according to equation 2.2. [7]

$$k_r^{'} = k_f^{'} e^{\left(\frac{\Delta E}{k_B T}\right)} \tag{2.2}$$

Addition of MSA, amine or water to either the MSA-amine-H_2O trimer or MSA-amine dimer could also be assumed to be collision limited. However, to reduce the complexity and computational cost of the mechanism, these reactions (k_4–k_8) are parameterized based on the experimental results under the assumption that the dependence of particle formation on gas-phase precursor concentrations can be captured without the inclusion of further intermediates

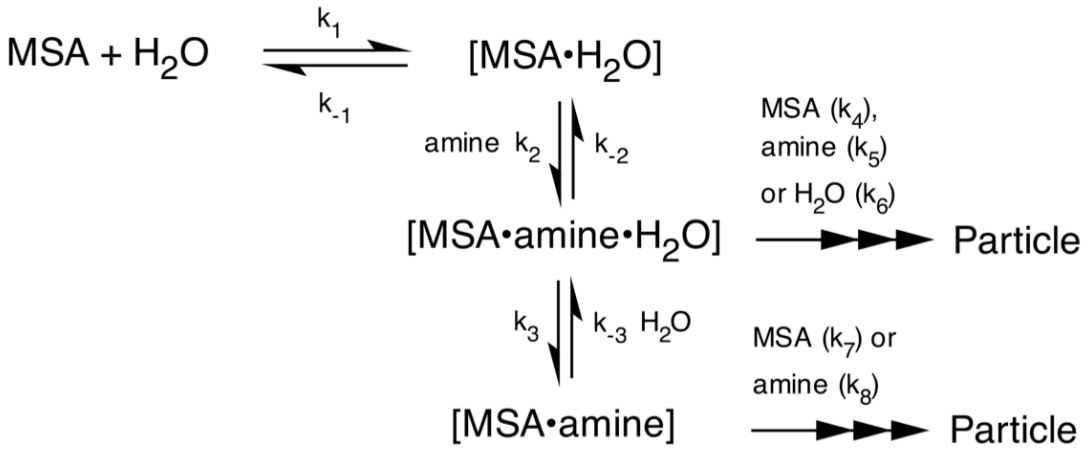

Figure 2.10: Proposed mechanism for particle formation from MSA, DMA or TMA, and water. Species labeled 'particle' are assumed to grow to detectable sizes.

into the mechanism. In this scheme, species labeled 'particle' are not the clusters expected from the addition of a single gas-phase molecule, but rather particles of a size detectable by the experimental system ($>\sim 5.8$ nm). The theoretical and experimentally fit rate constants used in the mechanism are presented in Table 2.5.

The kinetics mechanism was integrated using the commercially available kinetics software Acuchem for each set of experimental conditions.[252] Acuchem uses an integration method that is suitable for stiff equations, such as is expected in these types of kinetics equations. Varying the user-defined integration tolerance from 10^{-3} (the recommended value) to 10^{-6} changed the results by less than 0.2% under all experimental conditions.

A comparison of the modeled particle concentrations to those measured experimentally is presented in Figure 2.11. Error bars are calculated based on $\pm 25\%$ variability in the initial MSA and amine concentrations. As can be seen, the kinetics mechanism is able to reproduce well the experimental flow reactor data.

The inclusion of the energetically-unfavorable loss of water reaction in the particle formation scheme is in large part due to the experimentally observed dependence of water. As

Table 2.5: Rate constants used in kinetics model for particle formation from the MSA-amine-H_2O system shown in Figure 2.10.[149]

	TMA	ΔG (kcal mol^{-1})		DMA	ΔG (kcal mol^{-1})
k_1	6.58 (-10)[a]		k_1	6.58 (-10)[a]	
k_{-1}	5.53 (8)[b]	2.0	k_{-1}	5.53 (8)[b]	2.0
k_2	1.32 (-9)[a]		k_2	1.44 (-9)[a]	
k_{-2}	3.09 (1)[b]	12.3	k_{-2}	5.29 (0)[b]	13.4
k_3	9.96 (8)[b]	2.2	k_3	7.91 (6)[b]	5.0
k_{-3}	1.66 (-9)[a]		k_{-3}	1.49 (-9)[a]	
k_4	6.00 (-19)[a]		k_4	3.00 (-20)[c]	
k_5	5.00 (-19)[a]		k_5	1.00 (-20)[c]	
k_6	2.00 (-25)[a]		k_6	3.00 (-25)[c]	
k_7	5.00 (-20)[a]		k_7	1.00 (-20)[c]	
k_8	4.00 (-19)[a]		k_8	7.00 (-20)[c]	

[a]Assumed to be collision limited with zero activation energy. Calculated using equation 2.1.
[b]Calculated based on theoretical energies of formation using equation 2.2.
[c]Empirically fit.

mentioned above, water is always necessary to form significant numbers of particles, but in the case of excess TMA, no water dependence on the final particle concentration was seen between 4 and 20% RH. The formation of the MSA hydrate as the first step in the mechanism satisfies the requirement that water must be present to form particles and leads to a dependence on water in the number of particles formed. However, inclusion of the loss of water reaction (k_3 and k_{-3}) reduces the dependence of particle formation on gas-phase water concentration when particles are formed primarily through reactions 7 and 8, while particles formed through reactions 4–6 continue to depend on water. The experimentally observed dependence on water could then be modeled if particles formed under conditions of excess TMA go through reactions 7 and 8, while for excess DMA or MSA (in both the DMA and TMA systems), they are formed through reactions 4–6.

The way this is accomplished in the kinetics mechanism serves as an example of the benefits of an approach that combines theoretical and experimental results. While the rate constants k_4–k_8 are fit to the experimental results, it is the theoretical calculations that result in modeled particle formation going through reactions 7 and 8 for excess TMA and through

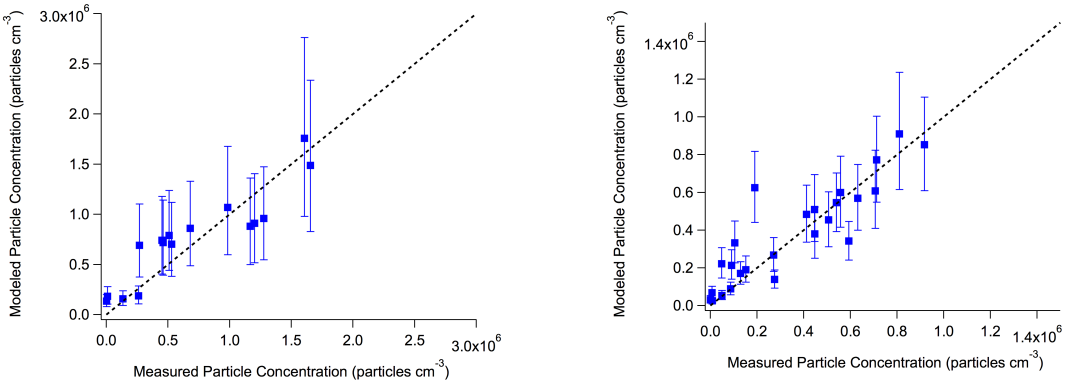

Figure 2.11: Comparison of modeled and measured particle concentrations for the MSA, H_2O and A) TMA or B) DMA systems. Error bars indicate the variability in the measured results based on ±25% initial gas-phase MSA and amine concentrations. The dashed line is a 1:1 line for reference.[149]

reactions 4-6 for excess DMA. As seen in the free energy diagrams (Fig. 2.9) and as listed in Table 2.5, more energy is required to remove water from MSA-DMA-H_2O to form MSA-DMA ($\Delta G = 5.0$ kcal mol^{-1}) than to go from MSA-TMA-H_2O to MSA-TMA ($\Delta G = 2.2$ kcal mol^{-1}) under standard conditions. This results in more particles being formed through reactions 7 and 8 for the excess TMA case, while reactions 4–6 play a greater role in the excess DMA case, reproducing the experimentally observed water dependence seen in Figure 2.6.

It is not the purpose of this work to develop a particle formation mechanism composed of an exhaustive list of intermediate clusters, as has been the focus of some purely theoretical approaches.[143,146,253] Indeed, in the real atmosphere, clusters not included in this mechanism (*e.g.*, the amine hydrate) exist and contribute in some way to the formation of larger clusters and particles. For example, in the absence of amines, MSA will form particles with water

(Fig. 2.6), and the mechanism proposed here would not capture this. However, when MSA amines and water are present, this mechanism is able to accurately predict the number of particles formed (Fig. 2.11). The inclusion of experimental results in the development of this model avoids one of the main limitations of a purely theoretically-based kinetics model for particle formation, *i.e.* that for clusters of more than just a few molecules, performing theoretical calculations of all possible clusters becomes unfeasible and their inclusion in a kinetics mechanism greatly increases its computational cost.[143] At the same time, the approach presented here has the advantage of being based on the fundamental physical processes at work, as opposed to a simple parameterization of experimental results. In addition, a similar mechanism starting from field measurement data and a parameterization of the most likely initial steps in particle formation, has successfully been implemented for the sulfuric acid/amine system.[126]

In relating measured particle concentrations directly to particle formation, it must be assumed that particle coagulation, growth and the wall loss of gas- and particle-phase species has a minimal effect on particle concentrations measured at 4.2 min reaction time. A justification for these assumptions is presented below. A more comprehensive approach to assessing the impact of these competing processes is described in section 5, where the kinetics mechanism described above is integrated while taking into account these associated processes.

2.3.4.1 Wall Loss of Particles

Most particle formation was observed to take place in less than 4.2 min and little if any increase in particle concentration was observed after 14 min reaction time. The effect of deposition loss of particles to the wall of the flow tube can be inferred from the measurements of particle concentration after particle formation has effectively ceased (*i.e.* after 14 min). Figure 2.12 shows the average normalized particle concentration between 9.2 and 24 min

relative to the measured concentrations at 9.2 min for each set of experimental conditions. These data indicate little change in particle concentration occurs between 14 and 24 min. The black line in Figure 2.12 is a weighted least squares fit of the data between 14 and 24 min to the following equation:

$$[P] = [P]_0 e^{-k_{wl}t} \tag{2.3}$$

Here, $[P]$ is the particle concentration at time t, $[P]_0$ is the particle concentration at 14 min reaction time and k_{wl} is the particle wall loss rate constant. The slight decrease in concentration observed corresponds to an effective loss rate of $k_{wl} \leq (7 \pm 7) \times 10^{-4}$ s^{-1} for particles whose GMD was 36 ± 24 nm ($2s$). This value represents an upper limit as coagulation of existing particles would also serve to decrease particle concentration, although this is expected to play a minor role as discussed in detail below. This low value for k_{wl} suggests particle wall loss will have a minor effect on measured size distributions compared to the effects of particle formation and growth, especially over the initial reaction times (0.0 – 9.2 min) where the largest changes in particle number concentration and size are observed.

2.3.4.2 Wall Loss of Gas-Phase Species

An estimate of wall loss of gas-phase MSA was determined by UPLC-ESI-MS from filter samples collected at various ports (*i.e.*, reaction times) in the flow tube in the absence of amines and at various RH (0 – 30%). The first-order rate constant for wall loss of MSA was found to be $(1 - 3) \cdot 10^{-3}$ s^{-1}. Using the largest value, the lifetime for MSA with respect to wall loss is approximately 6 min. This is much longer than the lifetime for the MSA forward reactions with water and the amines, which under our reaction conditions are milliseconds or less. To further assess the potential impacts, the model was run assuming that both MSA and the amines had wall-loss rate constants of 3×10^{-3} s^{-1}. Although the modeled particle

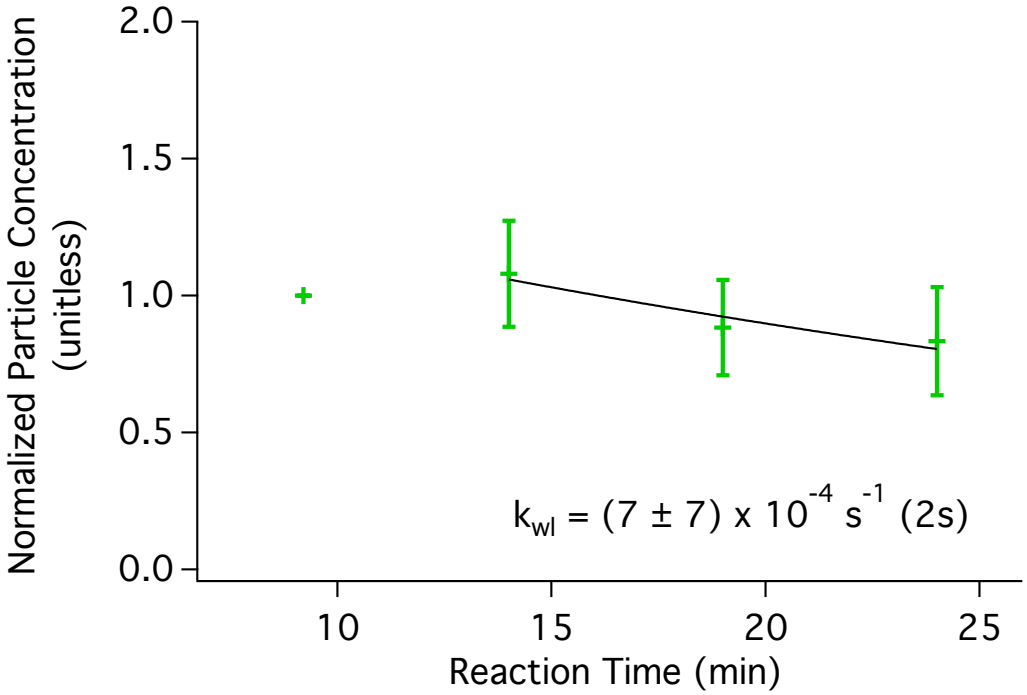

Figure 2.12: Average normalized particle concentrations for experimental conditions shown in Table 2.4 relative to the concentration measured at 9.2 min reaction time. Error bars are $\pm 2s$. Wall loss rate constant k_{wl} is calculated by a weighted least-squares fit of the data between 14 and 24 min reaction time to equation 2.3.

concentrations were reduced on average by 23%, the new values were still well within the error bars shown in Fig. 2.12.

2.3.4.3 Coagulation

To confirm that total particle concentration measurements at 4.2 min reaction time are an adequate indicator of the initial number of new particles formed, the reduction in number concentration from coagulation between particles must be small. Some flow reactor measurements were taken simultaneously at approximately 4 s reaction time as well as 4.2 min. Although the signal was less stable at 4 s, these measurements provide a means to determine the contribution from coagulation. The particle size distribution did not change significantly

between these two reaction times. Thus, if coagulation alters the measured particle number concentrations, it does so before 4 s reaction time.

An upper limit to coagulation was determined in the following manner. Using the formulation of Chan and Mozurkewich,[234] the maximum rate constant for coagulation corresponds to that between the smallest and largest particles in any given range. The range of particle sizes was taken to be 1 to 100 nm. (The geometric mean diameter for all experiments was well below 100 nm, and on average approximately 30 nm.) Because no bimodal peaks were observed, the maximum rate of coagulation would occur when particles were evenly distributed across the range of sizes. In this scenario, the rate of coagulation can be described by equation 2.4.

$$\frac{d[P]}{dt} = -0.5 * k_{avg}[P]^2 \tag{2.4}$$

Here, $[P]$ is the particle concentration and k_{avg} is the average coagulation rate constant for combinations of particles in this range, which is calculated to be 1.1×10^{-8} cm^3 particle^{-1} s^{-1} according to the formulation of Chan and Mozurkewich.[234] The 0.5 factor is to avoid double counting particles.

The maximum effect of coagulation would occur: (i) for the highest measured particle concentration and (ii) if all particles were formed immediately ($i.e.$, at reaction time t_0). Assuming these conditions, the maximum possible reduction in particle number concentration from coagulation can be determined by integrating equation 2.4 over reaction time t to yield equation 2.5.

$$[P]_0 = \frac{1}{\frac{1}{[P]_f} - 0.5 * k_{avg} t_f} \tag{2.5}$$

Here, $[P]_f$ is the measured particle concentration at time $t_f = 4$ s. The maximum measured $[P]_f$ under any set of conditions was 1.6×10^6 particles cm^{-3}. Using this value, the initial particle concentration, $[P]_0$ is calculated to be 1.7×10^6 particles cm^{-3}. This represents a reduction in particle concentration of 6% from coagulation. In no experiments was a flat particle size distribution observed that would have led to this maximum estimated coagulation rate described in equation 2.5. In addition, some finite time to form particles is required, further reducing the effect of coagulation. For these reasons, coagulation between particles is expected to be small enough that the total measured particle concentration at 4.2 min reaction time will be proportional to the new particles formed.

2.3.5 Atmospheric Implications

As mentioned in the introduction, MSA yields from DMS oxidation can be up to 3 times that of sulfuric acid,[59] and gas-phase MSA concentrations have been measured from 6 – 100% relative to gas-phase sulfuric acid concentrations (which are generally $10^5 - 10^7$ molecules cm^{-3})[7] in the coastal marine environment.[51] Amines are typically at the ppt level in air, but can reach several ppb or higher near sources.[88] To evaluate the impact of particle formation from MSA, amines and water in the atmosphere, the kinetics model described here was run at the atmopsherically relevent concentrations of: [MSA] = 10^6 molecules cm^{-3}, [DMA] or [TMA] = 500 ppt, and 30% RH. This results in particle formation at the rate of 0.004 – 0.02 particles cm^{-3} s^{-1}. For a comparison to the expected contribution from sulfuric acid under similar conditions, the parameterization of Kuang et al. of particle formation from sulfuric acid was calculated for [sulfuric acid] = 10^6 molecules cm^{-3}. (It should be noted that as this parameterization was based on field measurements, it would include the effect of ambient amine concentrations on particles formed from sulfuric acid.) The predicted rate of particle formation for this system is 0.01 – 10 particles cm^{-3} s^{-1}, indicating that under

some conditions the contribution of particle formation from MSA, amines and water could be comparable to that from sulfuric acid.

In addition to identifying an important source of new particles in the atmosphere, we believe this approach to modeling particle formation based on a combination of experiment and theory will prove useful for other systems as well. It avoids the computational limitations to a purely theoretical approach to modeling particle formation, while having the benfit of being based on the fundamental chemical processes at work, as opposed to a simple parameterization of experimental data.

Chapter 3

Gas-Phase Amine Measurements

3.1 Research Goals

As discussed in section 1.2, an important limitation to many existing techniques for measuring gas-phase amines is sample loss to instrument surfaces. This work aims to develop a simple, reliable method for measuring gas-phase ammonia and amines at typical atmospheric concentrations (ppt – ppm in air) by collection on an ion exchange resin and subsequent analysis by IC. In this work, two approaches were developed. The first is applicable to higher (ppb) concentrations while the second, for which a custom high-pressure resin holder cartridge was designed for in-line extraction on an IC system, has detection limits in the tens of ppt range for a 60 min sample. Loss to instrument surfaces is reduced by minimizing exposure of the sample to surfaces prior to measurement. This technique is shown to be accurate and reproducible, involve minimal sample preparation, and have relatively short sampling time, making it suitable for both laboratory and field studies. The evaluation of this technique is discussed in this chapter.

3.2 Experimental

3.2.1 Liquid-Phase Standards

Standard solutions for ammonia, MA, DMA, and TMA were prepared from their chloride salts in 0.1 M oxalic acid (Fluka). These include NH_4Cl (Sigma, 99.5%), CH_3NH_3Cl (Aldrich, 98.0%), $(CH_3)_2NH_2Cl$ (Aldrich, 99.0%), and $(CH_3)_3NHCl$ (Aldrich, 98.0%).

In the course of developing this method, there was some indication that amines and/or aminium ions in aqueous solution were being taken up in the walls of glass containers. To test whether, and to what extent, this was occurring, a standard solution containing between 10 and 30 ng/mL of the ammonium and aminium species in nanopure water was prepared and stored in plastic containers. A portion of this solution was placed in three 20 mL glass scintillation vials half filled with clean, dry borosilicate glass beads (Chemglass; P/N CG-1101-02) and allowed to sit for 60 min. The original standard solution (stored only in plastic) and those from the glass vials were then analyzed by IC. The peaks in the samples from the glass vials corresponding to ammonia and the amines were reduced, on average, by 13 – 23% compared to the original standard solution, indicating that amines are taken up by glass surfaces under neutral conditions. However, it should be noted that if the standard solution was acidic, no uptake on glass was observed. To avoid any potential wall loss, no glass was used in the preparation or storage of standards and samples used in this study.

3.2.2 Gas-Phase Standards

Mixtures of ammonia (Airgas; 0.812 ppm in N_2), MA (Airgas; 10 ppm in N_2), DMA (Airgas; 1.0 ppm in N_2), and TMA (Airgas; 1.0 ppm in N_2) in nitrogen were used to test the collection efficiency of the WCE resin (stated concentrations were those provided by the manufacturer

but as discussed in section 3.3.1, have considerable uncertainties associated with them). Gas-phase ammonia and amines from the gas cylinders were diluted with clean, dry air from an FTIR purge gas generator (Parker-Balston; model 75-62) for a total flow of 4.0 L min^{-1} and analyte concentrations of approximately 2 – 1000 ppb. Gas cylinder and purge-air flows were maintained using mass flow controllers (Alicat).

3.2.3 Cartridge preparation and analysis for higher (ppb) concentrations

Sampling cartridges were prepared by filling 2.5 mL non-fluorous polypropylene cartridges (Supelco; model 57602-U) with WCE resin (Resintech, model WACG) between two polyethylene frits (Supelco) as shown in Figure 3.1 (inset). WCE resin consists of acrylic/divinylbenzene beads terminated with carboxylic acid groups. The design of the cartridges minimizes the surfaces in contact with the sample prior to adsorption on the WCE resin, and those that are exposed are subsequently extracted with the resin. These cartridges were used to sample gas-phase standards in the ppb - ppm range in air to characterize the collection and extraction efficiency of WCE resin, and will be referred to as 'high-concentration cartridges'.

Samples were collected for 20 minutes at 1 – 2 L min^{-1} maintained using a mass flow controller (Alicat). Two cartridges in series (Fig. 3.1, hereafter referred as "primary" and "backup" cartridges) were used in all experiments to determine collection efficiency. Cartridges were extracted and regenerated by flushing five times with 10.0 mL 0.1 M oxalic acid (Fluka) to remove the collected ammonia and amines and return the resin to its protonated (-R-COOH) form. The first 10.0 mL extract was used as the sample. For the primary cartridge, the first two 10.0 mL extractions were analyzed to determine extraction efficiency. The cartridge was flushed another 3 times with 10.0 mL 0.1 M oxalic acid and the final rinse was used

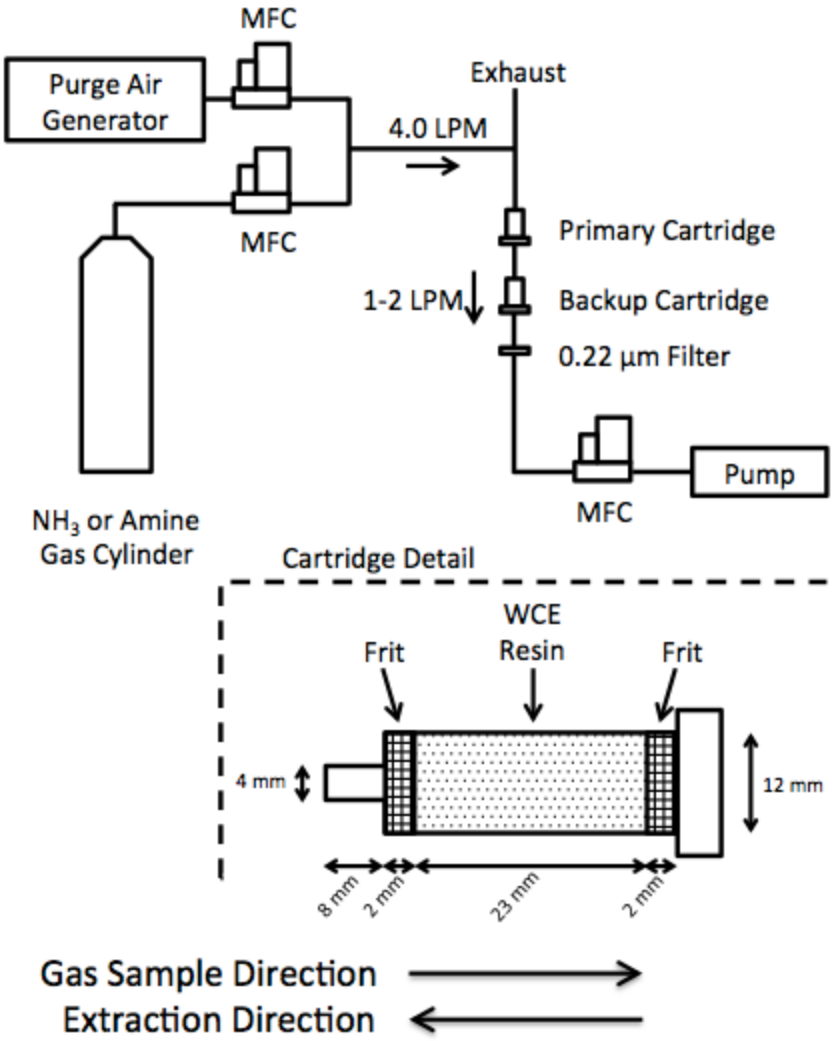

Figure 3.1: Schematic of experimental system used to determine cartridge measurement efficiency. MFC = mass flow controller. Inset shows a detailed view of the 'high-concentration cartridge.

as a blank for the subsequent sample. Samples were stored in 11 mL polypropylene vials (Metrohm, KITIC0008) prior to measurement.

Samples were analyzed by IC (Metrohm, model 850) with a Metrosep C4 250/4.0 cation column and equipped with a conductivity detector. The IC eluent was 0.00375 M oxalic acid and the flow rate was 0.9 mL/min. The IC column temperature was maintained at 30 C. The sample loop was 20 µL, and the total elution time was 24 minutes.

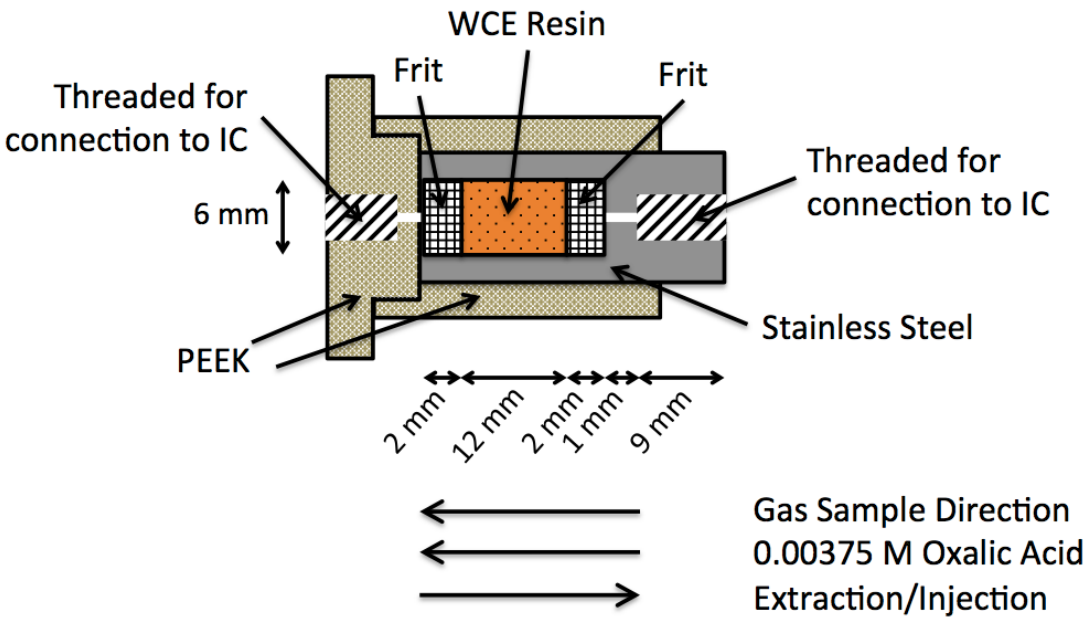

Figure 3.2: Schematic of 'low-concentration cartridge.

3.2.4 Cartridge preparation and analysis for lower (ppt) concentrations by in-line extraction and analysis

For ambient sampling, modified cartridges (Fig. 3.2) that could be used under the high-pressure conditions of the IC were designed for gas-phase collection and in-line extraction (*vide infra*). It should be noted that 'in-line' here refers to the method of extraction on the IC column and does not indicate that this is an on-line measurement technique. These cartridges were prepared using a PEEK analytical guard cartridge holder (Hamilton; model 79477) designed for use on high-pressure liquid chromatography systems and a custom-built stainless-steel insert containing WCE resin (Resintech, model WACG) between two polyethylene frits (Supelco). These are referred to as 'low-concentration cartridges' in the subsequent discussion. As for the 'high-concentration' cartridge, this design minimizes the amount of surface area that gas-phase samples are in contact with prior to adsorption on the WCE resin to $\sim$1 cm^2 of stainless steel and one of the polyethylene frits; however, adsorbates on both the frit and stainless steel are extracted along with those on the resin.

Prior to sampling, the low-concentration cartridges were flushed three times with 10.0 mL 0.1 M oxalic acid followed by clean, dry air for 20 min at 150 cm^3 min^{-1} to remove residual water from the last rinse. Gas-phase samples were pumped through the cartridge at 150 cm^3 min^{-1} for 45–50 min in the direction indicated in Figure 3.2. After sampling, the cartridge was filled with 60–80 μL 0.00375 M oxalic acid (IC eluent) using a syringe pump (New Era Pump Systems; model #NE-1000) in the same direction as the gas-phase sample (Fig. 3.2), to avoid injecting air into the IC system. The volume of eluent used to fill the cartridges was ∼5–10 μL lower than their predetermined capacity to prevent overfilling and loss of analyte. Any residual air left in the cartridges was not sufficient to cause problems during the IC runs.

Extraction and analysis were performed in-line on the IC by using two injectors in series, as shown in Figure 3.3. This procedure eliminates the separate extraction step and allows the entire collected sample to be injected onto the IC column, as opposed to extracting the cartridge with 10 mL of 0.1 M oxalic acid and then injecting only a 20 μL portion of the extract on the IC. Having the entire collected sample injected onto the IC column lowers the detection limit to a range suitable for atmospheric concentrations (Table 3.1). The first injector sample loop was loaded with 20 μL 0.1 M oxalic acid and the second injector was fitted with the low-concentration cartridge in place of a sample loop, oriented so the IC eluent flow will be in the direction indicated in Figure 3.2. All other IC conditions were as described in section 3.2.3.

At the beginning of the run, the sample loop containing the acid and the low-concentration cartridge were simultaneously injected. This allows the concentrated oxalic acid plug to extract the cartridge and push the analyte onto the column. After 0.25 min, the cartridge injector was returned to fill mode. Three to five sequential extractions of the cartridge were performed for each sample, depending on the measured ammonia and/or amine concentrations.

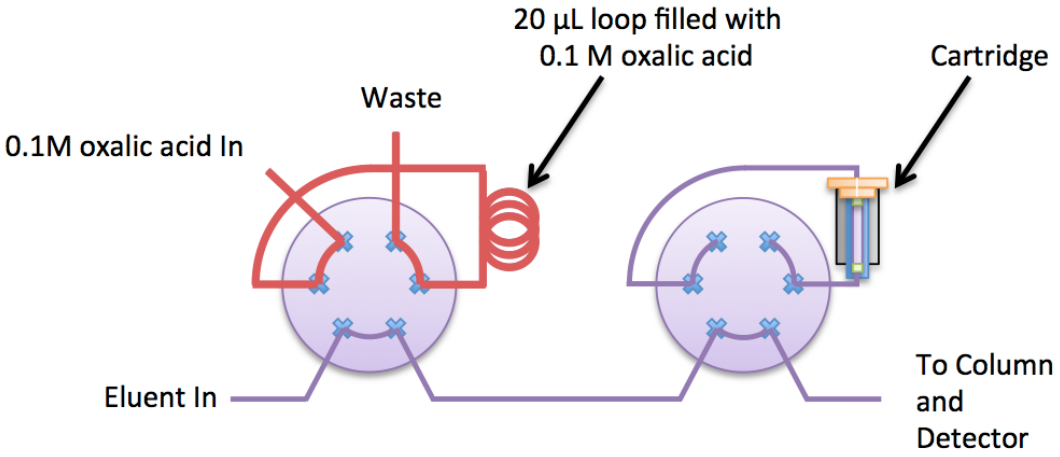

Figure 3.3: Schematic of the in-line system for simultaneous extraction and analysis of ammonia and amine samples by IC (shown immediately prior to injection). At the beginning of the IC run, both injectors are actuated, allowing the 0.1 M oxalic acid plug to extract the cartridge and push the amine/ammonia onto the IC column.

A series of experiments was performed to determine if breakthrough occurs in the low-concentration cartridges under conditions of high ammonia concentration as is often seen in the field samples.[88,254] Three low-concentration cartridges were prepared as described above, and one was kept as a blank. Gas-phase ammonia in N_2 from a gas cylinder (Airgas; 0.812 ppm in N_2) was then flowed through the remaining two cartridges in series for 50 min at 150 cm^3 min^{-1}. Three sets of samples were taken. After background subtraction, the measured NH_3 concentration on the backup cartridge was less than 7% of the total measured NH_3 (primary + backup) in all three cases, and was 4% of the total measured NH_3 on average. These results suggest minimal breakthrough occurs, even with high ammonia concentrations.

3.2.5 Field measurements in an agricultural area

Several field measurements using the low-concentration cartridges were performed in Chino, CA, USA. A 40 L steel chamber under vacuum was used as the pump. It was evacuated,

Table 3.1: Retention times and calculated detection limits for ammonia and amines. Errors shown are ±2s.

Species	Retention time (min)	Liquid-Phase Detection Limit (mol L^{-1} $\times 10^{-7}$)	Gas-Phase Detection Limit[a,b]	
			High-Concentration Cartridge (ppt in air)	Low-Concentration Cartridge (ppt in air)
Ammonia	7.5	2.3 ± 1.6	(2.8 ± 1.9) $\times 10^3$	12 ± 8
Methylamine	8.8	2.6 ± 1.7	(3.1 ± 2.1) $\times 10^3$	14 ± 9
Dimethylamine	11.8	3.5 ± 2.4	(4.3 ± 3.0) $\times 10^3$	19 ± 13
Trimethylamine	20.7	8.2 ± 5.6	(1.0 ± 0.7) $\times 10^4$	45 ± 31

[a]Detection limits are calculated from the average of the signal corresponding to 3/5 peak-to-peak noise from 10 cartridge samples.

[b]Gas-phase detection limits for the high-concentration cartridge samples are based on 1 L min^{-1} sampling for 20 min, extraction in 10 mL oxalic acid, and injection of 20 μL of the solution. For the low-concentration cartridge, detection limits are based on 150 cm^3 min^{-1} sampling for 60 min and in-line extraction on the IC.

fitted with a battery-powered mass flow controller (Alicat) and used to maintain a constant sample flow through the cartridges. This allowed sampling to be performed away from a power source without the need for a generator, which could have introduced exhaust-related artifacts. Samples were taken approximately 50 m away from cattle pens between 4 am and 6 am (before sunrise) between 28 August and 12 September 2013. On each day, one cartridge was prepared as described in section 3.2.4 and kept as a blank. These blanks were used for background subtraction of the sample chromatograms.

3.3 Results and Discussion

A typical chromatogram for the liquid standards used in the IC is shown in Figure 3.4. Peaks corresponding to NH_4^+, MA$-H^+$, DMA$-H^+$, TMA$-H^+$ and a small amount of Na^+ are present. Table 3.1 summarizes retention times and liquid-phase detection limits for ammonia, MA, DMA and TMA. These were calculated as the average concentration whose signal corresponds to 3/5 of the peak-to-peak noise from 10 typical cartridge measurements.[255] The standard deviation of this value is a measure of reproducibility. Errors in the estimated detection limits shown in Table 3.1 are ± two sample standard deviations. For the high-concentration cartridges, gas-phase detection limits were calculated for 20 min samples at 1.0 L min^{-1} sample flow followed by extraction in 10 mL 0.1 M oxalic acid. For the low-concentration cartridges, gas-phase detection limits were calculated for 60 min samples at 150 cm^3 min^{-1} sample flow followed by in-line extraction on the IC. Detection limits for the high- and low-concentration cartridges were in the low ppb and ppt range, respectively (see Table 3.1). It should be noted that with the current design of the low-concentration cartridges, 150 cm^3 min^{-1} is the maximum sample flow possible, however redesigning the cartridge to allow higher sampling flow would further lower the detection limits for this method.

3.3.1 Gas-phase standards using the high-concentration cartridges with off-line extraction

Oxalic acid is not retained by the cation column used in the IC and elutes at ∼2.5 min. The high concentration (0.1 M) of oxalic acid in the cartridge extracts compared to that of the IC eluent (0.00375 M) results in a characteristic negative broad signal initially as can be seen in a typical cartridge blank (Fig. 3.5a). For this reason, blanks are subtracted from cartridge samples before the peaks are integrated. A typical background-subtracted chromatogram for

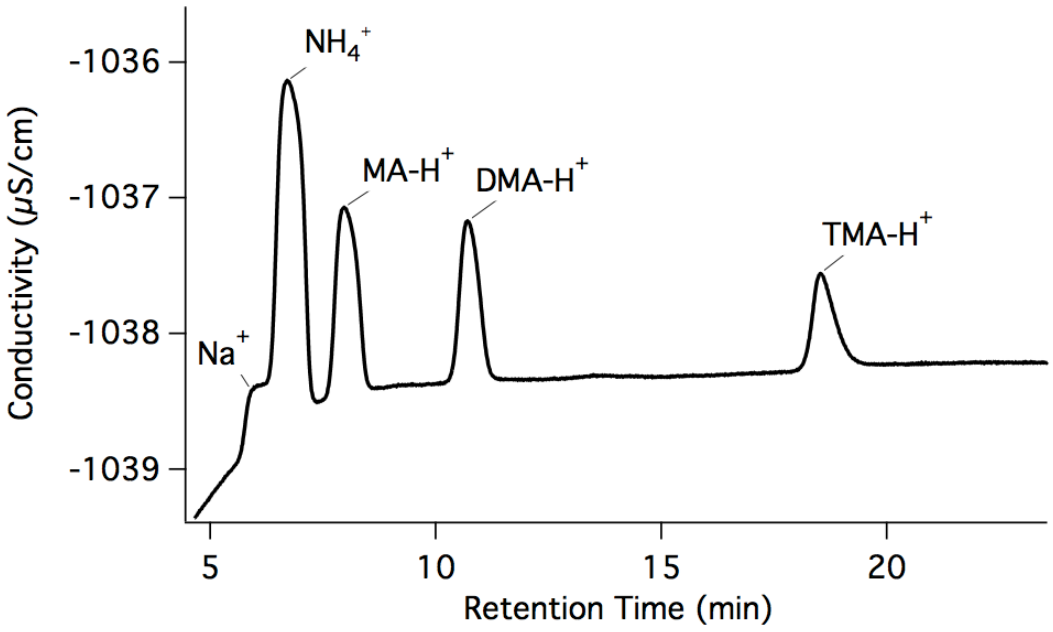

Figure 3.4: A typical ion chromatogram for the amine/ammonia standards in 0.1 M oxalic acid. Standards also included sodium methanesulfonate ($NaCH_3SO_3$; Aldrich; 98%) because of the nature of ongoing laboratory experiments at the time so that Na^+ was also present.

a DMA sample is shown in Figure 3.5b. Results from the gas-phase standard measurements are presented in Figure 3.6 and show measured ammonia and amine concentrations for the first and second extract of the primary cartridge, the first extract of the backup cartridge, as well as the total measured concentration (first and second extract of the primary cartridge plus the first extract of the backup cartridge).

WCE resin was originally designed to remove alkaline components from liquid solutions by reaction with the surface carboxylic acid groups.[256] To the best of our knowledge, its ability to take up gas-phase species has not been reported. For the three amines, the measured concentration from the backup cartridge was less than 5% of that of the primary cartridge (Fig. 3.6). This small amount of breakthrough indicates that WCE resin efficiently takes up gas-phase amines even at the relatively high flow rate of 1.0 L min^{-1}. For ammonia, this value is slightly higher (but still <10% of the primary cartridge), suggesting that the less-basic, more-volatile ammonia is trapped less efficiently than the amine species.

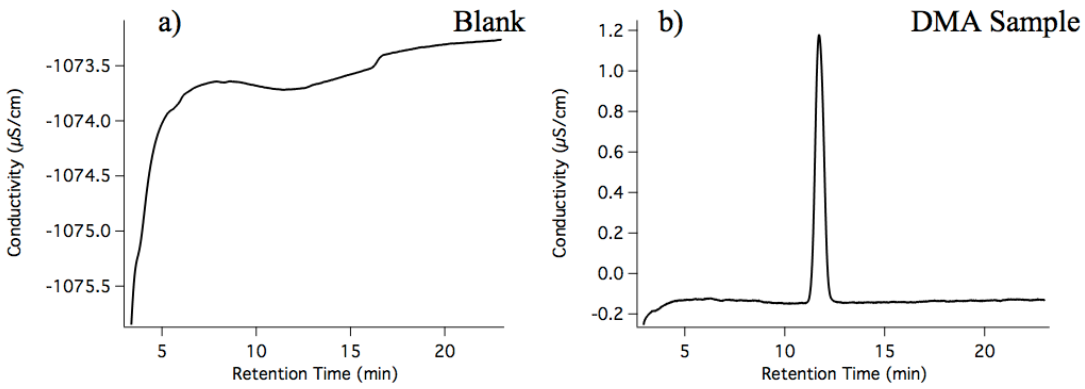

Figure 3.5: a) Chromatogram for a typical blank using high-concentration cartridges showing the characteristic baseline due to the high oxalic acid concentration in the cartridge extracts and b) a background subtracted ion chromatogram for a DMA sample (nominally 1.0 ppm in N_2; see section 3.3.1).

For cartridge extraction, an appropriate solvent must be able to efficiently extract the ammonia and amines, and be low enough in concentration to minimize effects on the baseline in the ion chromatogram (Fig. 3.5a). For regeneration of the WCE resin, the manufacturer recommends dilute hydrochloric or sulfuric acids. In our experiments, we chose oxalic acid as the extraction solvent due to its weak acidity [$pK_{a1} = 1.25$; $pK_{a2} = 3.81$][257] and its use as the IC eluent. As seen in Figure 3.6, the second extract of the primary cartridge using 10.0 mL of 0.1 M oxalic acid contains less than 15% of the analyte compared to that of the first extraction, indicating this method efficiently extracts the collected species. However, oxalic acid concentrations lower than 0.1 M were shown not to be sufficient. For DMA and TMA, a slight trend of increasing concentration of amine measured from the second extraction of the primary cartridge is evident, suggesting that at higher gas-phase concentrations, a shorter sample time, lower flow rate or multiple extractions may be required. However, such high concentrations of the amines (>0.5 ppm) have not been reported in air and hence are unlikely to present an analytical limitation for this technique as an ambient sampling method.

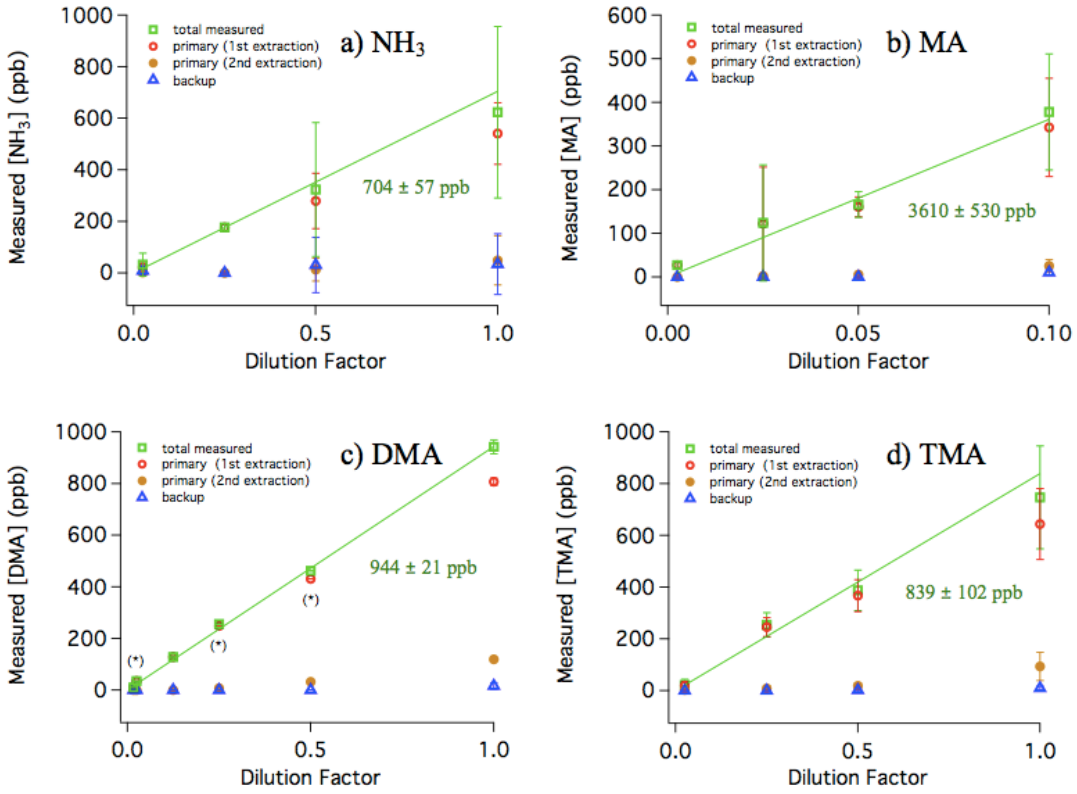

Figure 3.6: Results for measurements of gas-phase standards of a) ammonia, b) MA, c) DMA, and d) TMA using high-concentration cartridges, including the first and second extract of the primary cartridge and the first extract of the backup cartridge, as well as the total measured concentrations. The dilution factor for ammonia or amine from the gas cylinders diluted in air is shown on the x-axis, where 1.0 is the undiluted standard and 0.1 is a 10% mixture. Data points marked with an asterisk (*) do not have sufficient replicates to include error bars. The green lines are weighted least-squares fits, where the weights for each point are given by $w = (1/s^2)$ and s is the sample standard deviation of the measurements at each dilution. Slopes of fitted lines are shown in green ($\pm 2s$), and represent the measured undiluted standard concentrations. Labeled concentrations for the undiluted standards were: 0.812 ppm NH_3, 10 ppm MA, 1.0 ppm DMA, and 1.0 ppm TMA.

Figure 3.6 shows weighted least-squares fits (green lines) forced through (0,0) of the total measured concentrations of ammonia and the amines. These data indicate a linear trend of measured concentration with dilution and suggest good measurement efficiency for each of the gas-phase amines and ammonia. Error bars shown for individual data points are ± two sample standard deviations, and are based on at least three individual measurements. These values are used to calculate the errors in the weighted least-squares slopes shown

in Figure 3.6, which are a measure of the precision of this technique and are 2 – 15 % for ammonia, MA, DMA and TMA. These values are similar to those obtained for other techniques that have used gas-phase amine standards for characterization.[168] In addition, they likely represent an upper limit to the error associated with this technique as the system used to generate the gas-phase standards (Fig. 3.1) involves carefully regulated flow rates and many hours of conditioning. Some of the variability in the measurements, no doubt, reflects variability in the actual gas-phase concentrations and therefore is not intrinsic to the measurement technique.

As can be seen in Figure 3.6, the measured concentrations without dilution are lower than the manufacturer-provided concentrations of the gas cylinders (see section 3.2.2). While this could potentially be due to uptake of the amines on tubing walls prior to measurement, this seems unlikely as the system was conditioned for several hours at each concentration prior to sampling and no trend of increasing concentration was observed after conditioning. It is possible that the labeled concentrations of the cylinders are artificially high, as the manufacturer has expressed difficulty in preparing such low concentrations of these sticky compounds. However, the linear trend with dilution along with the negligible amounts measured in the backup cartridge and second extract of the primary cartridge indicate efficient measurement for this technique. To explore this further, two of the gas cylinders (NH_3 and MA) were analyzed by a different technique. Samples from the cylinders were bubbled through a 0.1 M oxalic acid solution at 30 cm^3 min^{-1} for 60 min, which was then analyzed by IC. These measured concentrations were within experimental error of those measured by cartridge collection ($[NH_3] = 575 \pm 128$ ppb; $[MA] = 4.40 \pm 0.58$ ppm). This comparison of measured to nominal concentrations also provides a cautionary note in terms of using commercially supplied amine or ammonia gas mixtures as calibration standards.

All the samples for the gas-phase standard measurements (both primary and backup) were collected on four high-concentration cartridges. These cartridges showed no noticeable degra-

dation in collection or extraction efficiency, even after hundreds of extractions without replacing the WCE resin. For example, on one day of sampling, measurements were made on TMA standards at 0.25, 0.5 and 1.0 dilution factor using two cartridges that had been used to different degrees. Cartridge A had seen ∼120 extractions and cartridge B ∼40 at the start of the day. Three measurements were made at each dilution, and each cartridge was used at least once at each dilution. The relative deviation from the mean was calculated for each measurement as:

$$d = \frac{(x - \mu)}{\mu} \tag{3.1}$$

where x is the measured concentration and μ is the mean value of the three replicate measurements at that dilution. The average of these deviations for each cartridge were, A: $d = +0.01 \pm 0.09(1s)$ and B: $d = -0.01 \pm 0.06(1s)$. Despite the small sample set, the deviations are very small and the cartridge that had seen more extractions (A) actually measured (very slightly) higher on average.

3.3.2 Results for field measurements using low-concentration cartridges

A typical chromatogram from an air sample taken in Chino, CA, on 28 August 2013 is shown in Figure 3.7. On each of the three days of sampling (28 August, 04 and 12 September 2013), two 45 – 50 min samples were taken. The results from all field measurements are presented in Table 3.2. Also included in Table 3.2 are the temperature, RH and weather conditions for each sample as reported by NOAA for the Chino Airport, which is <1 mile away from the sampling site.[258]

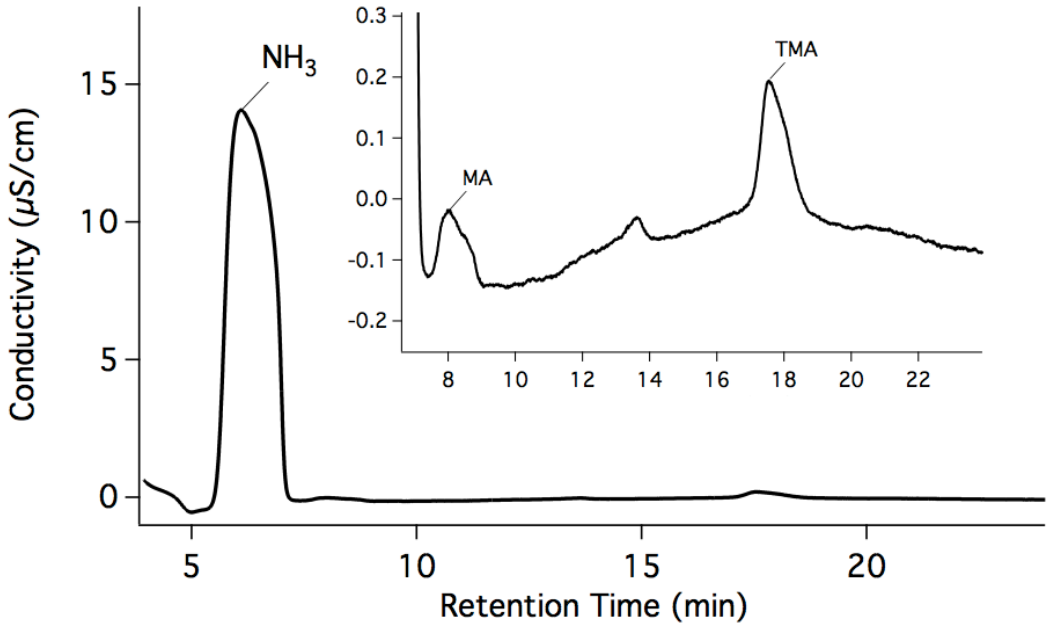

Figure 3.7: The background-subtracted chromatogram from the first extract of the cartridge for the sample taken 28 August 2013 at 4:22 AM in Chino, CA. Inset: same chromatogram magnified to show peaks for MA and TMA.

In all samples, peaks corresponding to NH_3 and TMA were observed, and in several samples a peak for MA and/or a peak at ∼14 min were present. In addition to the standards described in section 3.2.1, those for isopropylamine, ethylamine, diethylamine, butylamine and aniline were obtained and analyzed by IC, however their retention times did not correspond to the peak at ∼14 min, which remains unidentified. Also, diethylamine has been reported to coelute with TMA in some Dionex IC columns.[181,259,260] However, using the Metrohm column and IC conditions described in section 3.2.3, these two species were sufficiently well resolved to be distinguished.

Each sample cartridge was extracted in-line and analyzed by IC five times. The TMA peaks for the five extracts from a sample take on 28 August 2013 are shown in Figure 3.8. The trend in integrated peak areas with extraction for TMA (shown in boxes in Figure 3.8) indicates that five extractions are necessary to measure >97% of the collected species. Results for

Table 3.2: Results of field measurements taken in Chino, CA along with weather data from NOAA[a] for the Chino Airport

Date (2013)	Start Time	Duration (min)	[NH_3] (ppm)	[TMA] (ppb)	Temperature (°C)	RH (%)
28 Aug.	4:22 AM	45	0.90	6.8	21.1	57
28 Aug.	5:08 AM	45	1.5	6.7	20.6	57[b]
4 Sep.	3:55 AM	50	0.75	4.0	21.1	71
4 Sep.	4:47 AM	50	0.75	3.3	20.6	79
12 Sep.	3:53 AM	50	0.19	1.3	15.0	93[c]
12 Sep.	4:45 AM	50	0.49	4.5	14.4	90[c]

[a]Available at http://cdo.ncdc.noaa.gov/qclcd/QCLCD

[b]Haze

[c]Mist

ammonia show the same trend. While ammonia and TMA peaks were usually still present in the fifth extract, they represented $3 \pm 2\%$ ($2s$) for NH_3 and $1 \pm 3\%$ ($2s$) for TMA of the total over five extractions. However, the need for five extractions (∼2.5 hrs IC run time) is a limitation of this method over existing on-line techniques. Optimization of this method (*e.g.* modifying cartridge dimensions, extraction solvent, IC parameters, etc.) may be able to reduce the number of required extractions, thereby improving the efficiency of this technique.

The laboratory characterization of this technique was performed under dry conditions and showed near 100% collection efficiency as indicated by the small amount of analyte collected on the backup cartridges (Fig. 3.6). It is possible that ambient sampling at higher RH would reduce this efficiency, although this seems unlikely as WCE resin is designed and primarily used for extracting ions from liquid samples. Also, though the cartridges are flushed with clean, dry air prior to use, some residual water remains, which would exceed any water vapor in the gas-phase samples. For these reasons, the RH of the ambient samples is expected to have little affect on the measurement efficiency.

The first measurement on 12 September 2013 showed noticeably lower ammonia and TMA concentrations compared to the previous sampling periods. Several factors may contribute

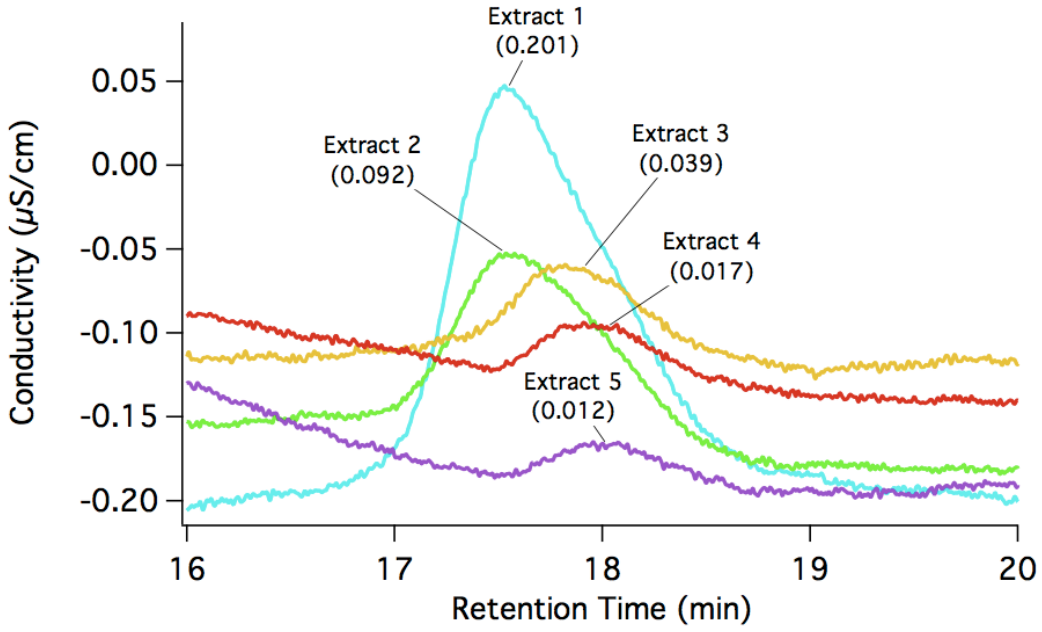

Figure 3.8: The background-subtracted chromatograms from all five extracts of the cartridge for the sample taken 28 August 2013 at 5:08 AM in Chino, CA. Image is magnified to show TMA peak. Integrated peak areas in (μS min) cm^{-1} are shown in parentheses. The slight shift in retention time at lower peak size was typical for TMA in both standards and samples.

to this difference. The temperature was lower and the RH higher on 12 September compared to the two previous sampling days. Also, mist was reported by the Chino Airport weather station on 12 September that had completely cleared up sometime between 5:38 and 5:53 am. Ammonia has been observed to be efficiently scavenged by water droplets during precipitation events.[123] Wet deposition onto mist droplets could account for the lower NH_3 and TMA concentrations on this day and also explain the increase in concentration between the first and second sample as the mist evaporated.

3.3.2.1 Agreement with Literature

The results of these field measurements are consistent with the range of published data on ammonia and amine concentrations in agricultural areas. Concentrations of ammonia and

TMA near cattle feedlots and enclosures in the range of 0.7 – 34 ppm NH_3[35,170,261] and 0 – 400 ppt TMA[261–263] have been reported. Inside cattle enclosures, TMA concentrations up to 0.6 – 7.6 ppb have been measured.[102,262,264] The ratio of TMA to NH_3 in this study, (4 – 9)$\times 10^{-3}$, is similar to that reported for indoor cattle enclosures as well as emissions from hay and silage.[102]

Chapter 4

Amine-Amine Displacement

4.1 Amine-Amine Displacement

Amine-amine displacement experiments were performed using the SPLAT-II mass spectrometer in collaboration with Dr. Alla Zelenyuk at Pacific Northwest National Lab's EMSL User Facility to explore the kinetics and extent of displacement of aminium species in MSA-amine particles by a different gas-phase amine. As discussed in chapter 1, MSA and amines are routinely detected in the particle phase, and while measurements of ammonia-amine displacement in sulfate salts have been performed under various RH conditions,[198,199] those for methanesulfonate salt have not. In addition, to our knowledge, an exploration of amine-amine (as opposed to ammonia-amine) exchange has not been reported in the literature for any salts. If there are species-specific effects of condensed-phase amines on the physical properties of particles, these will have implications for further growth, and make amine-amine exchange reactions a potentially important atmospheric process. Results from this study and a discussion of their impact on the atmosphere are presented in this chapter.

4.2 Experimental

Amine-amine displacement experiments were performed in Pacific Northwest National Lab's EMSL User Facility using the SPLAT-II mass spectrometer, in collaboration with Dr. Alla Zelenyuk. All experiments were performed in 100 L Teflon chambers with gas- and particle-phase species diluted with zero Air (OXARC). Particle size distributions were monitored using a SMPS consisting of a classifier (TSI; model 3080) and a differential mobility analyzer (TSI; model 3081) operated with 0.3 L min^{-1} sample flow and 3.0 L min^{-1} sheath flow.

Two types of experiments were performed that differed only in the source of aerosol particles. In the first type, gas-phase amine was added to a Teflon chamber containing particles formed from a *nebulized salt solution* of MSA and a different amine. In the second, gas-phase amine was added to a Teflon chamber containing particles formed from the *gas-phase reaction* of MSA and a different amine. The details of each type of experiment are described below.

4.2.1 SPLAT-II Mass Spectrometer

SPLAT-II is a single particle, laser ablation time-of-flight mass spectrometer described in detail elsewhere.[125] Briefly, particles entering SPLAT-II are focused with an aerodynamic lens that imparts the particles with a velocity proportional to their vacuum aerodynamic diameter. Particles are then detected by two optical detectors in series (spaced 10.5 cm apart) and sized according to the time between detection events. This delay time is then used to time two laser pulses 10.5 cm further down stream. The first (IR) pulse causes semi-volatile compounds to evaporate from the particle, while the second (UV) pulse, a few microseconds later, ionizes the evaporated compounds and ablates and ionizes the remaining nonvolatile species. Ionized species then enter a time-of-flight region before being detected.

SPLAT-II is capable of detecting particles down to ∼80 nm and can provide information on particle size, composition, density and morphology.[125,156–158]

4.2.2 Salt Standards Preparation

Standards of the MSA-amine/ammonia salts were individually prepared by mixing MSA (99.0%; Aldrich) with excess 28.7% NH_3 in H_2O (Aldrich), 40% MA in H_2O (Aldrich), 40% DMA in H_2O (Aldrich), or 40% TMA in H_2O (Aldrich) by adding the basic solution dropwise into a 20 mL glass scintillation vial containing ∼ 5 mL of the acid in an ice bath. These solutions were then dried under vacuum (Spin-Vap; Wheaton) to remove water and excess ammonia or amine. After re-exposure to lab air, some of the salts rapidly and visibly took up water to varying degrees, with MSA-NH_3 taking up the least water and MSA-TMA taking up the most. (Salts are referred to as, *e.g.* MSA-TMA for trimethylaminium methanesulfonate for clarity.) Uptake of water in the case of the MSA-TMA salt was sufficient to yield a viscous brine as can be seen in Figure 4.1. These results are consistent with the reported increase in hygroscopicity in going from ammonium to alkylaminium sulfate salts.[265]

4.2.3 Nebulized Salt Experiments

Salt standards described in Section 4.2.2 were dissolved in 100 mL Nanopure water (18.1 M, US Filter, model UHP-10) to make 3-4 mM salt solutions. Note that these concentrations are approximate because the salts had taken up water prior to being weighed as described in section 4.2.2. Particles of MSA-NH_3, MSA-MA, MSA-DMA and MSA-TMA were generated by flowing zero air through a nebulizer (Salter Labs; model 8913) filled with one of the salt solutions. Teflon chambers (∼100 L) were filled with zero air until they were ∼9 L from being full. The nebulized particles then were added at 3.0 L min^{-1} for ∼3 min resulting in ∼10:1 dilution of the nebulizer output in the chamber. Assuming the output of the nebulizer to

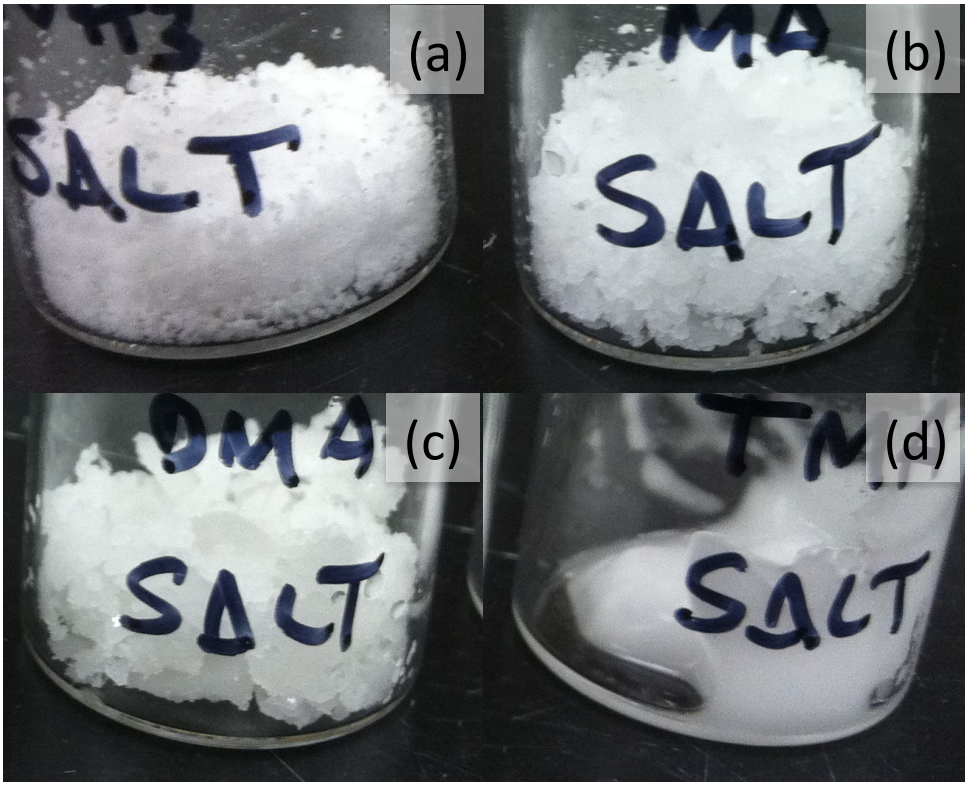

Figure 4.1: Image of prepared salts of a) MSA-NH_3, b) MSA-MA, c) MSA-DMA and d) MSA-TMA showing uptake of water when exposed to room air.

be 100% RH, this yields ∼10% RH in the chambers. Conditions for each of the experiments are given in Table 4.1.

4.2.4 Gas-Phase MSA Generation and Measurement

Gas-phase MSA was generated by flowing zero air through two traps in parallel containing liquid MSA (99.0%; Aldrich) at 3 L min^{-1}. Periodically, samples of gas-phase MSA exiting the traps were measured by collection on 0.45 μm Millipore filters followed by extraction in 20.0 mL nanopure H_2O and analysis by ultra performance liquid chromatography electrospray ionization mass spectrometry (UPLC-ESI-MS; Waters). These values were used to calculate the concentration of MSA in the Teflon chambers based on their known dilution in zero air.

Table 4.1: Conditions for nebulized salt experiments.

Salt	Nebulizer Flow Time (min)	Chamber Volume (L)	Dilution in Air	RH (%)
MSA-NH_3	3:20	112	10.2:1	8.9
MSA-MA	3:20	108	9.8:1	9.3
MSA-DMA	3:20	102	9.2:1	9.8
MSA-TMA	3:00	98	9.9:1	9.2

4.2.5 Particle Formation from Gas-Phase Precursors Experiments

In experiments on particles formed from the gas-phase reaction of MSA and ammonia or an amine, Teflon chambers were filled (fully or partially) with gas-phase MSA from the traps, followed by zero air to fill the chamber to near capacity. Gas-phase NH_3 (0.812 ppm in N_2; Airgas), MA (10 ppm in N_2; Airgas), DMA (1.4 ppm in N_2; Airgas), or TMA (13.4 ppm in N_2; Matheson) were then added such that the final ammonia/amine concentration in the chambers were between 2 and 200 ppb. It should be noted that these amine concentrations are based on the manufacturer stated concentrations, which may not be entirely accurate as discussed in section 3.3.1. It should also be noted that these experiments were all performed under nominally 'dry' conditions, although some water will be present.

4.2.6 Displacement Experiments

Displacement experiments were performed in which chambers prepared as described in sections 4.2.3 and 4.2.5 were subsequently exposed to a different gas-phase amine by flowing one of the gas-phase standards into the chamber in the same manner as described in section 4.2.5. The species involved along with their initial concentrations and other experimental conditions are given in Table 4.2.

Table 4.2: Conditions for amine-amine displacement experiments.

Nebulized Salt + Gas-Phase Amine

Salt	Dilution in Air	RH (%)	Displacing Amine	[Displacing Amine] (ppb)
MSA-NH_3	9.2:1	8.9	TMA	470
MSA-MA	9.1:1	9.3	TMA	9.7
MSA-MA	9.1:1	9.3	TMA	500
MSA-DMA	9.0:1	9.8	TMA	510
MSA-TMA	9.0:1	9.9	MA	500
MSA-TMA	9.0:1	10.2	DMA	350

Gas-Phase Particle Formation + Gas-Phase Amine

Initial Amine	[MSA] (ppb)	[Amine] (ppb)	Displacing Amine	[Displacing Amine] (ppb)
MA	8.3	11	TMA	8.2
DMA	3.8	5.4	TMA	4.3

4.3 Results and Discussion

4.3.1 Particles Prior to Displacement

Shown in Figure 4.2 are average mass spectra normalized to the total SPLAT-II MS signal for both the nebulized salt particles (black lines) and those formed in the gas phase (red lines). The signal from nebulized salt particles (black lines) are shown as negative values for clarity. While mass spectra are presented for nebulized MSA-NH_3 salt particles and those formed from the gas-phase reaction with MSA (Fig. 4.2), their low ionization efficiency compared to the amine-containing particles precludes quantification in any displacement experiments.

4.3.1.1 SPLAT-II Mass Spectra

In nebulized salt particles of MSA and the three amines, the dominant peak corresponds to $[M-H]^+$ for the amines (MA: m/z 30; DMA: m/z 44; TMA: m/z 58). This is consistent with reported electron ionization spectra[266] and well as typical UV ionization MS for alkylamines.[267–270] This peak is likely due to formation of the amine radical cation followed by loss of •H to yield $[R_2N{=}CH_2]^+$, as has been shown for the UV ionization of MA and DMA.[267,270] MSA-TMA particles give a strong peak at m/z 42 which may correspond to further loss of $•CH_3$ from the $[R_2N{=}CH_2]^+$ complex followed by loss of •H yielding $[H_2C{=}N{=}CH_2]^+$, as has been shown for electron ionization.[271]

Interestingly, for MSA-NH_3, -MA and -DMA salt particles, a large peak corresponding to $[M+CH_2-H]^+$ is also present. As this peak occurs for MSA-NH_3 particles (and is the dominant peak in this case), it is likely due to abstraction of CH_2 from MSA by the amine cation radical followed by loss of •H. This peak exists for MSA-TMA salt particles as well, but is quite small. This could indicate a role for –NH in the abstraction process, or may be a result of steric crowding. Similarly, Angelino and coworkers report mass spectra of particles con-

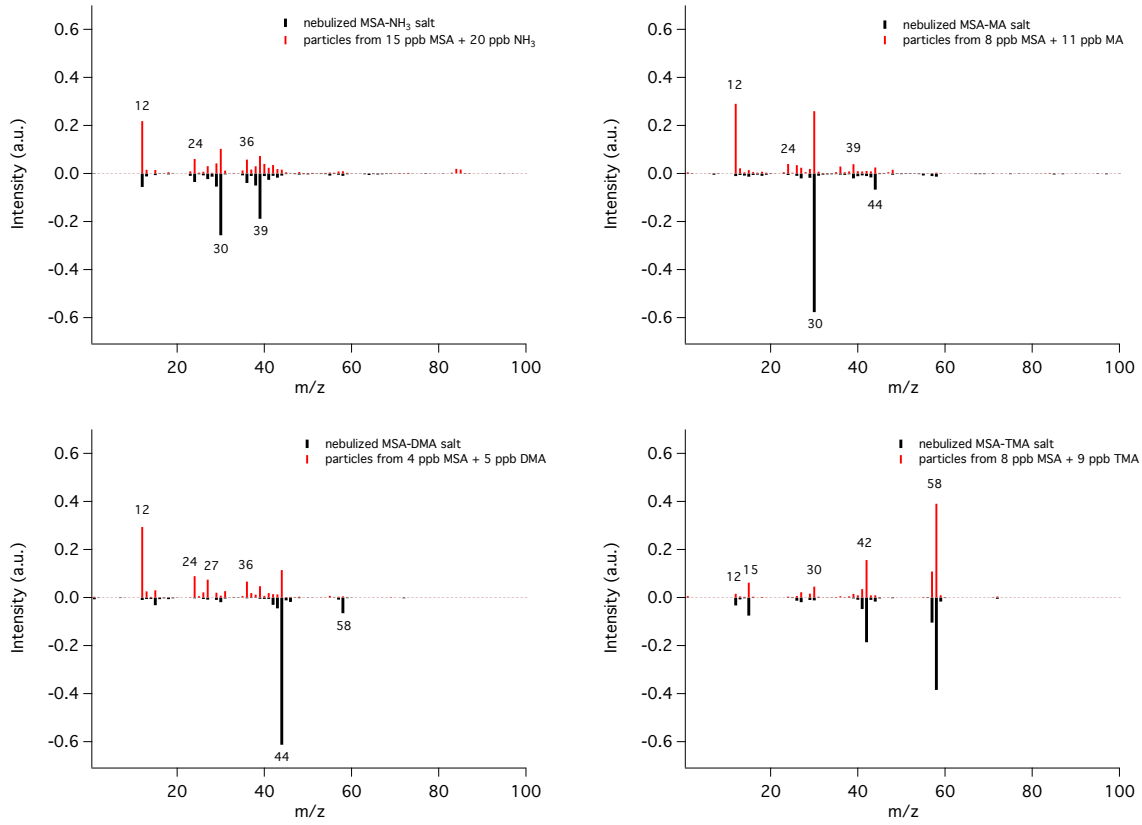

Figure 4.2: Average mass spectra normalized to the total SPLAT-II MS signal for both nebulized salt particles (black lines) and those formed by gas-phase reaction (red lines) for MSA and a) NH_3, b) MA, c) DMA and d) TMA. The signal from nebulized salt particles (black lines) are shown as negative values for clarity.

taining diethylamine (DEA) and TMA.[44] In DEA-water particles, a strong $[M+CH_2-H]^+$ was present, while for TMA-water particles, none was observed. In particles containing only amines and water, abstraction of CH_2 could only occur between amine molecules. For DEA-nitrate and TMA-nitrate particles, where amines could be expected to be coordinated with nitrate molecules with no available alkyl groups, no $[M+CH_2-H]^+$ were observed for either amine.[44]

Compared to particles nebulized from a salt solution, those formed by the gas-phase reaction of MSA with NH_3, MA and DMA showed increased fragmentation, with the dominant peak corresponding to C^+. In the case of MSA-TMA particles however, little difference in the

spectra is observed between the nebulized particles and those from the gas-phase reaction. One explanation for this could be water uptake on the particles. In the nebulized salt experiments the RH is ∼10%, while the gas-phase reactions of MSA and ammonia/amine were performed under dry conditions. Fragmentation of amine species from UV ionization is dependent on the ionizing conditions, including RH.[268,269,272] It could be expected that the particles formed from the gas-phase reaction under dry conditions would fragment differently than nebulized salt particles which would have taken up water, as is seen in the case of NH_3, MA and DMA. Of the four salts, TMA is the most hygroscopic, as can be seen in Figure 4.1. Even under the dry conditions of the gas-phase reaction to form particles, there may be sufficient water vapor available to adsorb to the MSA-TMA particles, reduce fragmentation, and result in little difference in the mass spectra between the nebulized MSA-TMA particles and those formed in the gas-phase reaction of MSA and TMA.

4.3.1.2 Particle Size Distributions

Size distributions determined by SMPS of the nebulized salt particles prior to displacement are shown in Figure 4.3a. SPLAT-II has a 50% cutoff efficiency for particles with d_p ∼80 nm.[125,157] Shown in the insets of Figure 4.3 are particles with d_p >80 nm, which should be accessible to SPLAT-II. (SPLAT-II size distributions for the nebulized salts are shown in Fig. 4.3c for comparison.) For particles formed from the nebulized salt solutions, little difference is seen between particles of different composition, with the bulk of the distributions being <80 nm, but having ∼500 particles cm^{-3} above 80 nm. Particles formed from the gas-phase reaction of MSA with ammonia or amine show more variability in size, especially in the case of MSA-NH_3 particles (Fig. 4.3b).

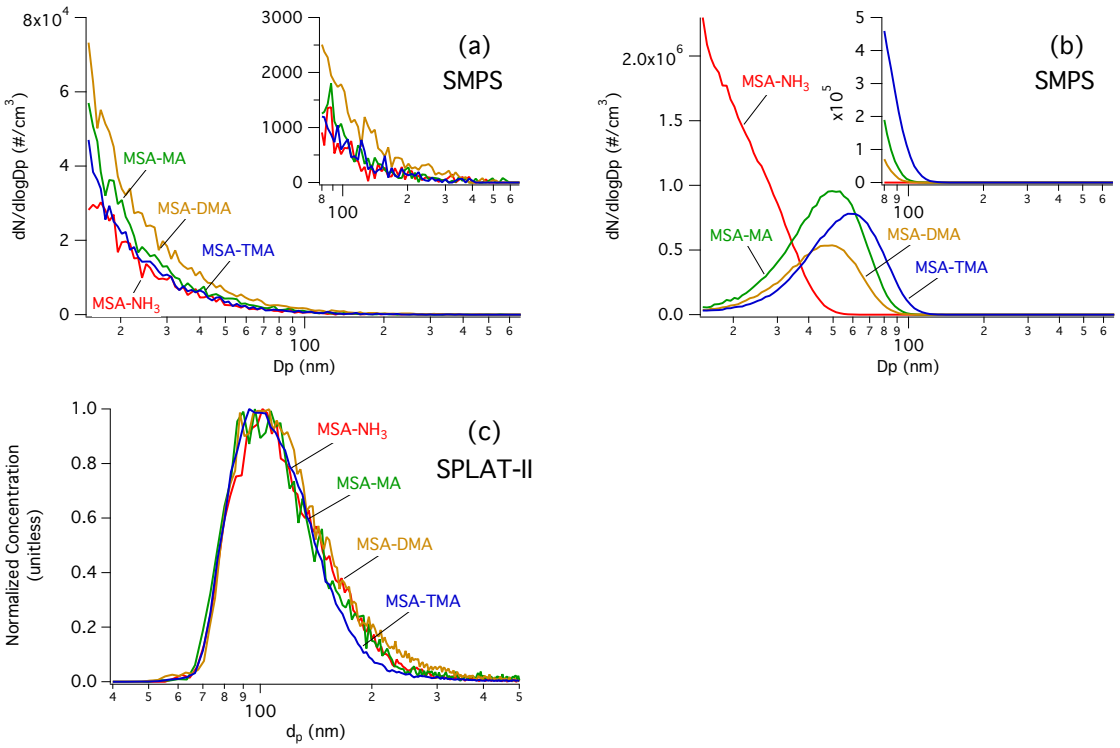

Figure 4.3: Particle size distributions for a) nebulized salt particles and b) particles formed from gas-phase reaction, prior to displacement experiments. Insets show particles with $d_p >$ 80 nm, corresponding to approximate distribution accessible to SPLAT-II. Shown in c) are the corresponding SPLAT-II size distributions for the nebulized salt particles, normalized to the peak concentrations for each distribution.

4.3.2 Amine-Amine Displacement

4.3.2.1 Particle Size Distributions

For nebulized MSA-NH_3 particles, size distributions were measured before and after addition of 500 ppb TMA (Fig. 4.4a). While number concentration decreases for particles <80 nm upon addition of the gas-phase amine, the size distribution visible to SPLAT-II remains relatively unchanged. The corresponding SPLAT-II size distributions show no significant change upon addition of gas-phase TMA (Fig. 4.4b). Thus, displacement rather than addition of the gas-phase amine is likely occurring (*i.e.*, the total amine + ammonia concentration in the particle-phase remains constant although the concentrations of the individual N-containing

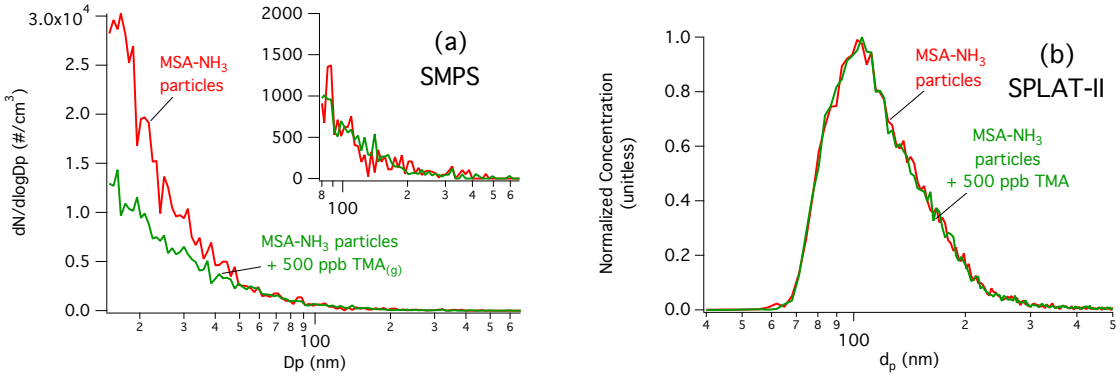

Figure 4.4: a) Particle size distributions of nebulized MSA-NH_3 particles before and after addition of gas-phase TMA. Inset shows particles with $d_p > 80$ nm, corresponding to approximate distribution accessible to SPLAT-II. b) Corresponding SPLAT-II size distributions, normalized to peak concentration for each distribution.

species in the particle phase change). For particles formed in the gas-phase, which showed wider variability in size and concentration depending on composition, the size distribution of MSA-MA and MSA-DMA particles shifts slightly to larger diameters after addition of gas-phase TMA (Fig. 4.5a,b). This shift is consistent with the continuous trend with time in the evolution of the particle size distribution, independent of the addition of TMA, as shown in Fig. 4.6. However, growth of particles by TMA (as opposed to displacement) cannot be ruled out as contributing to the observed shift in the particle size distribution, for particles formed by gas-phase reaction.

4.3.2.2 Quantification

To quantify amine-amine displacement, relative ionization efficiencies were calculated for MA, DMA and TMA particles. (As mentioned above, the ionization efficiency of NH_3 particles was too low to use in quantifying displacement.) A comparison was made of the average total single-particle SPLAT-II signal for MSA-MA, -DMA and -TMA particles of similar size. It was found that MSA-TMA particles had the highest average total signal (*i.e.*

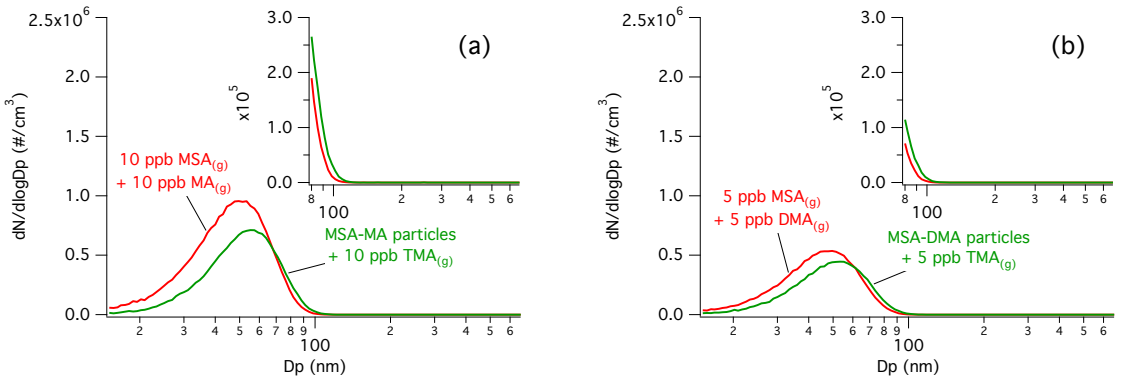

Figure 4.5: Size distributions of particles formed from the gas-phase reaction of a) 10 ppb MSA + 10 ppb MA and b) 5 ppb MSA + 5 ppb DMA, before and after addition of gas-phase TMA. Inset shows particles with $d_p > 80$ nm, corresponding to approximate distribution accessible to SPLAT-II.

ionization efficiency), a factor of 2.9 ± 0.4 $(2s)$ higher than MSA-MA particles, and a factor of 2.1 ± 0.4 $(2s)$ higher than those of MSA-DMA.

In displacement experiments, a gas-phase amine was introduced into a Teflon chamber containing particles composed of MSA and a different amine (either from nebulized salt or gas-phase reaction). The extent of amine-amine displacement was determined by monitoring the change in the SPLAT-II $[\mathrm{M}-\mathrm{H}]^+$ peaks for each of the amines (MA: m/z 30; DMA: m/z 44; TMA: m/z 58) upon introduction of the gas-phase displacing amine. The extent of displacement was determined using the following equation, a derivation of which is provided in appendix B.

$$\chi_a = \frac{f_{1b}^{\circ} - f_1}{\frac{e' e_a}{e_b}\left(f_1 - f_{1a}^{\circ}\right) - f_1 + f_{1b}^{\circ}}$$
$$f_{1a}^{\circ} \equiv \frac{h_{1a}^{\circ\prime}}{h_{1a}^{\circ\prime} + h_{2a}^{\circ\prime}} \qquad f_1 \equiv \frac{h_1'}{h_1' + h_2'} \qquad e' \equiv \frac{\left(h_{1a}^{\circ\prime} + h_{2a}^{\circ\prime}\right)}{\left(h_{1b}^{\circ\prime} + h_{2b}^{\circ\prime}\right)} \tag{4.1}$$

Here, χ_a is the fraction of the initial amine that remains in the particle phase (i.e. has not been displaced) and e_a is the ionization efficiency of the initial amine species. Numerical subscripts refer to a particular peak in the mass spectrum: 1 referring to the $[\mathrm{M}-\mathrm{H}]^+$ peak

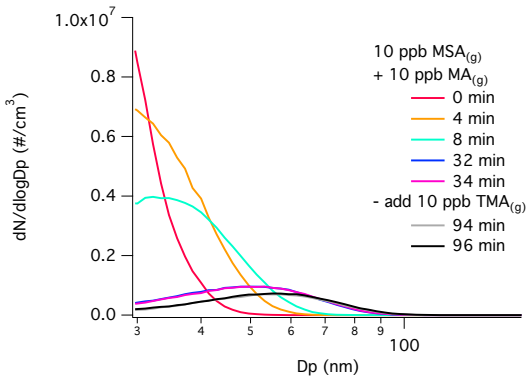

Figure 4.6: Evolution of the SMPS measured particle size distribution for the experiment starting with the gas-phase reaction of 10 ppb MSA with 10 ppb MA. All times shown are measured from introduction of MSA and MA. Addition of 10 ppb TMA occurred at ∼34 min reaction time.

for the initial amine and 2 to that for the displacing amine. Text subscripts refer to the initial (a) and displacing (b) amines. Normalized peak heights are designated $h^{'}$, such that for an experiment where TMA displaces MA, $h_{2a}^{\circ'}$ is the peak height of m/z 58 for pure MSA-MA particles and $h_1^{'}$ is the peak height of m/z 30 at any point during the experiment.

Using equation 4.1, the extent of displacement of the initial particle-phase amine is calculated as a function of reaction time for each set of conditions. The initial conditions and final extent of observed displacement are given in Table 4.3. The amount of initial gas-phase displacing amine in a given volume of air was in significant excess over the initial amount in the particle phase (at least a factor of five for the smallest gas-phase amine concentration and >100 times greater for amine concentrations in the hundreds of ppb). Gas-phase displacing amine concentrations can therefor be considered to be constant throughout the experiment.

In experiments starting with MSA-MA and MSA-DMA nebulized salts, despite the great excess of gas-phase TMA added, complete displacement does not occur even after allowing the reaction to continue overnight. This is in contrast to the reverse reactions of nebulized MSA-TMA salt particles with gas-phase MA or DMA, where TMA was completely displaced in less than 5 min. Comparable to this are findings by Qiu et al., who show displacement

Table 4.3: Initial conditions and extent of displacement for each experiment. Errors are calculated based on the $2s$ uncertainty in the ionization efficiencies.

Original Particle	Displacing Amine	[Displacing Amine] (ppb)	χ_a
Nebulized Salt + Gas-Phase Amine			
MSA-MA	TMA	9.7	0.98 ± 0.01
MSA-MA	TMA	500	0.32 ± 0.03
MSA-DMA	TMA	510	0.50 ± 0.05
MSA-TMA	MA	500	0.00 ± 0.00
MSA-TMA	DMA	350	0.03 ± 0.01
Gas-Phase Particle Formation + Gas-Phase Amine			
MSA-MA	TMA	8.2	0.73 ± 0.03
MSA-DMA	TMA	4.3	0.91 ± 0.02

of ammonia in $(NH_4)_2SO_4$ salt by gas-phase MA, DMA and TMA to be more favorable for less substituted amines (TMA < DMA < MA).[273]

4.3.2.3 Displacement of MA or DMA by TMA in Nebulized MSA-MA or MSA-DMA Salt Particles

As mentioned in section 4.3.1.1, experiments starting with nebulized salt are at ∼10% RH, and particles likely have taken up water vapor. As seen in Figure 4.1, the bulk MSA-amine salts take up water vapor at ambient (∼35%) RH to varying degrees with the MSA-TMA salt being the most hygroscopic. Based on the bulk properties of the salts, MSA-TMA particles are expected to be liquids, with rapid diffusion of gases into and out of the particles, consistent with the rapid, complete displacement observed here. Since gas-phase MA or DMA are in great excess in the experiments starting with nebulized MSA-TMA particles, essentially complete displacement occurs before the first SPLAT-II measurement ($<\sim$ 5 min).

In contrast, experiments starting with nebulized MSA-MA or MSA-DMA particles only result in partial displacement, despite introducing TMA in great excess. In the case of MSA-DMA particles with gas-phase TMA, displacement reached its final extent before the first SPLAT-II measurement (∼5 min reaction time). However, in experiments where gas-phase TMA was added to nebulized MSA-MA particles, while $> 40\%$ of the MA was replaced by TMA within 5 min reaction time, displacement continued for about an hour before reaching a final $\chi_{MA} = 0.32 \pm 0.03$ overnight, as seen in Fig. 4.7.

The observed time dependence of displacement of MA by TMA indicates that (at least up to $\sim$ 1 hr) this system has not reached an equilibrium state. Given that the added gas-phase TMA is in great excess, the lack of complete displacement of the particle-phase amine in the MSA-MA case clearly suggests that these particles are not liquid, unlike the MSA-TMA particles. (This may also be true for the displacement of DMA by TMA in MSA-DMA particles, although an equilibrium state cannot be ruled out in this case.) Similar effects related to particle phase have been seen for amine displacement in $(NH_4)_2SO_4$ particles exposed to triethylamine under various RH conditions.[198]

If MSA-MA particles were viscous solids or semi-solids, with diffusion in the particle-phase limiting displacement, it would be expected that χ_{MA} would decrease more rapidly for smaller particles. Figure 4.8a shows the fraction of MSA remaining in the particles as a function of particle size and reaction time, indicating that within experimental error, there is no significant dependence of the extent of displacement on particle size. This suggests that MSA-MA particles cannot be described simply as having one homogeneous, viscous phase. In experiments on displacement of NH_4^+ by DMA in small clusters of NH_4HSO_4, Bzdek et al.[197] show that there is a kinetic limitation to displacement of 'core' NH_4^+ molecules compared to those at the surface. Analogously, the larger MSA-MA particles used here could be treated as having a solid, crystalline core which does not undergo significant displacement within the time scale of these experiments, buried inside a 'shell' of gradually decreasing viscosity

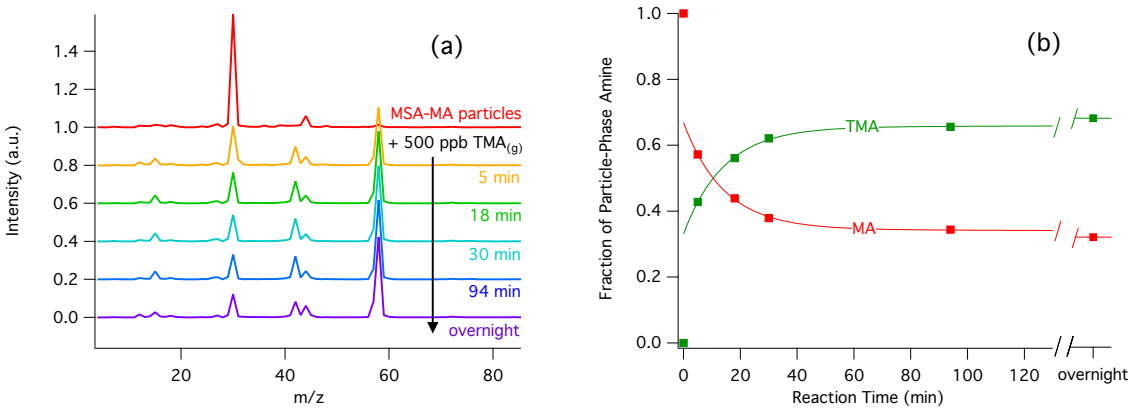

Figure 4.7: Time resolved (a) SPLAT-II mass spectra and (b) χ_{MA} and χ_{TMA}, for the reaction of nebulized MSA-MA salt particles with 500 ppb TMA.

which does undergo exchange with the gas-phase. For spherical particles, the data in Fig. 6 can be used to roughly calculate the ratio of the 'shell' thickness (r_{shell}) compared to the diameter of the particle (d_p), assuming the amine densities of the core and shell are the same, and approximating the system as having a clearly defined boundary between the 'core' (undisplaced) and 'shell' (displaced). Figure 4.8b shows that this ratio remains constant at $15 \pm 6\%$ across all particle sizes after 94 min reaction time (purple triangles).

The formation of an amorphous salt structure (as expected for the MSA-MA particle 'shell') may be the result of the nebulization process, where particles are formed under wet conditions and subsequently diluted with dry air. Similarly, particles formed by atomization of a $NaNO_3$ salt solution, were shown to be amorphous rather than crystalline by environmental scanning electron microscopy,[274] and SPLAT studies.[275,276]

4.3.2.4 Displacement in Particles Formed by Gas-Phase Reaction

In experiments starting with nebulized salt particles, an assumption of constant gas-phase concentration of the displacing amine could be made (sec. 4.3.2.2). This assumption cannot be made for experiments starting from particles formed in the gas-phase as the initial

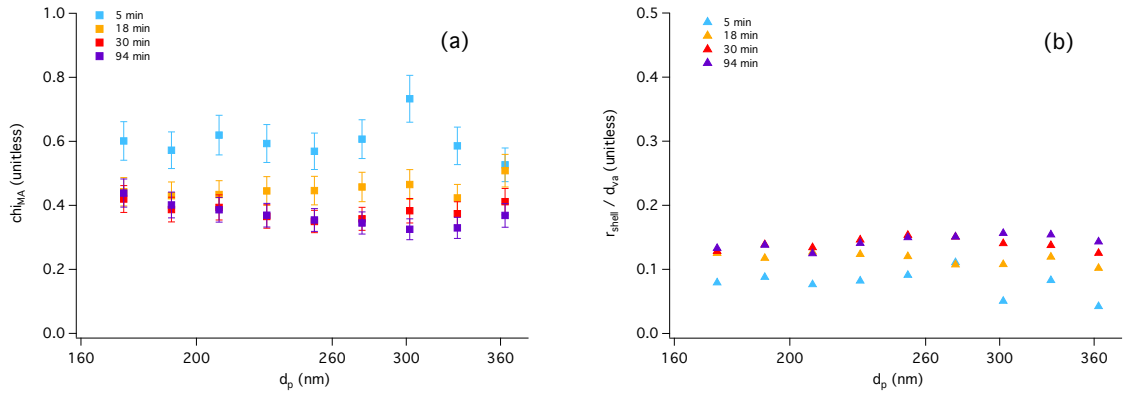

Figure 4.8: a) Dependence of displacement on particle size. Error bars are based on $1s$ uncertainty of particle mass spectra. b) Thickness of displaced shell (r_{shell}) relative to particle diameter (d_p) assuming spherical particles of uniform density.

amounts of particle-phase MA or DMA are on the same order as those of the initial gas-phase TMA. Therefore, quantitative arguments of displacement in these experiments are difficult, but some general observations may be made. First, complete displacement by TMA is not seen in either case as was seen with the nebulized salt particles. This is consistent with the core-shell structure of MSA-MA and MSA-DMA particles proposed in section 4.3.2.3. Also, the same trend is seen as with nebulized salt particles in which TMA displacement is greater for MSA-MA particles than for those of MSA-DMA.

As seen in Figure 4.9, MSA-MA particles accessible to SPLAT-II are smaller when formed in the gas-phase under 'dry conditions (gas-phase reaction; dashed green line) then when nebulized (solid green line). These smaller particles undergo greater displacement ($\chi_{MA} = 0.73$) than do the larger particles from nebulized salt solutions ($\chi_{MA} = 0.98$), when the added gas-phase TMA is $8-10$ ppb (Table 4.3). This is the case despite the drier conditions (where less water would be expected to be on the particle surface) and the lower initial concentration of the gas-phase displacing amine relative to initial concentration of the particle-phase amine in a given volume of air (due to the high number concentration of particles in the dry case; Fig. 4.9). This highlights the importance of particle size as well as water in predictions of amine displacement.

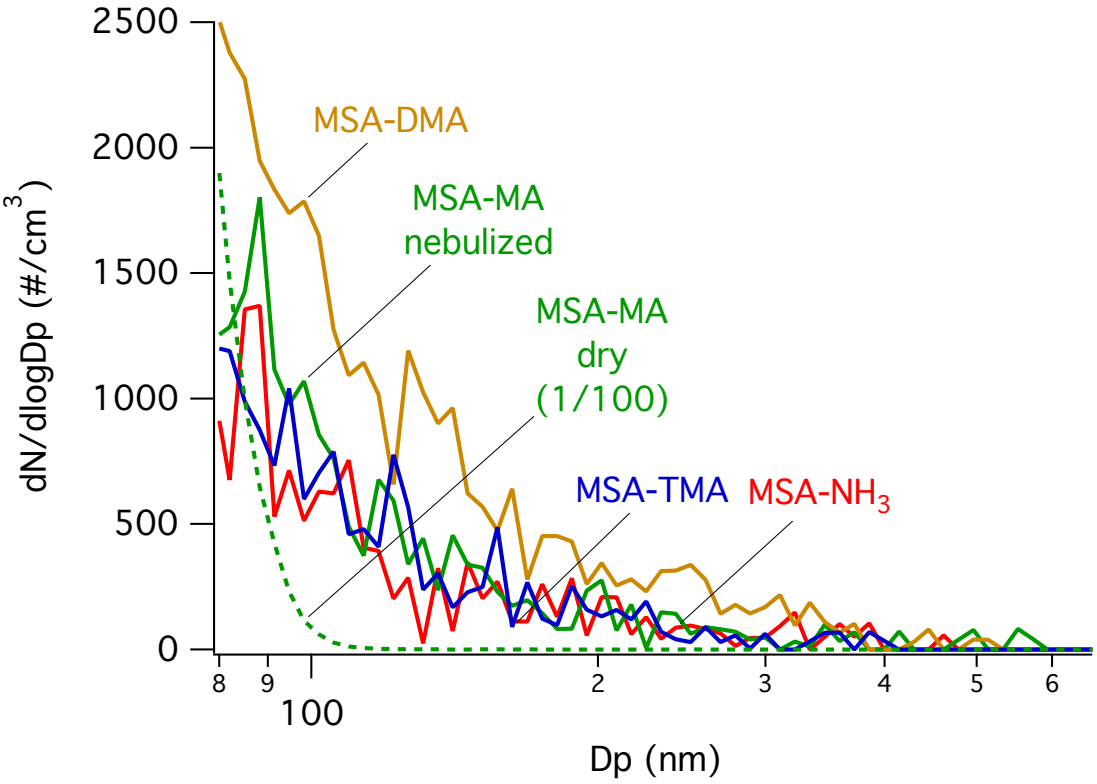

Figure 4.9: SMPS size distributions for particles formed from nebulized salt solutions (solid lines) and from the gas-phase reaction of MSA with MA (dashed line; scaled by 1/100).

4.3.2.5 Theoretical Calculations of MSA-MA, MSA-DMA and MSA-TMA Clusters

Theoretical calculations of clusters of MSA with MA, DMA, and TMA were performed by Dr. Mychel Varner of the Gerber Group at UCI in order to investigate the structure and energetics that may lead to the differences in water uptake observed in the bulk salts, and suggested by the displacement experiments.[277] Figure 4.10 present two stable isomers for clusters of MSA with TMA (a,b), DMA (c,d) and MA (e,f). A full discussion of the theoretical results is described in ref. 277. Briefly, as can be seen in Fig. 4.10, the less substituted amines are capable of forming more complex H-bonding networks, which would be expected to form denser, more stable structures, when extrapolated to a larger crystal structure. Stable crystal structures have been experimentally determined for MSA with

NH_3[278] or diisopropylamine,[279] both of which have a cyclic H-bonding network similar to that shown here for MSA-MA and MSA-DMA with C_i symmetry (Fig. 4.10c,e). TMA, having the fewest N-bound hydrogens, does not form such a structure but rather forms only ion pairs (Fig. 4.10a) or a weakly-bound hydrogen bridge structure (Fig. 4.10b),[280] and could therefor be expected to form a weaker crystal structure than either MSA-MA or MSA-DMA, which then would be more susceptible to water uptake. Thus, theoretical calculations support the trend in hygroscopicity of the bulk salts (Fig. 4.1) and the experimentally observed amine displacement.

4.3.3 Atmospheric Implications

Amines are increasingly being recognized as key players in new particle formation and growth.[15,37,42–44,49,126,142,149,260,281] Modeling particle growth from these small sizes up to sizes where particles can act as cloud condensation nuclei requires an understanding of the competition between co-condensing amine species. Amine exchange in ammonium-acid particles has been identified as a favorable process in both small (<3 nm)[195,196] and large (15 – 35 μm)[198] particles as well as the bulk ammonium salts[273,282] with implications for particle growth. Equally important is understanding the effect of particle-phase amines on the physical properties of particles (i.e. phase, hygroscopicity) which affects both aminium/ammonium displacement[198] and further growth.[265,283–285] This work presents evidence of amine-amine exchange in MSA-amine salt particles ∼100 nm in diameter that indicates kinetic limitations to displacement based on species-dependent physical properties of the aerosol particles.

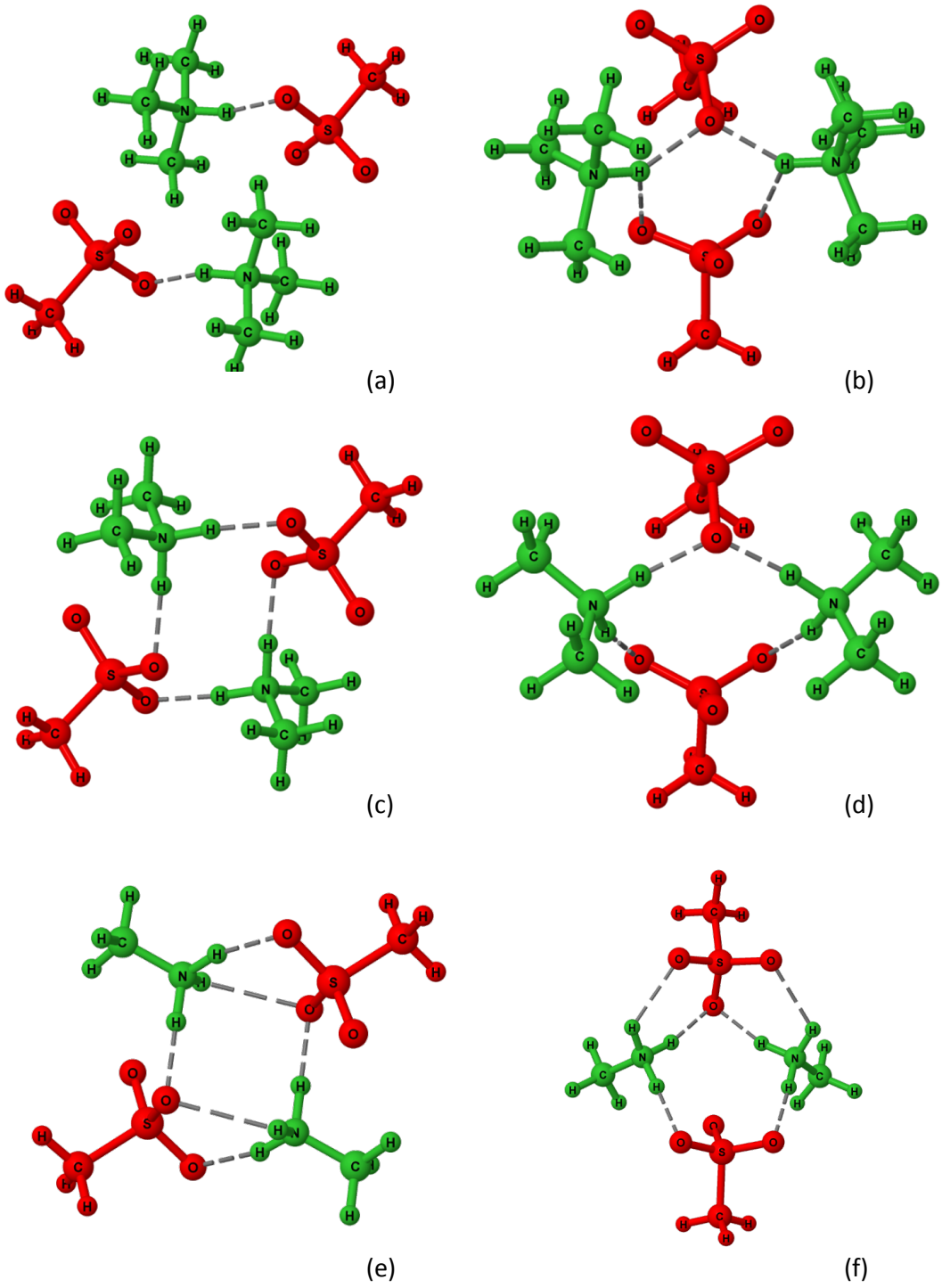

Figure 4.10: Theoretical calculations performed by Dr. Mychel Varner of the Gerber Group at UCI of $[MSA]_2[TMA]_2$ with a) C_i and b) C_s symmetry, $[MSA]_2[DMA]_2$ with c) C_i and d) C_s symmetry, and $[MSA]_2[MA]_2$ with e) C_i and f) C_s symmetry.[277]

Chapter 5

Flow Reactor Model

5.1 Research Goals

A kinetics model for particle formation and growth is under development to describe the MSA, amine, and water system investigated in chapter 2. This model integrates the GDE, described above, over the experimental reaction times used in the flow reactor studies and evaluates the suitability of the semi-empirical kinetics model for particle formation described in chapter 2 while accounting for particle growth, coagulation and wall loss. The development of this model is discussed in this chapter.

5.2 Model Development

This model integrates the general dynamic equation (eq. 1.1) over the reaction times accessible to the flow reactor system while keeping track of gas-phase precursor concentrations and size- and composition-resolved particle concentrations. The model code is written in C and makes use of the `gsl_odeiv2` functions available as part of the Gnu Scien-

tific Library[286] for integration of ordinary differential equations. The integration uses the `gsl_odeiv2_step_msbdf` stepper function, which is a variable-coefficient linear multistep backward differentiation formula method in Nordsieck form, and is suitable for stiff mathematical equations, such as are often encountered in systems of chemical kinetics equations.

5.2.1 Modeled Species

In addition to the three gas-phase precursor species (MSA, amine and water), the concentrations of the intermediate clusters used in the kinetics mechanism for particle formation described in section 2.3.4 are calculated as a function of reaction time t. Specifically, these clusters are the MSA hydrate, MSA-amine-water trimer, and the dry MSA-amine dimer. Gas-phase molecule and cluster concentrations are designated $y_g(t)$, where $g = 1, \ldots, n$. In this particular case of three gas-phase molecules and three clusters, $n = 6$. Particle-phase species are calculated as concentrations of MSA, amine or water in one of s discreet particle size bins, and labeled $y_{(i,q)}(t)$ where $i = 1, \ldots, s$ and $q = 1, \ldots, m$. Here, $m = 3$ and q represents one of the three particle phase species, either MSA, amine or water. All species concentrations are tracked in units of # cm^{-3}, *i.e.* number of molecules of gas- or particle-phase species per cm^3 of air. Particle number concentrations $p_i(t)$ are then calculated as follows.

$$p_i(t) = \left[\sum_{q=1}^{m} \frac{y_{(i,q)} MW_q}{N_A \rho_q} \right] \frac{1}{v_i} \tag{5.1}$$

Here, MW_q is the molecular weight of species q, ρ_q is its bulk density, N_A is Avagadro's number, and v_i is the volume of a single particle in size bin i.

As described by Sandu and Borden,[287] this treatment assumes that the continuous particle size distribution, $p(r,t)$, can be approximated as the linear combination of a discreet set of concentrations, p_i, of particles of radius r_i, such that,

$$\begin{aligned} p(r,t) &= \sum_{i=1}^{s} p_i(t)\phi_i(r) \\ \phi_i(r) &= \delta(r - r_i), \end{aligned} \tag{5.2}$$

where $\phi_i(r) = 0$ for $r \neq r_i$ and $\phi_i(r) = 1$ for $r = r_i$, and is referred to as size bin i. The effects of this discretization in particle-size space can be inferred by evaluating the effects of varying the number of size bins, s, on the modeled size distribution. This evaluation will be included in a future model sensitivity analysis.

Equation 5.1 further requires that particle densities can be approximated by a weighted average of the component bulk densities. The density of a concentrated salt particle would be expected to deviate from this simple approximation. An evaluation of the effects of this variation is made by two approaches. In addition to evaluating the model's sensitivity to particle densities, a comparison can be made to experimentally determined densities of the MSA-amine particles at a known RH.[277] The results of such a comparison will be included in a future model sensitivity analysis.

5.2.2 General Dynamics Equation

A formulation of the general dynamics equation in terms of multicomponent aerosols of discreet size is given in equation 5.3.

$$\frac{d}{dt}y_x(t) = \left(\frac{\partial y_x(t)}{\partial t}\right)_{\text{nucleation}} + \left(\frac{\partial y_x(t)}{\partial t}\right)_{\text{growth}} + \left(\frac{\partial y_x(t)}{\partial t}\right)_{\text{coagulation}} + \left(\frac{\partial y_x(t)}{\partial t}\right)_{\text{wall loss}} \tag{5.3}$$

Here, $y_x(t)$ is either gas-phase species concentration $y_g(t)$ or particle-phase species concentration $y_{(i,q)}(t)$. This equation along with the associated Jacobian is calculated for each species y at each time step. The individual components of equation 5.3 are discussed in the following sections.

5.2.3 Nucleation

As part of the analysis of the flow reactor experimental data, a kinetics mechanism for particle formation from MSA, amines and water was developed and is described in detail in section 2.3.4. The reaction scheme shown in Figure 2.10 is used as the basis of the nucleation portion of the GDE. Forward rate constants (k_1, k_2, k_{-3}) are taken to be collision limited, with reverse rate constants (k_{-1}, k_{-2}, k_3) calculated based on equation 2.2. Rate constants k_4–k_8 are fit to the experimental data. Calculated values for all the rate constants in the particle formation mechanism are shown in Table 2.5.

One important difference exists between the kinetics mechanism described in section 2.3.4 and that used here. In the mechanism described in section 2.3.4, the products of reactions 4–8 are taken to be particles of a detectable size ($d_p >\sim 5.8$ nm). Here, these reaction products are taken to be the clusters of MSA, amine and water expected from the addition of a single gas-phase molecule to the MSA-amine or MSA-amine-water clusters (Fig. 2.10). These clusters, or 'initial particles,' are then subject to condensational growth and coagulation until they reach sizes detectable by the SMPS system used. The result is that the experimentally-

fit rate constants used here are larger than those in Table 2.5, however a comparison can be made between the results of the comprehensive flow reactor model and the integration of the kinetics mechanism described in section 2.3.4.

The contribution to the rate of change in concentrations of the gas-phase and cluster species from each reaction in the nucleation mechanism are described in equation 5.4.

$$\begin{aligned} &\text{for A} + \text{B} \xrightarrow{k_x} \text{C where C is an intermediate cluster} \\ &\left(\frac{\partial y_A(t)}{\partial t}\right)_{\text{nucleation}} = -k_x[y_A(t)][y_B(t)] \\ &\left(\frac{\partial y_B(t)}{\partial t}\right)_{\text{nucleation}} = -k_x[y_A(t)][y_B(t)] \\ &\left(\frac{\partial y_C(t)}{\partial t}\right)_{\text{nucleation}} = k_x[y_A(t)][y_B(t)] \end{aligned} \tag{5.4}$$

However, when the product of the reaction is an 'initial particle,' the contribution to the rates of change of the involved species is described by equation 5.5.

$$\begin{aligned} &\text{for A} + \text{B} \xrightarrow{k_x} \text{C where C is an 'initial particle'} \\ &\left(\frac{\partial y_A(t)}{\partial t}\right)_{\text{nucleation}} = -k_x[y_A(t)][y_B(t)] \\ &\left(\frac{\partial y_B(t)}{\partial t}\right)_{\text{nucleation}} = -k_x[y_A(t)][y_B(t)] \\ &\left(\frac{\partial y_{(i,q)}(t)}{\partial t}\right)_{\text{nucleation}} = n_{(q,C)}k_x[y_A(t)][y_B(t)] \text{ for } q = 1, \ldots, m \end{aligned} \tag{5.5}$$

Here, $n_{(q,C)}$ is the number of molecules of species q in cluster C, and the size bin i is determined by an approximation of the volume of cluster C based on a linear combination of the densities of its components as described in section 5.2.1.

5.2.4 Growth

Models of growth in multicomponent aerosol systems are often derived in terms of the volume concentration,[287] $V_q(v,t)$, of particle-phase species q where v is the volume of an individual particle. Sandu and Borden present an equation for the growth portion of the GDE for a multicomponent aerosol that is given as equation 5.6.

$$\frac{\partial V_q(v,t)}{\partial t} = -\partial \left[V_q(v,t) \sum_k^m I_k(v) \right] / \partial v + V(v,t) I_q(v)/v \tag{5.6}$$

Here, m is the number of particle-phase species. For the MSA, amine, H_2O system, $m = 3$. The growth rate $I_q(v,t)$ is defined as the rate of change in volume of a single particle of volume v due to uptake of gas-phase species q, as shown in equation 5.7.

$$\frac{\partial v_q(v,t)}{\partial t} = I_q(v,t) v \tag{5.7}$$

In the semi-discretized system, the volume concentration is related to the number concentration of species q by equation 5.8.

$$\left(\frac{\partial y_{(i,q)}(t)}{\partial t} \right)_{\text{growth}} = \frac{\partial V_{(i,q)}(t)}{\partial t} \frac{\rho_q N_A}{MW_q} \tag{5.8}$$

Here, $V_{(i,q)}(t)$ is the total volume concentration of particle-phase species q in size bin i. A first order, backward in size-space semi-discretization of equation 5.6 yields equation 5.9.

$$\frac{\partial V_{(i,q)}(t)}{\partial t} = \sum_{k=1}^{m} \left[(V_{(i,q)} I_{(i,k)} - V_{(i-1,q)} I_{(i-1,k)})/\Delta v + V_{(i,k)} I_{(i,q)}/v_i \right] \tag{5.9}$$

The change in volume $(v_i - v_{i-1})$ is designated Δv, where v_i is the volume of particles in size bin i. What is then left to determine is the growth rate, $I_{(i,q)}(t)$. In the simplest approximation, each gas-phase species q condenses onto existing particles at a rate that depends only on its gas-phase concentration $y_g(t)$, such that,

$$I_{(i,q)}(t) = k^q_{\text{cond}} y_g(t) \frac{MW_q}{N_A \rho_q} \frac{1}{v_i}, \tag{5.10}$$

where k^q_{cond} is the second-order rate constant for condensational uptake. This rate constant is typically calculated as a collision limited reaction scaled by an effective uptake coefficient $\gamma(r, u_q)$ that includes a species-dependent mass accommodation coefficient, u_q.[288] The definition of $\gamma(r, u_q)$ is given by Verheggen.[288] The condensation rate constant can then be calculated as shown in equation 5.11.

$$k^q_{cond} = \pi \gamma(r_p, u_q) \left(r_p + r_g\right)^2 \nu_{(q,i)} \tag{5.11}$$

Here, r_p and r_g are the hard sphere collision radii of the particle and gas-phase species, respectively, and $\nu_{(q,i)}$ is their mean relative speed. A more complete treatment accounts for evaporation of particle-phase species, as shown in equation 5.12.

$$I_{(i,q)}(t) = \left[k^q_{\text{cond}} y_g(t) - k^q_{\text{evap}}\right] \frac{MW_q}{N_A \rho_q} \frac{1}{v_i}, \tag{5.12}$$

Here, k^q_{evap} is a first-order evaporation rate constant. In this system, MSA can be assumed to condense irreversibly onto particles due to its low vapor pressure, making $k^{MSA}_{\text{evap}} = 0$. Water will evaporate from particles based on its activity in the particle phase, and evaporation of particle-phase amines can be determined from their Henry's Law constants. These two cases are discussed below.

5.2.4.1 Water Evaporation

At equilibrium, condensation of water from the gas-phase is balanced by evaporation of particle-phase water based on its activity in solution, α_q ($q = H_2O$), such that,

$$k^q_{\text{cond}} y^0_g \alpha_q = k^q_{\text{evap}}. \tag{5.13}$$

In equation 5.13, y^0_g is the equilibrium vapor pressure of water. Substituting equation 5.13 into equation 5.12 yields:

$$I_{(v_i,q)}(t) = \left[k^q_{\text{cond}} y_g(t) - k^q_{\text{cond}} y^0_g(t)\alpha_q\right] \frac{MW_q}{N_A \rho_q}, \tag{5.14}$$

The Kelvin Effect increases evaporation from a liquid particle due to the free energy gained in reducing its radius.[7] This effect can be formulated as an increase in saturation vapor pressure, as shown in equation 5.15.

$$y^{0'}_g = y^0_g e^{\left(\frac{2\sigma_q MW_q}{r_i \rho_q N_A k_B T}\right)} \tag{5.15}$$

Here, σ_q is the surface tension of the particle (approximated as the surface tension of water), k_B is the Boltzmann constant, and T is temperature. Substituting the revised saturation vapor pressure, $y^{0'}_q$ in for y^0_q in equation 5.14 and rearranging yields equation 5.16.

$$I_{(v_i,q)}(t) = \left[y_q(t) - y^0_g(t)\alpha_q e^{\left(\frac{2\sigma_q MW_q}{r_i \rho_q N_A k_B T}\right)}\right] k^q_{\text{cond}} \frac{MW_q}{N_A \rho_q}, \tag{5.16}$$

The final value to calculate is α_q, for which we use the activity model of Dutcher et al.[232]. Equation 5.17 presents their equation for solute molality as a function of water activity (ref[231,232] Table 3, $n = 2$) rearranged to solve for water activity.

$$\alpha_q = \frac{1}{[2(K_A)^2(-1+C_{A,1})]}\Bigg(-2K_A + C_{A,1}K_A - C_{A,1}K_A m_A MW_q r_A + \sqrt{C_{A,1}}K_A\sqrt{C_{A,1} + 4m_A MW_q r_A - 2C_{A,1}m_A MW_q r_A + C_{A,1}(m_A)^2(MW_q)^2(r_A)^2}\Bigg) \tag{5.17}$$

The three parameters in their work for number of sorbed layers, $n = 2$, K_A, r_A and $C_{A,1}$ are taken as input parameters to the model. To the best of the author's knowledge, no experimental data on water activity in MSA-amine salt solutions exist, however an approximation may be made using the fit obtained by Dutcher et al. for NH_4NO_3, $K_A = 1.0036$, $r_A = 1.484$ and $C_{A,1} = 0.733$. The implications of this approximation will be included in a future model sensitivity analysis.

5.2.4.2 Amine Evaporation

Evaporation of amines from the particle phase can be calculated using Henry's Law, shown in equation 5.18.

$$y_g(t) = \frac{y_{(i,q)}(t)}{k_H y_{i,H_2O}(t)}\frac{N_{air}}{MW_{H_2O}} \tag{5.18}$$

Here, $y_g(t)$ is the gas-phase amine concentration, $y_{(i,q)}(t)$ is the particle-phase amine concentration and $y_{(i,H_2O)}(t)$ is the particle-phase water concentration. The Henry's Law constant, k_H for the amine is given in units of mol kg^{-1} atm^{-1}, and $N_{air} = 2.46 \times 10^{19}$ molecules

cm^{-3} atm^{-1} is the number concentration of air. At equilibrium, Henry's Law applies and the rate of condensation of gas-phase amine equals the rate of evaporation of amine from the particle-phase, such that,

$$k^q_{\text{evap}} = k^q_{\text{cond}} y_g \tag{5.19}$$

Substituting equation 5.18 into equation 5.19 yields the equation for the rate constant of evaporation given in equation 5.20.

$$k^q_{\text{evap}} = k^q_{\text{cond}} \frac{y_{(i,q)}(t)}{k_H y_{i,H_2O}(t)} \frac{N_{air}}{MW_{H_2O}} \tag{5.20}$$

Combining equations 5.12 and 5.20 with the rough approximation that condensed-phase amine that is neutralized by MSA will not evaporate, gives the full condensational growth equation for amine species,

$$I_{(v_i,q)}(t) = \left[y_g(t) - \frac{y_{(i,q)}(t) - y_{(i,MSA)}(t)}{k_H y_{i,H_2O}(t)} \frac{N_{air}}{MW_{H_2O}} \right] k^q_{\text{cond}} \frac{MW_q}{N_A \rho_q} \frac{1}{v_i}, \tag{5.21}$$

5.2.4.3 Combined Growth Equations

The rates of growth for MSA ($k_{evap} = 0$), water (eq. 5.16) and amine (eq. 5.21) are then,

$$I_{(v_i,MSA)}(t) = y_{MSA}(t) k_{\text{cond}}^{MSA} \frac{MW_{MSA}}{N_A \rho_{MSA}} \frac{1}{v_i} \tag{5.22a}$$

$$I_{(v_i,H_2O)}(t) = \left[y_{H_2O}(t) - y_{H_2O}^0(t) \alpha_{H_2O} e^{\left(\frac{2\sigma_{H_2O} MW_{H_2O}}{r_i \rho_{H_2O} N_A k_B T} \right)} \right] k_{\text{cond}}^{H_2O} \frac{MW_{H_2O}}{N_A \rho_{H_2O}} \tag{5.22b}$$

$$I_{(v_i,amine)}(t) = \left[y_{amine}(t) - \frac{y_{(i,amine)}(t) - y_{(i,MSA)}(t)}{k_H y_{i,H_2O}(t)} \frac{N_{air}}{MW_{H_2O}} \right] k_{\text{cond}}^{amine} \frac{MW_{amine}}{N_A \rho_{amine}} \frac{1}{v_i} \tag{5.22c}$$

5.2.5 Coagulation

The change in volume concentration of particle-phase species q in particles of volume v due to coagulation is given by Sandu and Borden as,[287]

$$\frac{\partial V_q(v,t)}{\partial t} = \int_0^v \frac{\beta_{(v-w,w)}}{w} V_q(v-w,t) V(w,t) dw - V_q(v,t) \int_0^\infty \frac{\beta_{(v,w)}}{w} V(w,t) dw \tag{5.23}$$

Here, the rate constant for the coagulation reaction of particles of volume $v - w$ and w to form particles of volume v is $\beta_{(v,w)}$, which takes the form of a second order rate constant. As described in section 5.2.4, $m = 3$ is the number of particle phase species for the MSA, amine, H_2O system. In the semi-discretized system, this becomes,[287]

$$\frac{\partial \mathbf{V}_q}{\partial t} = \left[(\mathbf{B} - \mathbf{C}) \times \sum_k^m \mathbf{V}_k \right] \cdot \mathbf{V}_q \tag{5.24}$$

The vector $\mathbf{V}_q = [V_{(0,q)}, V_{(1,q)}, \ldots V_{(n,q)}]^T$ is the volume concentration vector for particle-phase species q in n size bins. The tensors $\mathbf{B}$ and $\mathbf{C}$ are the production and loss terms for coagulation, respectively, and are defined in Sandu and Borden.[287]

The rate at which particles coagulate has been measured experimentally for particles of sulfuric acid and water.[234] As no experiments on coagulation in the MSA/amine/H_2O system have been reported, the parameterization of $\beta_{(v,w)}$ by Chan and Mozurkewich for sulfuric acid particles is used in this work.[234] This was chosen over the more computationally expensive, purely theoretical treatment of Sceats that requires knowledge of the Hamaker constant for the interacting particles, which has not been reported for this system.[235]

A scalar constant C_{coag} is used in the flow reactor model, to allow for differences in the role of long-range forces on coagulation in the MSA/amine/H_2O system compared to that of sulfuric acid/H_2O. This constant is taken as an input parameter to the model.

5.2.6 Wall Loss

Fuchs presents an equation for aerosol wall loss in a cylinder under laminar flow conditions,[243] which is given as equation 5.25.

$$\frac{n}{n_0} = 1 - 2.56\mu^{2/3} + 1.2\mu + 0.177\mu^{4/3} \tag{5.25}$$

Here, $\mu = D(v)x/R^2\tilde{v}$, where $D(v)$ is the particle diffusion coefficient of particles of volume v, x the length of the cylinder, R the radius of the cylinder, and $\tilde{v}$ the mean linear flow velocity. The value n/n_0 is the fraction of particles of volume v exiting the cylinder relative to the number of particles introduced. For particles formed in the gas phase in a cylinder, such as in the aerosol flow reactor used here, this equation does not strictly apply. Therefore,

wall loss in the flow reactor model is parameterized as the linear portion of this equation, 1.2μ, scaled by a constant C_{wl}, which is taken as an input parameter to the model, and is based on measured particle loss in the flow reactor, as described in section 2.3.4.1.

5.2.7 Model Organization

The code for the flow reactor model is contained in four files, which are described in the following sections.

5.2.7.1 `ft_sci_eq.c`

This file contains functions that return values for a variety of species and reaction properties (*i.e.* Brownian diffusion coefficients, reduced masses, collision limited rate constants, etc.). These functions are called in the calculation of the derivatives of species concentration by time and the Jacobian required by the stepper function.

5.2.7.2 `ft_ode_int.h`

This is a header file containing constants, definitions of the functions in `ft_ode_int.c` and `ft_sci_eq.c`, and the definitions of the two structures used, `ft_system` and `species`. Each model run requires one instance of `ft_system` which contains model parameters, such as the final reaction time and flow reactor radius. An instance of `ft_system` also includes an array of `species`, one for each gas-phase species, cluster and 'initial particle' used in the nucleation mechanism described in section 2.3.4 and discussed in section 5.2.3. Each instance of `species` contains properties of one of these species, such as hard shell collision radius and molecular weight.

5.2.7.3 `ft_ode_int.c`

This file contains the function called to run the model, `FT_ode_int`, which takes as parameters, an instance of `ft_system` containing the model parameters as described above, a string variable containing a text prefix to use for the generated output files, an empty two dimensional array of concentration by species and time, and a one-dimensional array containing particle diameters associated with the discreet size bins described in section 5.2.1. At the end of the model run, the concentration array is filled with the modeled species concentrations at a certain number of reaction times, and a set of output files is generated. These contain gas-phase species concentrations by time, particle concentrations by size and time, particle composition by size and time, particle-phase water activity by particle size and time, and a raw output file containing all values in the two-dimensional concentration array.

Also contained in `ft_ode_int.c` are functions that generate the coagulation tensors $\mathbf{B}$, $\mathbf{C}$, the wall loss rate constants $k_{wl}(v_i)$, and the time-independent portions of the growth rate constant $I_{(i,q)}(t)$, described in sections 5.2.5, 5.2.6 and 5.2.4, as well as functions that calculate time derivatives (`func`) and the Jacobian (`jac`) for the modeled species concentrations at each time step.

5.2.7.4 `run_ft_ode_int.c`

The previous three files are designed to be able to be implemented in an existing model, which can run the model over any time step Δt by loading an instance of `ft_system` with the model parameters and calling the function `FT_ode_int` as described above. In the absence of such a superstructure, this file provides the framework to load model parameters from a text input file, and run one or multiple instance of the model, perform sensitivity analyses, or perform diagnostic tests on the model. A sample input file is given in Appendix A along with a description of each input value.

Chapter 6

Conclusions

Atmospheric aerosol particles reduce visibility, have adverse effects on human health, and influence the Earth's climate through their ability to scatter and absorb radiation and affect cloud properties. Modeling the evolution of aerosol systems requires identification of the major gas-phase precursors that contribute to particle formation and growth, accurate measurement of their ambient concentrations, and an understanding of the mechanisms by which they react to form and grow particles.

This work identifies the reaction of MSA, amines and H_2O as a potentially important source of particle formation in the atmosphere. A simple kinetics model for particle formation from this system is presented. This model is based on the results of laboratory experiments using a unique flow reactor to investigate particle formation, as well as quantum chemical calculations of the structures and energies of formation of key intermediate clusters. This model is computationally inexpensive, making it suitable for inclusion in large scale regional and global air quality models. A more comprehensive model that includes the competing effects of particle growth, coagulation and wall loss is under development to further validate the kinetics mechanism, and aid in the evaluation of future flow reactor experiments.

Also presented is a new method for measuring gas-phase ammonia and amines, that is shown to be accurate and reproducible. This technique is inexpensive, has fast ($\sim$1 hr) time resolution, and has detection limits in the tens of ppt range, making it suitable for atmospheric measurements. Finally, amine-amine displacement is explored in aminium methanesulfonate salt particles. The extent of displacement of one amine species in the particle phase by a different gas-phase amine is shown to depend on particle phase (i.e. whether a particle behaves like a liquid or has a solid salt core). Amine-amine displacement reactions will have important effects on particle growth, as particle-phase amines are suggested to have species-specific effects on hygroscopicity.

These findings will aid in the development of accurate models of atmospheric aerosol systems, reducing the uncertainty in predicting their long-term effects on visibility, human health, and climate.

Bibliography

[1] W. Hinds, *Aerosol Technology: Properties, Behavior, and Measurement of Airborne Particles*, Wiley-Interscience, 2nd ed.

[2] R. Michaels and M. Kleinman, Incidence and apparent health significance of brief airborne particle excursions. *Aerosol Sci. Tech.* **32**(2), 93–105 (2000).

[3] P. Moller, J. Folkmann, L. Forchhammer, E. Brauner, P. Danielsen, L. Risom, and S. Loft, Air pollution, oxidative damage to DNA, and carcinogenesis. *Cancer Lett.* **266**(1), 84–97 (2008).

[4] C. A. Pope, J. B. Muhlestein, H. T. May, D. G. Renlund, J. L. Anderson, and B. D. Horne, Ischemic heart disease events triggered by short-term exposure to fine particulate air pollution. *Circ. J.* **114**(23), 2443–2448 (2006).

[5] C. A. Pope III and D. W. Dockery, Health effects of fine particulate air pollution: Lines that connect. *J. Air Waste Manage. Assoc.* **56**(6), 709–742 (2006).

[6] I. Colbeck and M. Lazaridis, Aerosols and environmental pollution. *Naturwissenschaften.* **97**(2), 117–131 (2010).

[7] B. Finlayson-Pitts and J. Pitts, *Chemistry of the upper and lower atmosphere – theory, experiments and applications*, Academic Press.

[8] IPCC, 2013: Climate change 2013: The physical science basis. contribution of working group 1 to the fifth assessment report of the intergovernmental panel on climate change.

[9] J. Seinfeld and S. Pandis, *Atmospheric chemistry and physics: from air pollution to climate change*, Wiley-Interscience.

[10] D. W. Dockery, C. A. Pope, X. Xu, J. D. Spengler, J. H. Ware, M. E. Fay, B. G. Ferris, and F. E. Speizer, An Association between Air Pollution and Mortality in Six U.S. Cities. **329**(24), 1753–1759 (1993).

[11] T. Bartos, P. Cupr, J. Klánová, and I. Holoubek, Which compounds contribute most to elevated airborne exposure and corresponding health risks in the Western Balkans? *Environ. Int.* **35**(7), 1066–1071 (2009).

[12] J. Schnelle-Kreis, U. Kupper, M. Sklorz, J. Cyrys, J. Briede, A. Peters, and R. Zimmermann, Daily measurement of organic compounds in ambient particulate matter in Augsburg, Germany: New aspects on aerosol sources and aerosol related health effects. *Biomarkers.* **14**, 39–44 (2009).

[13] M. Posfai and P. R. Buseck, Nature and Climate Effects of Individual Tropospheric Aerosol Particles. *Annu. Rev. Earth Planet. Sci.* **38**, 17–43 (2010).

[14] M. Andreae and D. Rosenfeld, Aerosol-cloud-precipitation interactions. Part 1. The nature and sources of cloud-active aerosols. *Earth-Sci. Rev.* **89**(1), 13–41 (2008).

[15] B. Bzdek and M. Johnston, New particle formation and growth in the troposphere. *Anal. Chem.* **82**, 7871–7878 (2010).

[16] J. Merikanto, D. V. Spracklen, G. W. Mann, S. J. Pickering, and K. S. Carslaw, Impact of nucleation on global CCN. *Atmos. Chem. Phys.* **9**(21), 8601–8616 (2009).

[17] M. Kulmala and V. Kerminen, On the formation and growth of atmospheric nanoparticles. *Atmos. Res.* **90**(2), 132–150 (2008).

[18] R. Zhang, A. Khalizov, L. Wang, M. Hu, and W. Xu, Nucleation and Growth of Nanoparticles in the Atmosphere. *Chem. Rev.* **112**(3), 1957–2011 (2012).

[19] T. Berndt, O. Boge, F. Stratmann, J. Heintzenberg, and M. Kulmala, Rapid formation of sulfuric acid particles at near-atmospheric conditions. *Science.* **307**(5710), 698–700 (2005).

[20] R. Y.-W. Chang, S. J. Sjostedt, J. R. Pierce, T. N. Papakyriakou, M. G. Scarratt, S. Michaud, M. Levasseur, W. R. Leaitch, and J. P. D. Abbatt, Relating atmospheric and oceanic DMS levels to particle nucleation events in the Canadian Arctic. *J. Geophys. Res.-Atmos.* **116** (2011) DOI:10.1029/2011JD015926.

[21] S. M. Kreidenweis and J. H. Seinfeld, Nucleation of sulfuric acid-water and methanesulfonic acid-water solution particles: Implications for the atmospheric chemistry of organosulfur species. *Atmos. Environ.* **22**(2), 283–296 (1988).

[22] C. Kuang, P. H. McMurry, A. V. McCormick, and F. L. Eisele, Dependence of nucleation rates on sulfuric acid vapor concentration in diverse atmospheric locations. *J. Geophys. Res.* **113** (2008) DOI:200810.1029/2007JD009253.

[23] P. Mirabel and J. L. Katz, Binary homogeneous nucleation as a mechanism for the formation of aerosols. *J. Chem. Phys.* **60**(3), 1138–1144 (1974).

[24] M. Noppel, H. Vehkamaki, and M. Kulmala, An improved model for hydrate formation in sulfuric acid-water nucleation. *J. Chem. Phys.* **116**(1), 218–228 (2002).

[25] L. Russell, S. Pandis, and J. Seinfeld, Aerosol production and growth in the marine boundary-layer. *J. Geophys. Res.-Atmos.* **99**, 20989–21003 (1994).

[26] M. Sipila, T. Berndt, T. Petaja, D. Brus, J. Vanhanen, F. Stratmann, J. Patokoski, R. Mauldin, A. Hyvarinen, H. Lihavainen, and M. Kulmala, The role of sulfuric acid in atmospheric nucleation. *Science*. **327**(5970), 1243–1246 (2010).

[27] A. Sorokin, X. Vancassel, and P. Mirabel, Kinetic model for binary homogeneous nucleation in the H_2O-H_2SO_4 system: Comparison with experiments and classical theory of nucleation. *J. Chem. Phys.* **123**(24) (2005) DOI:10.1063/1.2141511.

[28] R. Weber, J. Marti, P. McMurry, F. Eisele, D. Tanner, and A. Jefferson, Measurements of new particle formation and ultrafine particle growth rates at a clean continental site. *J. Geophys. Res.-Atmos.* **102**, 4375–4385 (1997).

[29] B. Wyslouzil, J. Seinfeld, R. Flagan, and K. Okuyama, Binary nucleation in acid-water systems 2. sulfuric acid-water and a comparison with methanesulfonic acid-water. *J. Chem. Phys.* **94**(10), 6842–6850 (1991).

[30] C. Clement and I. Ford, Gas-to-particle conversion in the atmosphere: I. Evidence from empirical atmospheric aerosols. *Atmos. Environ.* **33**(3), 475–487 (1999).

[31] M. E. Erupe, D. R. Benson, J. Li, L.-H. Young, B. Verheggen, M. Al-Refai, O. Tahboub, V. Cunningham, F. Frimpong, A. A. Viggiano, and S.-H. Lee, Correlation of aerosol nucleation rate with sulfuric acid and ammonia in Kent, Ohio: An atmospheric observation. *J. Geophys. Res.-Atmos.* **115** (2010) DOI:10.1029/2010JD013942.

[32] D. Brus, K. Neitola, A.-P. Hyvarinen, T. Petaja, J. Vanhanen, M. Sipila, P. Paasonen, M. Kulmala, and H. Lihavainen, Homogenous nucleation of sulfuric acid and water at close to atmospherically relevant conditions. *Atmos. Chem. Phys.* **11**(11), 5277–5287 (2011).

[33] T. Anttila, H. Vehkamaki, I. Napari, and M. Kulmala, Effect of ammonium bisulphate formation on atmospheric water-sulphuric acid-ammonia nucleation. *Boreal Environ. Res.* **10**(6), 511–523 (2005).

[34] K. C. Barsanti, P. H. McMurry, and J. N. Smith, The potential contribution of organic salts to new particle growth. *Atmos. Chem. Phys.* **9**(9), 2949–2957 (2009).

[35] N. Hiranuma, S. D. Brooks, D. C. Thornton, and B. W. Auvermann, Atmospheric ammonia mixing ratios at an open-air cattle feeding facility. *J. Air Waste Manage. Assoc.* **60**(2), 210–218 (2010).

[36] D. R. Benson, J. H. Yu, A. Markovich, and S.-H. Lee, Ternary homogeneous nucleation of H_2SO_4, NH_3, and H_2O under conditions relevant to the lower troposphere. *Atmos. Chem. Phys.* **11**(10), 4755–4766 (2011).

[37] T. Berndt, F. Stratmann, M. Sipila, J. Vanhanen, T. Petaja, J. Mikkila, A. Gruner, G. Spindler, R. Mauldin, J. Curtius, M. Kulmala, and J. Heintzenberg, Laboratory study on new particle formation from the reaction OH + SO_2: influence of experimental conditions, H_2O vapour, NH_3 and the amine tert-butylamine on the overall process. *Atmos. Chem. Phys.* **10**(15), 7101–7116 (2010).

[38] F. Yu, Effect of ammonia on new particle formation: A kinetic H_2SO_4-H_2O-NH_3 nucleation model constrained by laboratory measurements. *J. Geophys. Res.-Atmos.* **111** (2006) DOI:10.1029/2005JD005968.

[39] J. Kirkby, J. Curtius, J. Almeida, E. Dunne, J. Duplissy, S. Ehrhart, A. Franchin, S. Gagne, L. Ickes, A. Kuerten, A. Kupc, A. Metzger, F. Riccobono, L. Rondo, S. Schobesberger, G. Tsagkogeorgas, D. Wimmer, A. Amorim, F. Bianchi, M. Breitenlechner, A. David, J. Dommen, A. Downard, M. Ehn, R. C. Flagan, S. Haider, A. Hansel, D. Hauser, W. Jud, H. Junninen, F. Kreissl, A. Kvashin, A. Laaksonen, K. Lehtipalo, J. Lima, E. R. Lovejoy, V. Makhmutov, S. Mathot, J. Mikkila, P. Minginette, S. Mogo, T. Nieminen, A. Onnela, P. Pereira, T. Petaja, R. Schnitzhofer, J. H. Seinfeld, M. Sipila, Y. Stozhkov, F. Stratmann, A. Tome, J. Vanhanen, Y. Viisanen, A. Vrtala, P. E. Wagner, H. Walther, E. Weingartner, H. Wex, P. M. Winkler, K. S. Carslaw, D. R. Worsnop, U. Baltensperger, and M. Kulmala, Role of sulphuric acid, ammonia and galactic cosmic rays in atmospheric aerosol nucleation. *Nature.* **476**(7361), 429–U77 (2011).

[40] J. Almeida, S. Schobesberger, A. Kürten, I. K. Ortega, O. Kupiainen-Määttä, A. P. Praplan, A. Adamov, A. Amorim, F. Bianchi, M. Breitenlechner, A. David, J. Dommen, N. M. Donahue, A. Downard, E. Dunne, J. Duplissy, S. Ehrhart, R. C. Flagan, A. Franchin, R. Guida, J. Hakala, A. Hansel, M. Heinritzi, H. Henschel, T. Jokinen, H. Junninen, M. Kajos, J. Kangasluoma, H. Keskinen, A. Kupc, T. Kurtén, A. N. Kvashin, A. Laaksonen, K. Lehtipalo, M. Leiminger, J. Leppä, V. Loukonen, V. Makhmutov, S. Mathot, M. J. McGrath, T. Nieminen, T. Olenius, A. Onnela, T. Petäjä, F. Riccobono, I. Riipinen, M. Rissanen, L. Rondo, T. Ruuskanen, F. D. Santos, N. Sarnela, S. Schallhart, R. Schnitzhofer, J. H. Seinfeld, M. Simon, M. Sipilä, Y. Stozhkov, F. Stratmann, A. Tomé, J. Tröstl, G. Tsagkogeorgas, P. Vaattovaara, Y. Viisanen, A. Virtanen, A. Vrtala, P. E. Wagner, E. Weingartner, H. Wex, C. Williamson, D. Wimmer, P. Ye, T. Yli-Juuti, K. S. Carslaw, M. Kulmala, J. Curtius, U. Baltensperger, D. R. Worsnop, H. Vehkamäki, and J. Kirkby, Molecular understanding of sulphuric acid-amine particle nucleation in the atmosphere. *Nature.* **502**(7471), 359–363 (2013).

[41] H. Yu, R. McGraw, and S.-H. Lee, Effects of amines on formation of sub-3 nm particles and their subsequent growth. *Geophys. Res. Lett.* **39** (2012) DOI:10.1029/2011GL050099.

[42] J. Smith, K. Barsanti, H. Friedli, M. Ehn, M. Kulmala, D. Collins, J. Scheckman, B. Williams, and P. McMurry, Observations of aminium salts in atmospheric nanoparticles and possible climatic implications. *PNAS.* **107**(15), 6634–6639 (2010).

[43] J. M. Creamean, A. P. Ault, J. E. Ten Hoeve, M. Z. Jacobson, G. C. Roberts, and K. A. Prather, Measurements of aerosol chemistry during new particle formation events at a remote rural mountain site. *Environ. Sci. Technol.* **45**(19), 8208–8216 (2011).

[44] S. Angelino, D. Suess, and K. Prather, Formation of aerosol particles from reactions of secondary and tertiary alkylamines: Characterization by aerosol time-of-flight mass spectrometry. *Environ. Sci. Technol.* **35**(15), 3130–3138 (2001).

[45] X. Tang, D. Price, E. Praske, D. Vu, K. Purvis-Roberts, P. J. Silva, D. R. Cocker III, and A. Asa-Awuku, CCN activity of aliphatic amine secondary aerosol. *Atmos. Chem. Phys. Discuss.* **14**(1), 31–56 (2014).

[46] R. Zhang, I. Suh, J. Zhao, D. Zhang, E. C. Fortner, X. Tie, L. T. Molina, and M. J. Molina, Atmospheric New Particle Formation Enhanced by Organic Acids. *Science.* **304**(5676), 1487–1490 (2004).

[47] T. Berndt, O. Böge, and F. Stratmann, Formation of atmospheric H_2SO_4/H_2O particles in the absence of organics: A laboratory study. *Geophys. Res. Lett.* **33** (2006) DOI:200610.1029/2006GL026660.

[48] M. Facchini, S. Decesari, M. Rinaldi, C. Carbone, E. Finessi, M. Mircea, S. Fuzzi, F. Moretti, E. Tagliavini, D. Ceburnis, and C. O'Dowd, Important source of marine secondary organic aerosol from biogenic amines. *Environ. Sci. Technol.* **42**(24), 9116–9121 (2008).

[49] C. Muller, Y. Iinuma, J. Karstensen, D. van Pinxteren, S. Lehmann, T. Gnauk, and H. Herrmann, Seasonal variation of aliphatic amines in marine sub-micrometer particles at the Cape Verde islands. *Atmos. Chem. Phys.* **9**(24), 9587–9597 (2009).

[50] H. Bardouki, H. Berresheim, M. Vrekoussis, J. Sciare, G. Kouvarakis, K. Oikonomou, J. Schneider, and N. Mihalopoulos, Gaseous (DMS, MSA, SO_2, H_2SO_4 and DMSO) and particulate (sulfate and methanesulfonate) sulfur species over the northeastern coast of Crete. *Atmos. Chem. Phys.* **3**, 1871–1886 (2003).

[51] H. Berresheim, T. Elste, H. Tremmel, A. Allen, H. Hansson, K. Rosman, M. Dal Maso, J. Makela, M. Kulmala, and C. O'Dowd, Gas-aerosol relationships of H_2SO_4, MSA, and OH: Observations in the coastal marine boundary layer at Mace Head, Ireland. *J. Geophys. Res.-Atmos.* **107** (2002) DOI:10.1029/2000JD000229.

[52] L. Chen, J. Wang, Y. Gao, G. Xu, X. Yang, Q. Lin, and Y. Zhang, Latitudinal distributions of atmospheric MSA and MSA/nss-SO_4^{2-} ratios in summer over the high latitude regions of the Southern and Northern Hemispheres. *J. Geophys. Res.-Atmos.* **117** (2012) DOI:10.1029/2011JD016559.

[53] A. Sorooshian, L. Padro, A. Nenes, G. Feingold, A. McComiskey, S. Hersey, H. Gates, H. Jonsson, S. Miller, G. Stephens, R. Flagan, and J. Seinfeld, On the link between ocean biota emissions, aerosol, and maritime clouds: Airborne, ground, and satellite measurements off the coast of California. *Global Biogeochem. Cy.* **23**, GB4007 (2009) DOI:10.1029/2009GB003464.

[54] H. Berresheim, J. W. Huey, R. P. Thorn, F. L. Eisele, D. J. Tanner, and A. Jefferson, Measurements of dimethyl sulfide, dimethyl sulfoxide, dimethyl sulfone, and aerosol ions at Palmer Station, Antarctica. *J. Geophys. Res.* **103**, 1629–1637 (1998).

[55] J. M. Makela, S. Yli-Koivisto, V. Hiltunen, W. Seidl, E. Swietlicki, K. Teinila, M. Sillanpaa, I. K. Koponen, J. Paatero, K. Rosman, and K. Hameri, Chemical composition of aerosol during particle formation events in boreal forest. *Tellus Ser. B-Chem. Phys. Meteorol.* **53**(4), 380–393 (2001).

[56] V. Kerminen, M. Aurela, R. Hillamo, and A. Virkkula, Formation of particulate MSA: Deductions from size distribution measurements in the Finnish Arctic. *Tellus Ser. B-Chem. Phys. Meteorol.* **49**(2), 159–171 (1997).

[57] C. Gaston, K. Pratt, X. Qin, and K. Prather, Real-time detection and mixing state of methanesulfonate in single particles at an inland urban location during a phytoplankton bloom. *Environ. Sci. Technol.* **44**(5), 1566–1572 (2010).

[58] H. Allen, E. Raymond, and G. Richmond, Surface structural studies of methanesulfonic acid at air aqueous solution interfaces using vibrational sum frequency spectroscopy. *J. Phys. Chem. A.* **105**(9), 1649–1655 (2001).

[59] R. Dingenen, N. R. Jensen, J. Hjorth, and F. Raes, Peroxynitrate formation during the night-time oxidation of dimethylsulfide: Its role as a reservoir species for aerosol formation. *J. Atmos. Chem.* **18**(3), 211–237 (1994).

[60] R. Mauldin, C. Cantrell, M. Zondlo, E. Kosciuch, F. Eisele, G. Chen, D. Davis, R. Weber, J. Crawford, D. Blake, A. Bandy, and D. Thornton, Highlights of OH, H_2SO_4, and methane sulfonic acid measurements made aboard the NASA P-3B during transport and chemical evolution over the Pacific. *J. Geophys. Res.-Atmos.* **108** (2003) DOI:10.1029/2003JD003410.

[61] B. Wyslouzil, J. Seinfeld, R. Flagan, and K. Okuyama, Binary nucleation in acid-water systems 1. methanesulfonic acid-water. *J. Chem. Phys.* **94**(10), 6827–6841 (1991).

[62] I. Barnes, K. H. Becker, and N. Mihalopoulos, An FTIR product study of the photooxidation of dimethyl disulfide. *J. Atmos. Chem.* **18**(3), 267–289 (1994).

[63] S. Hatakeyama, M. Okuda, and H. Akimoto, Formation of sulfur-dioxide and methanesulfonic-acid in the photo-oxidation of dimethyl sulfide in the air. *Geophys. Res. Lett.* **9**(5), 583–586 (1982).

[64] G. S. Tyndall and A. R. Ravishankara, Atmospheric oxidation of reduced sulfur species. *Int. J. Chem. Kinet.* **23**(6), 483–527 (1991).

[65] L. Zhu, A. Nenes, P. H. Wine, and J. M. Nicovich, Effects of aqueous organosulfur chemistry on particulate methanesulfonate to non–sea salt sulfate ratios in the marine atmosphere. *J. Geophys. Res.* **111**, D05316 (2006) DOI:10.1029/2005JD006326.

[66] K. P. Capaldo and S. N. Pandis, Dimethylsulfide chemistry in the remote marine atmosphere: Evaluation and sensitivity analysis of available mechanisms. *J. Geophys. Res.* **102**, 23251–23267 (1997).

[67] I. V. Patroescu, I. Barnes, K. H. Becker, and N. Mihalopoulos, FT-IR product study of the OH-initiated oxidation of DMS in the presence of NO_x. *Atmos. Environ.* **33**(1), 25–35 (1998).

[68] T. Chen and M. Jang, Secondary organic aerosol formation from photooxidation of a mixture of dimethyl sulfide and isoprene. *Atmos. Environ.* **46**, 271–278 (2012).

[69] T. Bates, B. Lamb, A. Guenther, J. Dignon, and R. Stoiber, Sulfur emissions to the atmosphere from natural sources. *J. Atmos. Chem.* **14**, 315–337 (1992).

[70] A. Kettle and M. Andreae, Flux of dimethylsulfide from the oceans: A comparison of updated data seas and flux models. *J. Geophys. Res.-Atmos.* **105**, 26793–26808 (2000).

[71] A. Kettle, T. Rhee, M. von Hobe, A. Poulton, J. Aiken, and M. Andreae, Assessing the flux of different volatile sulfur gases from the ocean to the atmosphere. *J. Geophys. Res.-Atmos.* **106**, 12193–12209 (2001).

[72] S. Yvon, E. Saltzman, D. Cooper, T. Bates, and A. Thompson, Atmospheric sulfur cycling in the tropical Pacific marine boundary layer (12 °S,135 °W): A comparison of field data and model results. 1. Dimethylsulfide. *J. Geophys. Res.* **101**, 6899–6909 (1996).

[73] M. Andreae and H. Raemdonck, Dimethyl sulfide in the surface ocean and the marine atmosphere - a global view. *Science.* **221**(4612), 744–747 (1983).

[74] M. Andreae, R. Ferek, F. Bermond, K. Byrd, R. Engstrom, S. Hardin, P. Houmere, F. LeMarrec, H. Raemdonck, and R. Chatfield, Dimethyl Sulfide in the marine atmosphere. *J. Geophys. Res.-Atmos.* **90**, 2891–2900 (1985).

[75] A. Feilberg, D. Liu, A. P. S. Adamsen, M. J. Hansen, and K. E. N. Jonassen, Odorant emissions from intensive pig production measured by online proton-transfer-reaction mass spectrometry. *Environ. Sci. Technol.* **44**(15), 5894–5900 (2010).

[76] J. Filipy, B. Rumburg, G. Mount, H. Westberg, and B. Lamb, Identification and quantification of volatile organic compounds from a dairy. *Atmos. Environ.* **40**(8), 1480–1494 (2006).

[77] S. Gay, D. Schmidt, C. Clanton, K. Janni, L. Jacobson, and S. Weisberg, Odor, total reduced sulfur, and ammonia emissions from animal housing facilities and manure storage units in Minnesota. *Appl. Eng. Agric.* **19**(3), 347–360 (2003).

[78] K.-H. Kim, E.-C. Jeon, Y.-S. Koo, M.-S. Im, and Y.-H. Youn, An on-line analysis of reduced sulfur gases in the ambient air surrounding a large industrial complex. *Atmos. Environ.* **41**(18), 3829–3840 (2007).

[79] K.-H. Kim, Emissions of reduced sulfur compounds (RSC) as a landfill gas (LFG): A comparative study of young and old landfill facilities. *Atmos. Environ.* **40**(34), 6567–6578 (2006).

[80] F. Lunn and J. Van de Vyver, Sampling and analysis of air in pig houses. *Agric. Environ.* **3**(2), 159–169 (1977).

[81] I. Barnes, V. Bastian, K. H. Becker, and R. D. Overath, Kinetic studies of the reactions of IO, BrO, and ClO with dimethylsulfide. *Int. J. Chem. Kinet.* **23**(7), 579–591 (1991).

[82] S. Hatakeyama, K. Izumi, and H. Akimoto, Yield of SO_2 and formation of aerosol in the photo-oxidation of DMS under atmospheric conditions. *Atmos. Environ.* **19**(1), 135–141 (1985).

[83] G. S. Tyndall and A. R. Ravishankara, Kinetics and mechanisms of the reactions of methylthiyl with oxygen and nitrogen dioxide at 298 K. *J. Phys. Chem.* **93**(6), 2426–2435 (1989).

[84] G. S. Tyndall, J. P. Burrows, W. Schneider, and G. K. Moortgat, Rate coefficient for the reaction between NO_3 radicals and dimethyl sulphide. *Chem. Phys. Lett.* **130**(5), 463–466 (1986).

[85] R. L. Mauldin, E. Kosciuch, B. Henry, F. L. Eisele, R. Shetter, B. Lefer, G. Chen, D. Davis, G. Huey, and D. Tanner, Measurements of OH, HO_2+RO_2, H_2SO_4, and MSA at the south pole during ISCAT 2000. *Atmos. Environ.* **38**(32), 5423–5437 (2004).

[86] D. Davis, G. Chen, P. Kasibhatla, A. Jefferson, D. Tanner, F. Eisele, D. Lenschow, W. Neff, and H. Berresheim, DMS oxidation in the Antarctic marine boundary layer: Comparison of model simulations and held observations of DMS, DMSO, $DMSO_2$, H_2SO_4(g), MSA(g), and MSA(p). *J. Geophys. Res.* **103**, 1657 (1998).

[87] F. Yin, D. Grosjean, R. C. Flagan, and J. H. Seinfeld, Photooxidation of dimethyl sulfide and dimethyl disulfide. II: Mechanism evaluation. *J. Atmos. Chem.* **11**(4), 365–399 (1990).

[88] X. Ge, A. Wexler, and S. Clegg, Atmospheric amines - Part I. A review. *Atmos. Environ.* **45**(3), 524–546 (2011).

[89] N. Anderson, R. Strader, and C. Davidson, Airborne reduced nitrogen: ammonia emissions from agriculture and other sources. *Environ. Int.* **29**, 277–286 (2003).

[90] S. W. Gibb, R. F. C. Mantoura, and P. S. Liss, Ocean-atmosphere exchange and atmospheric speciation of ammonia and methylamines in the region of the NW Arabian Sea. *Glob. Biogeochem. Cycle.* **13**(1), 161–177 (1999).

[91] Y. Li, J. J. Schwab, and K. L. Demerjian, Measurements of ambient ammonia using a tunable diode laser absorption spectrometer: Characteristics of ambient ammonia emissions in an urban area of New York City. *J. Geophys. Res.* **111**, D10S02 (2006) DOI:10.1029/2005JD006275.

[92] M. Norman, C. Spirig, V. Wolff, I. Trebs, C. Flechard, A. Wisthaler, R. Schnitzhofer, A. Hansel, and A. Neftel, Intercomparison of ammonia measurement techniques at an intensively managed grassland site (Oensingen, Switzerland). *Atmos. Chem. Phys.* **9**(8), 2635–2645 (2009).

[93] F. Özogul and Y. Özogul, The ability of biogenic amines and ammonia production by single bacterial cultures. *Eur Food Res Technol.* **225**(3), 385–394 (2007).

[94] C. Perrino, M. Catrambone, A. Di Menno Di Bucchianico, and I. Allegrini, Gaseous ammonia in the urban area of Rome, Italy and its relationship with traffic emissions. *Atmospheric Environment.* **36**(34), 5385–5394 (2002).

[95] W. R. Pierson and W. W. Brachaczek, Emissions of ammonia and amines from vehicles on the road. *Environ. Sci. Technol.* **17**(12), 757–760 (1983).

[96] M. A. Sutton, U. Dragosits, Y. S. Tang, and D. Fowler, Ammonia emissions from non-agricultural sources in the UK. *Atmos. Environ.* **34**(6), 855–869 (2000).

[97] K. Toda, J. Li, and P. K. Dasgupta, Measurement of Ammonia in Human Breath with a Liquid-Film Conductivity Sensor. *Anal. Chem.* **78**(20), 7284–7291 (2006).

[98] I. Trebs, F. Meixner, J. Slanina, R. Otjes, P. Jongejan, and M. Andreae, Real-time measurements of ammonia, acidic trace gases and water-soluble inorganic aerosol species at a rural site in the Amazon Basin. *Atmos. Chem. Phys.* **4**(4), 967–987 (2004).

[99] J. D. Whitehead, I. D. Longley, and M. W. Gallagher, Seasonal and Diurnal Variation in Atmospheric Ammonia in an Urban Environment Measured Using a Quantum Cascade Laser Absorption Spectrometer. *Water Air Soil Pollut.* **183**(1), 317–329 (2007).

[100] M. Akyüz, Simultaneous determination of aliphatic and aromatic amines in ambient air and airborne particulate matters by gas chromatography-mass spectrometry. *Atmos. Environ.* **42**(16), 3809–3819 (2008).

[101] M. E. Cablk, E. E. Szelagowski, and J. C. Sagebiel, Characterization of the volatile organic compounds present in the headspace of decomposing animal remains, and compared with human remains. *Forensic Sci. Int.* **220**(1), 118–125 (2012).

[102] U. Kuhn, J. Sintermann, C. Spirig, M. Jocher, C. Ammann, and A. Neftel, Basic biogenic aerosol precursors: Agricultural source attribution of volatile amines revised. *Geophys. Res. Lett.* **38**(16) (2011) DOI:10.1029/2011GL047958.

[103] A. Mosier, C. Andre, and F. Viets, Identification of aliphatic amines volatilized from cattle feedyard. *Environ. Sci. Technol.* **7**(7), 642–644 (1973).

[104] J.-Q. Ni, W. P. Robarge, C. Xiao, and A. J. Heber, Volatile organic compounds at swine facilities: A critical review. *Chemosphere.* **89**(7), 769–788 (2012).

[105] G. Schade and P. Crutzen, Emission of aliphatic amines from animal husbandry and their reactions: Potential source of N_2O and HCN. *J. Atmos. Chem.* **22**(3), 319–346 (1995).

[106] J. M. Lobert, D. H. Scharffe, W. M. Hao, and P. J. Crutzen, Importance of biomass burning in the atmospheric budgets of nitrogen-containing gases. *Nature.* **346**(6284), 552–554 (1990).

[107] N. Borduas, J. P. D. Abbatt, and J. G. Murphy, Gas phase oxidation of monoethanolamine (MEA) with OH radical and ozone: kinetics, products, and particles. *Environ. Sci. Technol.* **47**(12), 6377–6383 (2013).

[108] A. Schreiber, P. Zapp, and W. Kuckshinrichs, Environmental assessment of German electricity generation from coal-fired power plants with amine-based carbon capture. *Int. J. Life Cycle Assess.* **14**(6), 547–559 (2009).

[109] C. J. Nielsen, H. Herrmann, and C. Weller, Atmospheric chemistry and environmental impact of the use of amines in carbon capture and storage (CCS). *Chem. Soc. Rev.* **41**(19), 6684–6704 (2012).

[110] G. T. Rochelle, Amine Scrubbing for CO_2 Capture. *Science.* **325**(5948), 1652–1654 (2009).

[111] A. Sexton and G. Rochelle, Reaction Products from the Oxidative Degradation of Monoethanolamine. *Ind. Eng. Chem. Res.* **50**(2), 667–673 (2011).

[112] S. Das, M. N. Schuchmann, H.-P. Schuchmann, and C. V. Sonntag, The production of the superoxide radical anion by the OH radical-induced oxidation of trimethylamine in oxygenated aqueous solution. The kinetics of the hydrolysis of (hydroxymethyl)dimethylamine. *Chemische Berichte.* **120**(3), 319–323 (1987).

[113] X. Tang, D. Price, E. Praske, S. A. Lee, M. A. Shattuck, K. Purvis-Roberts, P. J. Silva, A. Asa-Awuku, and D. R. Cocker, NO_3 radical, OH radical and O_3-initiated secondary aerosol formation from aliphatic amines. *Atmos. Environ.* **72**, 105–112 (2013).

[114] G. Yan-Bo, G. Mao-Fa, and W. Wei-Gang, Rate Constants for the Gas Phase Reactions of Ozone with Diethylamine and Triethylamine. *Acta Phys.-Chim. Sin.* **26**(7), 1768–1772 (2010).

[115] F. L. Eisele, Natural and transmission line produced positive ions. *J. Geophys. Res.-Atmos.* **94**, 6309–6318 (1989).

[116] P. McMurry, A review of atmospheric aerosol measurements. *Atmos. Environ.* **34**(12), 1959–1999 (2000).

[117] D. Brus, A.-P. Hyvarinen, Y. Viisanen, M. Kulmala, and H. Lihavainen, Homogeneous nucleation of sulfuric acid and water mixture: experimental setup and first results. *Atmos. Chem. Phys.* **10**(6), 2631–2641 (2010).

[118] J. Duplissy, M. Enghoff, K. Aplin, F. Arnold, H. Aufmhoff, M. Avngaard, U. Baltensperger, T. Bondo, R. Bingham, K. Carslaw, J. Curtius, A. David, B. Fastrup, S. Gagne, F. Hahn, R. Harrison, B. Kellett, J. Kirkby, M. Kulmala, L. Laakso, A. Laaksonen, E. Lillestol, M. Lockwood, J. Makela, V. Makhmutov, N. Marsh, T. Nieminen, A. Onnela, E. Pedersen, J. Pedersen, J. Polny, U. Reichl, J. Seinfeld, M. Sipila, Y. Stozhkov, F. Stratmann, H. Svensmark, J. Svensmark, R. Veenhof, B. Verheggen, Y. Viisanen, P. Wagner, G. Wehrle, E. Weingartner, H. Wex, M. Wilhelmsson, and

P. Winkler, Results from the CERN pilot CLOUD experiment. *Atmos. Chem. Phys.* **10**(4), 1635–1647 (2010).

[119] M. E. Erupe, A. A. Viggiano, and S.-H. Lee, The effect of trimethylamine on atmospheric nucleation involving H_2SO_4. *Atmos. Chem. Phys.* **11**(10), 4767–4775 (2011).

[120] K. Iida, M. Stolzenburg, and P. McMurry, Effect of working fluid on sub-2 nm particle detection with a laminar flow ultrafine condensation particle counter. *Aerosol Sci. Tech.* **43**(1), 81–96 (2009).

[121] J. Jiang, M. Chen, C. Kuang, M. Attoui, and P. McMurry, Electrical mobility spectrometer using a diethylene glycol condensation particle counter for measurement of aerosol size distributions down to 1 nm. *Aerosol Sci. Tech.* **45**(4), 510–521 (2011).

[122] J. Jiang, J. Zhao, M. Chen, F. L. Eisele, J. Scheckman, B. J. Williams, C. Kuang, and P. H. McMurry, First Measurements of Neutral Atmospheric Cluster and 1-2 nm Particle Number Size Distributions During Nucleation Events. *Aerosol Sci. Technol.* **45**(4), II–V (2011) DOI:10.1080/02786826.2010.546817.

[123] R. A. Ellis, J. G. Murphy, M. Z. Markovic, T. C. VandenBoer, P. A. Makar, J. Brook, and C. Mihele, The influence of gas-particle partitioning and surface-atmosphere exchange on ammonia during BAQS-Met. *Atmos. Chem. Phys.* **11**(1), 133–145 (2011).

[124] A. Zelenyuk and D. Imre, Single Particle Laser Ablation Time-of-Flight Mass Spectrometer: An Introduction to SPLAT. **39**(6), 554–568 (2005).

[125] A. Zelenyuk, J. Yang, E. Choi, and D. Imre, SPLAT II: An aircraft compatible, ultrasensitive, high precision instrument for in-situ characterization of the size and composition of fine and ultrafine particles. *Aerosol Sci. Tech.* **43**(5), 411–424 (2009).

[126] M. Chen, M. Titcombe, J. Jiang, C. Jen, C. Kuang, M. L. Fischer, F. L. Eisele, J. I. Siepmann, D. R. Hanson, J. Zhao, and P. H. McMurry, Acid–base chemical reaction model for nucleation rates in the polluted atmospheric boundary layer. *PNAS.* **109**(46), 18713–18718 (2012).

[127] J. Zhao, F. Eisele, M. Titcombe, C. Kuang, and P. McMurry, Chemical ionization mass spectrometric measurements of atmospheric neutral clusters using the cluster-CIMS. *J. Geophys. Res.-Atmos.* **115** (2010) DOI:10.1029/2009JD012606.

[128] B. R. Bzdek, J. W. DePalma, D. P. Ridge, J. Laskin, and M. V. Johnston, Fragmentation Energetics of Clusters Relevant to Atmospheric New Particle Formation. *J. Am. Chem. Soc.* **135**(8), 3276–3285 (2013).

[129] C. Kuang, I. Riipinen, S. Sihto, M. Kulmala, A. McCormick, and P. McMurry, An improved criterion for new particle formation in diverse atmospheric environments. **10**(17), 8469–8480 (2010).

[130] M. Ehn, J. A. Thornton, E. Kleist, M. Sipilä, H. Junninen, I. Pullinen, M. Springer, F. Rubach, R. Tillmann, B. Lee, F. Lopez-Hilfiker, S. Andres, I.-H. Acir, M. Rissanen, T. Jokinen, S. Schobesberger, J. Kangasluoma, J. Kontkanen, T. Nieminen, T. Kurtén, L. B. Nielsen, S. Jørgensen, H. G. Kjaergaard, M. Canagaratna, M. D. Maso, T. Berndt, T. Petäjä, A. Wahner, V.-M. Kerminen, M. Kulmala, D. R. Worsnop, J. Wildt, and T. F. Mentel, A large source of low-volatility secondary organic aerosol. *Nature.* **506**(7489), 476–479 (2014).

[131] S. M. Kreidenweis, F. Yin, S.-C. Wang, D. Grosjean, R. C. Flagan, and J. H. Seinfeld, Aerosol formation during photooxidation of organosulfur species. *Atmos. Environ.* **25**(11), 2491–2500 (1991).

[132] A. Metzger, B. Verheggen, J. Dommen, J. Duplissy, A. Prevot, E. Weingartner, I. Riipinen, M. Kulmala, D. Spracklen, K. Carslaw, and U. Baltensperger, Evidence for the role of organics in aerosol particle formation under atmospheric conditions. *PNAS.* **107**(15), 6646–6651 (2010).

[133] T. Berndt, M. Sipilä, F. Stratmann, T. Petäjä, J. Vanhanen, J. Mikkilä, J. Patokoski, R. Taipale, R. L. Mauldin III, and M. Kulmala, Enhancement of atmospheric H_2SO_4 / H_2O nucleation: organic oxidation products versus amines. *Atmos. Chem. Phys.* **14**(2), 751–764 (2014).

[134] M. Ezell, S. Johnson, Y. Yu, V. Perraud, E. Bruns, M. Alexander, A. Zelenyuk, D. Dabdub, and B. Finlayson-Pitts, A new aerosol flow system for photochemical and thermal studies of tropospheric aerosols. *Aerosol Sci. Tech.* **44**(5), 329–338 (2010).

[135] S. Kreidenweis, R. Flagan, J. Seinfeld, and K. Okuyama, Binary Nucleation of Methanesulfonic Acid and Water. *J. Aerosol Sci.* **20**(5), 585–607 (1989).

[136] P. H. McMurry and D. Grosjean, Gas and aerosol wall losses in Teflon film smog chambers. *Environ. Sci. Technol.* **19**(12), 1176–1182 (1985).

[137] X. Zhang, C. D. Cappa, S. H. Jathar, R. C. McVay, J. J. Ensberg, M. J. Kleeman, and J. H. Seinfeld, Influence of vapor wall loss in laboratory chambers on yields of secondary organic aerosol. *PNAS.* **111**(16), 5802–5807 (2014).

[138] J. W. DePalma, B. R. Bzdek, D. J. Doren, and M. V. Johnston, Structure and Energetics of Nanometer Size Clusters of Sulfuric Acid with Ammonia and Dimethylamine. *J. Phys. Chem. A.* **116**(3), 1030–1040 (2012).

[139] T. Kurten and H. Vehkamaki in *Advances in Quantum Chemistry, Vol 55: Applications of Theoretical Methods to Atmospheric Science*, J. R. Sabin and E. Brandas, Eds., Vol. 55; Elsevier Academic Press Inc; pages 407–427.

[140] A. Krishtal, P. Senet, and C. Van Alsenoy, Influence of Structure on the Polarizability of Hydrated Methane Sulfonic Acid Clusters. *J. Chem. Theory Comput.* **4**(12), 2122–2129 (2008).

[141] V. Loukonen, I.-F. W. Kuo, M. J. McGrath, and H. Vehkamäki, On the stability and dynamics of (sulfuric acid) (ammonia) and (sulfuric acid) (dimethylamine) clusters: A first-principles molecular dynamics investigation. *Chem. Phys.* **428**, 164–174 (2014).

[142] V. Loukonen, T. Kurten, I. K. Ortega, H. Vehkamaki, A. A. H. Padua, K. Sellergi, and M. Kulmala, Enhancing effect of dimethylamine in sulfuric acid nucleation in the presence of water - a computational study. *Atmos. Chem. Phys.* **10**(10), 4961–4974 (2010).

[143] M. J. McGrath, T. Olenius, I. K. Ortega, V. Loukonen, P. Paasonen, T. Kurten, M. Kulmala, and H. Vehkamaki, Atmospheric Cluster Dynamics Code: a flexible method for solution of the birth-death equations. *Atmos. Chem. Phys.* **12**(5), 2345–2355 (2012).

[144] B. Mmereki and D. Donaldson, Ab initio and density functional study of complexes between the methylamines and water. *J. Phys. Chem. A.* **106**(13), 3185–3190 (2002).

[145] A. B. Nadykto, A. Al Natsheh, F. Yu, K. V. Mikkelsen, and J. Herb in *Advances in Quantum Chemistry, Vol 55: Applications of Theoretical Methods to Atmospheric Science*, J. R. Sabin and E. Brandas, Eds., Vol. 55; Elsevier Academic Press Inc; pages 449–478.

[146] I. K. Ortega, O. Kupiainen, T. Kurten, T. Olenius, O. Wilkman, M. J. McGrath, V. Loukonen, and H. Vehkamaki, From quantum chemical formation free energies to evaporation rates. *Atmos. Chem. Phys.* **12**(1), 225–235 (2012).

[147] M. Rozenberg, A. Loewenschuss, and C. J. Nielsen, H-Bonded Clusters in the Trimethylamine/Water System: A Matrix Isolation and Computational Study. *J. Phys. Chem. A.* **116**(16), 4089–4096 (2012).

[148] L. Wang, Clusters of Hydrated Methane Sulfonic Acid $CH_3SO_3H(H_2O)_n$ (n = 15): A Theoretical Study. *J. Phys. Chem. A.* **111**(18), 3642–3651 (2007).

[149] M. L. Dawson, M. E. Varner, V. Perraud, M. J. Ezell, R. B. Gerber, and B. J. Finlayson-Pitts, Simplified mechanism for new particle formation from methanesulfonic acid, amines, and water via experiments and *ab initio* calculations. *PNAS.* **109**(46), 18719–18724 (2012).

[150] A. Sorooshian, F. J. Brechtel, Y. Ma, R. J. Weber, A. Corless, R. C. Flagan, and J. H. Seinfeld, Modeling and Characterization of a Particle-into-Liquid Sampler (PILS). *Aerosol Sci. Technol.* **40**(6), 396–409 (2006).

[151] R. J. Weber, D. Orsini, Y. Daun, Y.-N. Lee, P. J. Klotz, and F. Brechtel, A Particle-into-Liquid Collector for Rapid Measurement of Aerosol Bulk Chemical Composition. *Aerosol Sci. Technol.* **35**(3), 718–727 (2001).

[152] D. A. Orsini, Y. Ma, A. Sullivan, B. Sierau, K. Baumann, and R. J. Weber, Refinements to the particle-into-liquid sampler (PILS) for ground and airborne measurements of water soluble aerosol composition. *Atmos. Environ.* **37**(9), 1243–1259 (2003).

[153] T. Nordmeyer and K. A. Prather, Real-Time Measurement Capabilities Using Aerosol Time-of-Flight Mass Spectrometry. *Anal. Chem.* **66**(20), 3540–3542 (1994).

[154] K. A. Prather, T. Nordmeyer, and K. Salt, Real-time characterization of individual aerosol particles using time-of-flight mass spectrometry. *Anal. Chem.* **66**(9), 1403–1407 (1994).

[155] A. Laskin, J. Laskin, and S. A. Nizkorodov, Mass spectrometric approaches for chemical characterisation of atmospheric aerosols: critical review of the most recent advances. *Environ. Chem.* **9**(3), 163–189 (2012).

[156] T. D. Vaden, D. Imre, J. Beranek, and A. Zelenyuk, Extending the capabilities of single particle mass spectrometry: I. Measurements of aerosol number concentration, size distribution, and asphericity. *Aerosol Sci. Technol.* **45**(1), 113–124 (2011).

[157] T. D. Vaden, D. Imre, J. Beranek, and A. Zelenyuk, Extending the capabilities of single particle mass spectrometry: II. Measurements of aerosol particle density without dma. *Aerosol Sci. Technol.* **45**(1), 125–135 (2011).

[158] A. Zelenyuk, J. Yang, C. Song, R. A. Zaveri, and D. Imre, A new real-time method for determining particles' sphericity and density: Application to secondary organic aerosol formed by ozonolysis of alpha-pinene. *Environ. Sci. Technol.* **42**(21), 8033–8038 (2008).

[159] D. R. Benson, A. Markovich, M. Al-Refai, and S.-H. Lee, A Chemical Ionization Mass Spectrometer for ambient measurements of Ammonia. *Atmos. Meas. Tech.* **3**(4), 1075–1087 (2010).

[160] H. Yu and S.-H. Lee, Chemical ionisation mass spectrometry for the measurement of atmospheric amines. *Environ. Chem.* **9**(3), 190–201 (2012).

[161] D. R. Hanson, P. H. McMurry, J. Jiang, D. Tanner, and L. G. Huey, Ambient pressure proton transfer mass spectrometry: detection of amines and ammonia. *Environ. Sci. Technol.* **45**(20), 8881–8888 (2011).

[162] R. Blake, P. Monks, and A. Ellis, Proton-transfer reaction mass spectrometry. *Chem. Rev.* **109**(3), 861–896 (2009).

[163] D. Liu, A. Feilberg, A. P. Adamsen, and K. E. Jonassen, The effect of slurry treatment including ozonation on odorant reduction measured by in-situ PTR-MS. *Atmos. Environ.* **45**(23), 3786–3793 (2011).

[164] H. Tanimoto, N. Aoki, S. Inomata, J. Hirokawa, and Y. Sadanaga, Development of a PTR-TOFMS instrument for real-time measurements of volatile organic compounds in air. *Int. J. Mass Spectrom.* **263**(1), 1–11 (2007).

[165] F. L. Eisele and D. J. Tanner, Identification of ions in continental air. *J. Geophys. Res.-Atmos.* **95**, 20539–20550 (1990).

[166] J. Cape, S. Cornell, T. Jickells, and E. Nemitz, Organic nitrogen in the atmosphere — Where does it come from? A review of sources and methods. *Atmos. Res.* **102**(1), 30–48 (2011).

[167] S. Fuselli, G. Benedetti, and R. Mastrangeli, Determination of methylamines in air using activated-charcoal traps and gas-chromatographic analysis with an alkali flame detector (AFD). *Atmos. Environ.* **16**(12), 2943–2946 (1982).

[168] M. Fournier, J. Lesage, C. Ostiguy, and H. Van Tra, Sampling and analytical methodology development for the determination of primary and secondary low molecular weight amines in ambient air. *J. Environ. Monit.* **10**(3), 379–386 (2008).

[169] L. Gronberg, P. Lovkvist, and J. Jonsson, Determination of aliphatic-amines in air by membrane enrichment directly coupled to a gas-chromatograph. *Chromatographia.* **33**(1), 77–82 (1992).

[170] G. Huang, J. Hou, and X. Zhou, A measurement method for atmospheric ammonia and primary amines based on aqueous sampling, OPA derivatization and HPLC analysis. *Environ. Sci. Technol.* **43**(15), 5851–5856 (2009).

[171] I.-H. Chang, C.-G. Lee, and D. S. Lee, Development of an Automated Method for Simultaneous Determination of Low Molecular Weight Aliphatic Amines and Ammonia in Ambient Air by Diffusion Scrubber Coupled to Ion Chromatography. *Anal. Chem.* **75**(22), 6141–6146 (2003).

[172] T. Nishikawa and K. Kuwata, Liquid chromatographic determination of low molecular weight aliphatic amines in air via derivatization with 7-chloro-4-nitro-2,1,3-benzoxadiazole. *Anal. Chem.* **56**(11), 1790–1793 (1984).

[173] N. A. Santagati, E. Bousquet, A. Spadaro, and G. Ronsisvalle, Analysis of aliphatic amines in air samples by HPLC with electrochemical detection. *J. Pharm. Biomed. Anal.* **29**(6), 1105–1111 (2002).

[174] D. Scheiner, Determination of ammonia and Kjeldahl nitrogen by indophenol method. *Water Res.* **10**(1), 31–36 (1976).

[175] L. Solórzano, Determination of ammonia in natural waters by the phenol hypochlorite method. *Limnol Oceanogr.* **14**(5), 799–801 (1969).

[176] K. Toda, T. Koga, T. Tanaka, S.-I. Ohira, J. M. Berg, and P. K. Dasgupta, Miniature open channel scrubbers for gas collection. *Talanta.* **82**(5), 1870–1875 (2010).

[177] G. Zhang, P. K. Dasgupta, and D. Shen, Measurement of atmospheric ammonia. *Environ. Sci. Technol.* **23**(12), 1467–1474 (1989).

[178] R. Bethea and R. Narayan, Identification of Beef-Cattle Feedlot Odors. *Trans. ASAE.* **15**(6), 1135–1137 (1972).

[179] L. Gronberg, P. Lovkvist, and J. Jonsson, Measurement of Aliphatic-Amines in Ambient Air and Rainwater. *Chemosphere*. **24**(10), 1533–1540 (1992).

[180] A. P. Praplan, F. Bianchi, J. Dommen, and U. Baltensperger, Dimethylamine and ammonia measurements with ion chromatography during the CLOUD4 campaign. *Atmos. Meas. Tech.* **5**(9), 2161–2167 (2012).

[181] T. VandenBoer, M. Markovic, A. Petroff, M. Czar, N. Borduas, and J. Murphy, Ion chromatographic separation and quantitation of alkyl methylamines and ethylamines in atmospheric gas and particulate matter using preconcentration and suppressed conductivity detection. *J. Chromatogr. A*. **1252**, 74–83 (2012).

[182] N. D. Boscher, T. Bohn, P. Heier, F. Moisy, B. Untereiner, K. Heinze, and P. Choquet, Optical sensing responses of CrIIICl(TPP)(H_2O)-based coatings obtained by an atmospheric pressure plasma method – Application to the detection of volatile amines. *Sensors and Actuators B: Chemical*. **191**, 553–560 (2014).

[183] M. L. Cable, A. M. Stockton, M. F. Mora, and P. A. Willis, Low-Temperature Microchip Nonaqueous Capillary Electrophoresis of Aliphatic Primary Amines: Applications to Titan Chemistry. *Anal. Chem.* **85**(2), 1124–1131 (2013).

[184] F. C. Fehsenfeld, L. G. Huey, E. Leibrock, R. Dissly, E. Williams, T. B. Ryerson, R. Norton, D. T. Sueper, and B. Hartsell, Results from an informal intercomparison of ammonia measurement techniques. *J.-Geophys.-Res.* **107**, 4812 (2002).

[185] M. Kirchner, S. Braeutigam, M. Ferm, M. Haas, M. Hangartner, P. Hofschreuder, A. Kasper-Giebl, H. Römmelt, J. Striedner, W. Terzer, L. Thöni, H. Werner, and R. Zimmerling, Field intercomparison of diffusive samplers for measuring ammonia. *J. Environ. Monit.* **1**(3), 259–265 (1999).

[186] J. J. Schwab, Y. Li, M.-S. Bae, K. L. Demerjian, J. Hou, X. Zhou, B. Jensen, and S. C. Pryor, A Laboratory Intercomparison of Real-Time Gaseous Ammonia Measurement Methods. *Environ. Sci. Technol.* **41**(24), 8412–8419 (2007).

[187] K. von Bobrutzki, C. F. Braban, D. Famulari, S. K. Jones, T. Blackall, T. E. L. Smith, M. Blom, H. Coe, M. Gallagher, M. Ghalaieny, M. R. McGillen, C. J. Percival, J. D. Whitehead, R. Ellis, J. Murphy, A. Mohacsi, A. Pogany, H. Junninen, S. Rantanen, M. A. Sutton, and E. Nemitz, Field inter-comparison of eleven atmospheric ammonia measurement techniques. *Atmos. Meas. Tech.* **3**(1), 91–112 (2010).

[188] H. A. Wiebe, K. G. Anlauf, E. C. Tuazon, A. M. Winer, H. W. Biermann, B. R. Appel, P. A. Solomon, G. R. Cass, T. G. Ellestad, K. T. Knapp, E. Peake, C. W. Spicer, and D. R. Lawson, A comparison of measurements of atmospheric ammonia by filter packs, transition-flow reactors, simple and annular denuders and fourier transform infrared spectroscopy. *Atmos. Environ.* **24**(5), 1019–1028 (1990).

[189] E. Williams, S. Sandholm, J. Bradshaw, J. Schendel, A. Langford, P. Quinn, P. Lebel, S. Vay, P. Roberts, R. Norton, B. Watkins, M. Buhr, D. Parrish, J. Calvert, and

F. Fehsenfeld, An Intercomparison of 5 Ammonia Measurement Techniques. *J. Geophys. Res.-Atmos.* **97**, 11591–11611 (1992).

[190] M. J. Hansen, A. P. S. Adamsen, and A. Feilberg, Recovery of odorants from an olfactometer measured by proton-transfer-reaction mass spectrometry. *Sensors.* **13**(6), 7860–7871 (2013).

[191] N. Nishino, K. D. Arquero, M. L. Dawson, and B. J. Finlayson-Pitts, Infrared studies of the reaction of methanesulfonic acid with trimethylamine on surfaces. *Environ. Sci. Technol.* **48**(1), 323–330 (2013).

[192] P. Brimblecombe and S. L. Clegg, The solubility and behaviour of acid gases in the marine aerosol. *J. Atmos. Chem.* **7**(1), 1–18 (1988).

[193] S. Clegg and P. Brimblecombe, The solubility of methanesulfonic acid and its implications for atmospheric chemistry. *Environ. Technol. Lett.* **6**(7), 269–278 (1985).

[194] G. Biskos, P. R. Buseck, and S. T. Martin, Hygroscopic growth of nucleation-mode acidic sulfate particles. *J. Aerosol. Sci.* **40**(4), 338–347 (2009).

[195] B. R. Bzdek, D. P. Ridge, and M. V. Johnston, Amine exchange into ammonium bisulfate and ammonium nitrate nuclei. *Atmos. Chem. Phys.* **10**(8), 3495–3503 (2010).

[196] B. R. Bzdek, D. P. Ridge, and M. V. Johnston, Reactivity of methanesulfonic acid salt clusters relevant to marine air. *J. Geophys. Res.-Atmos.* **116** (2011) DOI:10.1029/2010JD015217.

[197] B. R. Bzdek, D. P. Ridge, and M. V. Johnston, Size-dependent reactions of ammonium bisulfate clusters with dimethylamine. *J. Phys. Chem. A.* **114**(43), 11638–11644 (2010).

[198] L. P. Chan and C. K. Chan, Displacement of ammonium from aerosol particles by uptake of triethylamine. *Aerosol Sci. Technol.* **46**(2), 236–247 (2012).

[199] L. P. Chan and C. K. Chan, Role of the aerosol phase state in ammonia/amines exchange reactions. *Environ. Sci. Technol.* **47**(11), 5755–5762 (2013).

[200] E. Debry, B. Sportisse, and B. Jourdain, A stochastic approach for the numerical simulation of the general dynamics equation for aerosols. *J. Comput. Phys.* **184**(2), 649–669 (2003).

[201] E. Debry and B. Sportisse, Numerical simulation of the general dynamic equation (GDE) for aerosols with two collocation methods. *Appl. Numer. Math.* **57**(8), 885–898 (2007).

[202] K. Lehtinen and M. Kulmala, A model for particle formation and growth in the atmosphere with molecular resolution in size. *Atmos. Chem. Phys.* **3**, 251–257 (2003).

[203] T. Gaydos, C. Stanier, S. Pandis, and S. Pandis, Modeling of in situ ultrafine atmospheric particle formation in the eastern United States. *J. Geophys. Res.-Atmos.* **110** (2005) DOI:10.1029/2004JD004683.

[204] M. Karl, C. Leck, A. Gross, and L. Pirjola, A study of new particle formation in the marine boundary layer over the central Arctic Ocean using a flexible multicomponent aerosol dynamic model. *Tellus Ser. B-Chem. Phys. Meteorol.* **64** (2012) DOI:10.3402/tellusb.v64i0.17158.

[205] V. Kerminen and M. Kulmala, Analytical formulae connecting the 'real' and the 'apparent' nucleation rate and the nuclei number concentration for atmospheric nucleation events. *J. Aerosol Sci.* **33**(4), 609–622 (2002).

[206] H. Korhonen, K. Lehtinen, and M. Kulmala, Multicomponent aerosol dynamics model UHMA: model development and validation. *Atmos. Chem. Phys.* **4**, 757–771 (2004).

[207] C. Pilinis, J. H. Seinfeld, and C. Seigneur, Mathematical modeling of the dynamics of multicomponent atmospheric aerosols. *Atmos. Environ.* **21**(4), 943–955 (1987).

[208] M. Shiraiwa, C. Pfrang, T. Koop, and U. Poeschl, Kinetic multi-layer model of gas-particle interactions in aerosols and clouds (KM-GAP): linking condensation, evaporation and chemical reactions of organics, oxidants and water. *Atmos. Chem. Phys.* **12**(5), 2777–2794 (2012).

[209] T. Yli-Juuti, K. Barsanti, L. Hildebrandt Ruiz, A.-J. Kieloaho, U. Makkonen, T. Petäjä, T. Ruuskanen, M. Kulmala, and I. Riipinen, Model for acid-base chemistry in nanoparticle growth (MABNAG). *Atmos. Chem. Phys.* **13**(24), 12507–12524 (2013).

[210] Y. Zhang, C. Seigneur, J. Seinfeld, M. Jacobson, and F. Binkowski, Simulation of Aerosol Dynamics: A Comparative Review of Algorithms Used in Air Quality Models. **31**(6), 487–514 (1999).

[211] A. Castleman, P. Holland, and R. Keesee, Properties of ion clusters and their relationship to hetero-molecular nucleation. *J. Chem. Phys.* **68**(4), 1760–1767 (1978).

[212] A. Castleman and I. Tang, Role of small clusters in nucleation about ions. *J. Chem. Phys.* **57**(9), 3629–3638 (1972).

[213] M. Kulmala, K. Lehtinen, and A. Laaksonen, Cluster activation theory as an explanation of the linear dependence between formation rate of 3nm particles and sulphuric acid concentration. *Atmos. Chem. Phys.* **6**, 787–793 (2006).

[214] D. Kaschiev, On the relation between nucleation work, nucleus size and nucleation rate. *J. Chem. Phys.* **76**(10), 5098–5102 (1982).

[215] J. Curtius, Nucleation of atmospheric aerosol particles. *Comptes Rendus Phys.* **7**(9), 1027–1045 (2006).

[216] R. K. Bowles, R. McGraw, P. Schaaf, B. Senger, J. C. Voegel, and H. Reiss, A molecular based derivation of the nucleation theorem. *J. Chem. Phys.* **113**(11), 4524–4532 (2000).

[217] H. Du, A. B. Nadykto, and F. Yu, Quantum-mechanical solution to fundamental problems of classical theory of water vapor nucleation. *Phys. Rev. E.* **79**(2) (2009) DOI:10.1103/PhysRevE.79.021604.

[218] D. W. Oxtoby and D. Kashchiev, A general relation between the nucleation work and the size of the nucleus in multicomponent nucleation. *J. Chem. Phys.* **100**(10), 7665 (1994).

[219] H. Vehkamäki, M. J. McGrath, T. Kurtén, J. Julin, K. E. J. Lehtinen, and M. Kulmala, Rethinking the application of the first nucleation theorem to particle formation. *J. Chem. Phys.* **136**(9) (2012) DOI:doi:10.1063/1.3689227.

[220] I. Ford, Statistical mechanics of nucleation: a review. *P. I. Mech. Eng. C-J. Mec.* **218**(8), 883–899 (2004).

[221] A. S. Ansari and S. N. Pandis, Prediction of multicomponent inorganic atmospheric aerosol behavior. *Atmos. Environ.* **33**(5), 745–757 (1999).

[222] S. L. Clegg, P. Brimblecombe, and A. S. Wexler, Thermodynamic model of the system H^+-NH_4^+-Na^+-SO_4^{2-}-NB_3^--Cl^--H_2O at 298.15 K. *J. Phys. Chem. A.* **102**(12), 2155–2171 (1998).

[223] S. L. Clegg, P. Brimblecombe, and A. S. Wexler, Thermodynamic Model of the System $H^+NH_4^+SO_4^{2-}NO_{3<sub>-H<sub>2}O$ at Tropospheric Temperatures. *J. Phys. Chem. A.* **102**(12), 2137–2154 (1998).

[224] D. L. Bones, J. P. Reid, D. M. Lienhard, and U. K. Krieger, Comparing the mechanism of water condensation and evaporation in glassy aerosol. *PNAS.* **109**(29), 11613–11618 (2012).

[225] C. S. Dutcher, A. S. Wexler, and S. L. Clegg, Surface Tensions of Inorganic Multicomponent Aqueous Electrolyte Solutions and Melts. *J. Phys. Chem. A.* **114**(46), 12216–12230 (2010).

[226] S. A. Edwards and D. R. M. Williams, Surface tension of electrolyte solutions: Comparing the effects of ionic dispersion forces and solvation. *Europhys. Lett.* **74**(5), 854–860 (2006).

[227] S. L. Clegg, J. H. Seinfeld, and P. Brimblecombe, Thermodynamic modelling of aqueous aerosols containing electrolytes and dissolved organic compounds. *J. Aerosol Sci.* **32**(6), 713–738 (2001).

[228] S. L. Clegg and J. H. Seinfeld, Thermodynamic Models of Aqueous Solutions Containing Inorganic Electrolytes and Dicarboxylic Acids at 298.15 K. 1. The Acids as Nondissociating Components. *J. Phys. Chem. A.* **110**(17), 5692–5717 (2006).

[229] S. L. Clegg and K. S. Pitzer, Thermodynamics of multicomponent, miscible, ionic solutions: generalized equations for symmetrical electrolytes. *J. Phys. Chem.* **96**(8), 3513–3520 (1992).

[230] S. L. Clegg, K. S. Pitzer, and P. Brimblecombe, Thermodynamics of multicomponent, miscible, ionic solutions. Mixtures including unsymmetrical electrolytes. *J. Phys. Chem.* **96**(23), 9470–9479 (1992).

[231] C. S. Dutcher, X. Ge, A. S. Wexler, and S. L. Clegg, Statistical Mechanics of Multilayer Sorption: 2. Systems Containing Multiple Solutes. *J. Phys. Chem. C.* **116**(2), 1850–1864 (2012).

[232] C. S. Dutcher, X. Ge, A. S. Wexler, and S. L. Clegg, Statistical Mechanics of Multilayer Sorption: Extension of the Brunauer–Emmett–Teller (BET) and Guggenheim–Anderson–de Boer (GAB) Adsorption Isotherms. *J. Phys. Chem. C.* **115**(33), 16474–16487 (2011).

[233] E. Amado G and L. H. Blanco, Osmotic and activity coefficients of aqueous solutions of KCl at temperatures of 283.15, 288.15, 293.15 and 298.15 K: A new isopiestic apparatus. *Fluid Phase Equilibria*. **226**(0), 261–265 (2004).

[234] T. W. Chan and M. Mozurkewich, Measurement of the coagulation rate constant for sulfuric acid particles as a function of particle size using tandem differential mobility analysis. *J. Aerosol Sci.* **32**(3), 321–339 (2001).

[235] M. Sceats, Brownian coagulation in aerosols - the role of long range forces. *J. Colloid Interface Sci.* **129**(1), 105–112 (1989).

[236] H. Bai and P. Biswas, Deposition of lognormally distributed aerosols accounting for simultaneous diffusion, thermophoresis and coagulation. *J. Aerosol Sci.* **21**(5), 629–640 (1990).

[237] J. G. Crump and J. H. Seinfeld, Turbulent deposition and gravitational sedimentation of an aerosol in a vessel of arbitrary shape. *J. Aerosol Sci.* **12**(5), 405–415 (1981).

[238] C. N. Davies, Definitive equations for the fluid resistance of spheres. *Proc. Phys. Soc.* **57**(4), 259–270 (1945).

[239] C. Davies, Diffusion and sedimentation of aerosol particles from poiseuille flow in pipes. *J. Aerosol Sci.* **4**(4), 317–328 (1973).

[240] M. Alonso, F. Alguacil, and C.-H. Huang, Analytical approximation to the fully developed concentration profile of diffusive aerosol particles in laminar flow in a circular tube. *J. Aerosol Sci.* **41**(4), 413–417 (2010).

[241] Y. K. Chen and C. P. Yu, Particle Deposition from Duct Flows by Combined Mechanisms. *Aerosol Sci. Technol.* **19**(3), 389–395 (1993).

[242] M. Alonso and F. J. Alguacil, Penetration of aerosol undergoing combined electrostatic dispersion and diffusion in a cylindrical tube. *J. Aerosol Sci.* **38**(5), 481–493 (2007).

[243] N. Fuchs and A. Sutugin, *Highly dispersed aerosols*, Ann Arbor Science Publishers, Inc.

[244] K. J. Noone and H.-C. Hansson, Calibration of the TSI 3760 condensation nucleus counter for nonstandard operating conditions. *Aerosol Sci. Technol.* **13**(4), 478–485 (1990).

[245] G. Mordas, H. E. Manninen, T. Petäjä, P. P. Aalto, K. Hämeri, and M. Kulmala, On Operation of the Ultra-Fine Water-Based CPC TSI 3786 and Comparison with Other TSI Models (TSI 3776, TSI 3772, TSI 3025, TSI 3010, TSI 3007). *Aerosol Sci. Technol.* **42**(2), 152–158 (2008).

[246] G. P. Ayers, R. W. Gillett, and J. L. Gras, On the vapor pressure of sulfuric acid. *Geophys. Res. Lett.* **7**(6), 433–436 (1980).

[247] I. N. Tang and H. R. Munkelwitz, Determination of vapor pressure from droplet evaporation kinetics. *J. Colloid Interface Sci.* **141**(1), 109–118 (1991).

[248] S. Li, W. Qian, and F. Tao, Ionic dissociation of methanesulfonic acid in small water clusters. *Chem. Phys. Lett.* **438**(4), 190–195 (2007).

[249] S. Li, L. Zhang, W. Qin, and F. Tao, Intermolecular structure and properties of the methanesulfonic acid-ammonia system in small water clusters. *Chem. Phys. Lett.* **447**(1), 33–38 (2007).

[250] D. J. Millen and G. W. Mines, Hydrogen bonding in the gas phase. Part 5. Infrared spectroscopic investigation of O-H *** N complexes formed by water: ammonia monohydrate and amine and pyridine monohydrates. **73**(3), 369 (1977).

[251] A. Givan, A. Loewenschuss, and C. J. Nielsen, Infrared spectrum and ab initio calculations of matrix isolated methanesulfonic acid species and its 1 : 1 water complex. *J. Mol. Struct.* **748**(1), 77–90 (2005).

[252] W. Braun, J. Herron, and D. Kahaner, Acuchem - a Computer-Program for Modeling Complex Chemical-Reaction Systems. *Int. J. Chem. Kinet.* **20**(1), 51–62 (1988).

[253] M. Kulmala, Dynamical atmospheric cluster model. *Atmos. Res.* **98**(2), 201–206 (2010).

[254] X. Ge, A. Wexler, and S. Clegg, Atmospheric amines - Part II. Thermodynamic properties and gas/particle partitioning. *Atmos. Environ.* **45**(3), 561–577 (2011).

[255] D. Skoog, F. Holler, and T. Nieman, *Principles of Instrumental Analysis*, Harcourt Brace & Company, 5 ed.

[256] R. Kunin and R. E. Barry, Carboxylic, Weak Acid Type, Cation Exchange Resin. *Ind. Eng. Chem.* **41**(6), 1269–1272 (1949).

[257] in *CRC Handbook of Chemistry and Physics*, W. Haynes, Ed.; 93rd ed.

[258] NOAA, Quality controlled local climatological data.

[259] S. Murphy, J. Sorooshian, J. Kroll, N. Ng, P. Chhabra, C. Tong, J. Surratt, E. Knipping, R. Flagan, and J. Seinfeld, Secondary aerosol formation from atmospheric reactions of aliphatic amines. *Atmos. Chem. Phys.* **7**(9), 2313–2337 (2007).

[260] T. C. VandenBoer, A. Petroff, M. Z. Markovic, and J. G. Murphy, Size distribution of alkyl amines in continental particulate matter and their online detection in the gas and particle phase. *Atmos. Chem. Phys.* **11**(9), 4319–4332 (2011).

[261] S. Trabue, K. Scoggin, L. McConnell, R. Maghirang, E. Razote, and J. Hatfield, Identifying and tracking key odorants from cattle feedlots. *Atmos. Environ.* **45**(25), 4243–4251 (2011).

[262] T. Fujii and T. Kitai, Determination of trace levels of trimethylamine in air by gas chromatography/surface ionization organic mass spectrometry. *Anal. Chem.* **59**(2), 379–382 (1987).

[263] K. Kuwata, E. Akiyama, Y. Yamazaki, H. Yamasaki, and Y. Kuge, Trace determination of low molecular weight aliphatic amines in air by gas chromatograph. *Anal. Chem.* **55**(13), 2199–2201 (1983).

[264] G. Kallinger and R. Niessner, Laboratory investigation of annular denuders as sampling system for the determination of aliphatic primary and secondary amines in stack gas. *Mikrochim Acta.* **130**(4), 309–316 (1999).

[265] D. Hu, C. Li, H. Chen, J. Chen, X. Ye, L. Li, X. Yang, X. Wang, A. Mellouki, and Z. Hu, Hygroscopicity and optical properties of alkylaminium sulfates. *J. Environ Sci.* **26**(1), 37–43 (2014).

[266] NIST chemistry webbook.

[267] W. Jie, Z. Bing, F. Li, G. Wenyue, Z. Liandi, Z. Shudong, and C. Jiye, Multiphoton ionization of ethylamine and dimethylamine enhanced by resonance excitation to the 3s Rydberg state. *Acta Phys.-Chim. Sin.* **13**(8), 732–735 (1997).

[268] G. Siuzdak and J. J. BelBruno, Laser multiphoton dissociation/ionization of butylamines: competitive processes in radical cations. *J. Phys. Chem.* **94**(11), 4559–4565 (1990).

[269] G. Siuzdak and J. J. BelBruno, Multiphoton ionization studies of amines with UV-VIS lasers. *Appl. Phys. B.* **50**(3), 221–226 (1990).

[270] L. Xiaojun, Z. Bing, F. Li, G. Wenyue, Z. Jingang, C. Jiye, L. Yiqun, and Z. Shikang, Study of the multiphoton ionization mass spectra methylamine. *Acta Phys.-Chim. Sin.* **12**(11), 981–985 (1996).

[271] G. Hvistendahl and K. Undheim, High resolution mass spectrometry of trimethylamine. *Org. Mass Spectrom.* **3**(6), 821–824 (1970).

[272] K. R. Neubauer, M. V. Johnston, and A. S. Wexler, Humidity effects on the mass spectra of single aerosol particles. *Atmospheric Environment.* **32**(14), 2521–2529 (1998).

[273] C. Qiu, L. Wang, V. Lal, A. F. Khalizov, and R. Zhang, Heterogeneous reactions of alkylamines with ammonium sulfate and ammonium bisulfate. *Environ. Sci. Technol.* **45**(11), 4748–4755 (2011).

[274] R. C. Hoffman, A. Laskin, and B. J. Finlayson-Pitts, Sodium nitrate particles: physical and chemical properties during hydration and dehydration, and implications for aged sea salt aerosols. *Journal of Aerosol Science.* **35**(7), 869–887 (2004).

[275] A. Zelenyuk, M. J. Ezell, V. Perraud, S. N. Johnson, E. A. Bruns, Y. Yu, D. Imre, M. L. Alexander, and B. J. Finlayson-Pitts, Characterization of organic coatings on hygroscopic salt particles and their atmospheric impacts. *Atmospheric Environment.* **44**(9), 1209–1218 (2010).

[276] A. Zelenyuk, Y. Cai, L. Chieffo, and D. Imre, High Precision Density Measurements of Single Particles: The Density of Metastable Phases. *Aerosol Sci. Technol.* **39**(10), 972 (2005).

[277] M. Dawson, M. Varner, V. Perraud, M. Ezell, J. Wilson, A. Zelenyuk, R. Gerber, and B. Finlayson-Pitts, Amine-Amine Exchange in Aminium-Methanesulfonate Aerosols. *in preparation.*

[278] C. H. Wei, Structure of ammonium methanesulfonate. *Acta Cryst. C.* **42**(12), 1839–1842 (1986).

[279] G. J. Reiss and M. K. Meyer, Diisopropylammonium methanesulfonate. **67**(8), o2169–o2169 (2011) DOI:10.1107/S1600536811029382.

[280] G. R. Desiraju, Hydrogen bridges in crystal engineering: Interactions without borders. *Acc. Chem. Res.* **35**(7), 565–573 (2002).

[281] J. Ruiz-Jiménez, S. Hautala, J. Parshintsev, T. Laitinen, K. Hartonen, T. Petäjä, M. Kulmala, and M.-L. Riekkola, Aliphatic and aromatic amines in atmospheric aerosol particles: Comparison of three ionization techniques in liquid chromatography-mass spectrometry and method development. *Talanta.* **97**, 55–62 (2012).

[282] Y. Liu, C. Han, C. Liu, J. Ma, Q. Ma, and H. He, Differences in the reactivity of ammonium salts with methylamine. *Atmos. Chem. Phys.* **12**(11), 4855–4865 (2012).

[283] S. L. Clegg, C. Qiu, and R. Zhang, The deliquescence behaviour, solubilities, and densities of aqueous solutions of five methyl- and ethyl-aminium sulphate salts. *Atmos. Environ.* **73**, 145–158 (2013).

[284] A. Lavi, N. Bluvshtein, E. Segre, L. Segev, M. Flores, and Y. Rudich, Thermochemical, cloud condensation nucleation ability, and optical properties of alkyl aminium sulfate aerosols. *J. Phys. Chem. C.* **117**(43), 22412–22421 (2013).

[285] C. Qiu and R. Zhang, Physiochemical properties of alkylaminium sulfates: Hygroscopicity, thermostability, and density. *Environ. Sci. Technol.* **46**(8), 4474–4480 (2012).

[286] M. Galassi, J. Davies, J. Theiler, B. Gough, G. Jungman, P. Alken, M. Booth, F. Rossi, and R. Ulerich, *GNU Scientific Library Reference Manual for GSL Version 1.16*, 3 ed.

[287] A. Sandu and C. Borden, A framework for the numerical treatment of aerosol dynamics. *Appl. Numer. Math.* **45**(4), 475–497 (2003).

[288] B. Verheggen and M. Mozurkewich, An inverse modeling procedure to determine particle growth and nucleation rates from measured aerosol size distributions. *Atmos. Chem. Phys.* **6**, 2927–2942 (2006).

Appendix A

Sample Model Input File

What follows is a sample input file containing parameters used in the flow reactor model. Table A.1 describes the input parameters and use in the model.

[CCOAG] 1.0

[CWL] 104.17

[K_A] 1.00

[r_A] 1.484

[C_A1] 0.733

[NUM_MOLEC] 3

[RXN_TIME] 1500.0

[DENSITY_EST] 1769.0

[SURF_TENS] 0.072

[D_VAP] 8.79349e-6

[ALPHA] 0.0

[MFP_AIR] 6.57895e-8

[VISC_AIR] 1.86086e-5

[FT_RADIUS] 0.0381

[DP_RANGE] 3.0

[SPECIES]

# name	conc	kwl	MW	density	HSCR	E_act	SVP	HLC	Alpha	ClorP	nMSA	nAmine	nWater
#	(#/cc)	(1/s)	(g/mol)	(g/m^3)	(m)	NA	(#/cc)	(mol/(kg*atm))	unitless				
1MSA	4.31e09	0.002	96.11	1480000	2.73e-10	1e-20	0	0.0	0.025	0	1	0	0
2TMA	2.95e11	0.002	59.11	670000	2.73e-10	1e-20	0	9.6	0.012	0	0	1	0
3H2O	3.54e17	0.002	18.02	1000000	8.00e-11	6.5e-20	6.83e17	0.0	1.0	0	0	0	1
4MH	0	0.002	114.13	1240000	3.50e-10	0	0	0.0	0.01	0	1	0	1
5MTH	0	0.002	173.24	1050000	6.30e-10	0	0	0.0	0.06	0	1	1	1

```
6MT     0       0.002   155.22  1075000 5.50e-10        0       0       0.0             0.01    0       1       1       0
7Part1  0       0       0       0       8.00e-10        0       0       0.0             0.0     1       2       1       1
8Part2  0       0       0       0       8.00e-10        0       0       0.0             0.0     1       1       2       1
9Part3  0       0       0       0       8.00e-10        0       0       0.0             0.0     1       1       1       2
10Part4 0       0       0       0       8.00e-10        0       0       0.0             0.0     1       2       1       0
11Part5 0       0       0       0       8.00e-10        0       0       0.0             0.0     1       1       2       0
[END_SPECIES]


[RXNS]
# name  Reac1   Reac2   Prod1   Prod2   RateConst
k1      1       3       4       0       6.58e-10
k-1     4       0       1       3       5.53e8
k2      4       2       5       0       1.32e-9
k-2     5       0       4       2       3.09e1
k3      5       0       6       3       9.96e8
k-3     6       3       5       0       1.66e-9
k4      5       1       7       0       1e-15
k5      5       2       8       0       9e-16
k6      5       3       9       0       3e-22
k7      6       1       10      0       4e-17
k8      6       2       11      0       3e-16
[END_RXNS]
[END]
```

Table A.1: Description of input file parameters.

Input Parameter	Description	Units
CCOAG	scalar enhancement to coagulation, C_{coag}	unitless
CWL	scalar enhancement to particle wall loss, C_{wl}	unitless
K_A	Dutcher et al. activity model parameter, k_A	unitless
r_A	Dutcher et al. activity model parameter, r_A	unitless
C_A1	Dutcher et al. activity model parameter, C_{A1}	unitless
NUM_MOLEC	number of particle phase species, m	unitless
	($m = 3$ for the MSA/amine/H_2O system)	
RXN_TIME	reaction time over which to integrate	s
DENSITY_EST	estimated particle density, ρ	kg m^{-3}
SURF_TENS	estimated particle surface tension, σ	N m^{-1}
D_VAP	gas-phase diffusion coefficient	m^2 s^{-1}
	(used in calculation of uptake coefficient, γ)	
ALPHA	not used	
MFP_AIR	mean free path in air	m
	(used in calculation of diffusion coefficient, D)	
VISC_AIR	absolute viscosity of air	kg m^{-1} s^{-1}
	(used in calculation of diffusion coefficient, D)	
FT_RADIUS	flow tube radius, R	m
DP_RANGE	range of particle diameter, d_p, to integrate over in log scale	unitless

Species Parameters

name	label for gas-phase species	
conc	initial gas-phase concentration	# cm^{-3}
kwl	gas-phase wall loss rate constant, $k_w l$	s^{-1}
MW	molecular weight, MW	g mol^{-1}

Table A.1: (continued)

Input Parameter	Description	Units
`density`	bulk density, ρ	g m^{-3}
`HSCR`	estimated hard sphere collision radius, r_g	m
`E_act`	not used	
`SVP`	saturation vapor pressure, y_q^0	# cm^{-3}
`HLC`	Henry's Law coefficient, k_H	mol kg^{-1} atm^{-1}
`Alpha`	mass accommodation coefficient, u_q	unitless
`ClorP`	0 for gas-phase species or intermediate clusters, 1 for initial particles	unitless
`nMSA`	number of MSA molecules in cluster or particle	unitless
`nAmine`	number of amine molecules in cluster or particle	unitless
`nH2O`	number of H_2O molecules in cluster or particle	unitless

Reaction Parameters

`name`	label for reaction	unitless
`React1`	index of reactant 1	unitless
`React2`	index reactant 2	unitless
`Prod1`	index of product 1	unitless
`Prod2`	index of product 2	unitless
`RateConst`	rate constant for reaction	s^{-1} or cm^3 s^{-1}

Appendix B

Derivation of Displacement Equation

A derivation of equation 4.1 follows. In general, subscripted numbers refer to a specific m/z peak, subscripted ($_\Sigma$) refers to the sum of all m/z peaks in the spectrum, subscripted letters refer to a specific amine, superscipted (^{0}) refers to the pure (one-amine) salt, and superscripted ($'$) refers to a normalized peak height.

The $[M-H]^+$ peak heights for the original and displacing amines are used for quantification of displacement and are refered to as h_1 and h_2. For the mass spectrum of a single particle of a known size, the height for each of these peaks can be calculated as,

$$h_1 = h_{1a}^0 \chi_a + h_{1b}^0 \chi_b \tag{B.1a}$$

$$h_2 = h_{2a}^0 \chi_a + h_{2b}^0 \chi_b \tag{B.1b}$$

where χ_a is the fraction of total amine in the particle that is amine a, such that $\chi_a + \chi_b = 1$ and h_{1a}^0 is the height of peak 1 for a single particle of the same size that contains only MSA and amine a. The other variables are defined in a similar manner. Equations B.1a and B.1b

assume that the size and total amine concentration remains the same upon displacement, which seems reasonable based on a comparison of the particle size distributions before and after reaction (fig. 4.5) and the similarity of the measured particle densities for each type of particle.[277] The normalized peak height is then:

$$h_1^{'} = \frac{h_1}{h_\Sigma} \tag{B.2a}$$

$$h_2^{'} = \frac{h_2}{h_\Sigma} \tag{B.2b}$$

The relative ionization efficiency for pure salt particles of each amine is:

$$\frac{e_a}{e_b} = \frac{h^0_{\Sigma a}}{h^0_{\Sigma b}} \tag{B.3}$$

Combining equations B.1a, B.1b, B.2a, B.2b and B.3 yields:

$$h_1^{'} h_\Sigma = h^{0'}_{1a} h^0_{\Sigma a} \chi_a + h^{0'}_{1b} \frac{e_b}{e_a} h^0_{\Sigma a} \chi_b \tag{B.4a}$$

$$h_2^{'} h_\Sigma = h^{0'}_{2a} h^0_{\Sigma a} \chi_a + h^{0'}_{2b} \frac{e_b}{e_a} h^0_{\Sigma a} \chi_b \tag{B.4b}$$

Taking eq. B.4a divided by (eq. B.4a + eq. B.4b), cancelling common terms, and rearranging gives equation B.5.

$$\frac{h_1^{'}}{h_1^{'} + h_2^{'}} = \frac{h^{0'}_{1a} \chi_a - h^{0'}_{1b} \frac{e_b}{e_a} \chi_a + h^{0'}_{1b} \frac{e_b}{e_a}}{\chi_a \left[\left(h^{0'}_{1a} + h^{0'}_{2a} \right) - \frac{e_b}{e_a} \left(h^{0'}_{1b} + h^{0'}_{2b} \right) \right] + \frac{e_b}{e_a} \left(h^{0'}_{1b} + h^{0'}_{2b} \right)} \tag{B.5}$$

Now, we define the following four terms,

$$f_1 \equiv \frac{h_1^{'}}{h_1^{'} + h_2^{'}} \qquad f_{1a}^0 \equiv \frac{h_{1a}^{0'}}{h_{1a}^{0'} + h_{2a}^{0'}} \qquad f_{1b}^0 \equiv \frac{h_{1b}^{0'}}{h_{1b}^{0'} + h_{2b}^{0'}} \qquad e^{'} \equiv \frac{h_{1a}^{0'} + h_{2a}^{0'}}{h_{1b}^{0'} + h_{2b}^{0'}} \tag{B.6}$$

Substituting the definitions in equation B.6 into equation B.5 yields:

$$f_1 = \frac{f_{1a}^0 \chi_a - \frac{f_{1b}^0 e_b}{e^{'} e_a} \chi_a + \frac{f_{1b}^0 e_b}{e^{'} e_a}}{\chi_a \left(1 - \frac{e_b}{e^{'} e_a}\right) + \frac{e_b}{e^{'} e_a}} \tag{B.7}$$

Rearranging to solve for χ_a results in equation 4.1:

$$\chi_a = \frac{f_{1b}^0 - f_1}{\frac{e^{'} e_a}{e_b}(f_1 - f_{1a}^0) - f_1 + f_{1b}^0} \tag{B.8}$$